Conformational study of cinchona and ephedra alkaloids

Dijkstra, Gerard Durk Henk

CONFORMATIONAL STUDY OF CINCHONA AND EPHEDRA ALKALOIDS

RIJKSUNIVERSITEIT GRONINGEN

CONFORMATIONAL STUDY OF CINCHONA AND EPHEDRA ALKALOIDS

PROEFSCHRIFT

Ter verkrijging van het doctoraat in de
Wiskunde en Natuurwetenschappen
aan de Rijksuniversiteit Groningen
op gezag van de
Rector Magnificus Dr. L. J. Engels
in het openbaar te verdedigen op
vrijdag 5 april 1991
des namiddags te 4.00 uur
door

Gerard Durk Henk Dijkstra
geboren op 21 februari 1958
te Groningen

EERSTE PROMOTOR: PROF. DR. R. M. KELLOGG
TWEEDE PROMOTOR: PROF. DR. H. WIJNBERG

The computer and molecular modelling facilities used for this work were provided by Royal Dutch Shell

Aan allen die hebben bijgedragen aan het tot stand komen van dit proefschrift betuig ik mijn hartelijke dank

voor mijn ouders
voor emmy en wouter

CONTENTS

1

INTRODUCTION

1.1 SCOPE OF THIS THESIS

Chirality and Nature are closely associated. Living organisms use chiral catalysts (enzymes) to synthesize many of their chemical constituents. Over millions of years the complex compositions of enzymes have developed into efficient and specific catalysts for the synthesis (and breakdown) of chiral organic compounds. Because of the complexity of enzymatic reactions, it is difficult to study the details of their reaction mechanisms directly from experiments. Recently several breakthroughs in the design and the synthesis of organic catalysts have taken place. With these catalysts it is possible to control the stereoselectivity of some reactions with efficiencies rivalling those of enzymes. In many cases these chiral organic catalysts are, like enzymes, natural products or their derivatives. However, such catalysts are much smaller than enzymes and are thus better suited to mechanistic studies. A recent example is given by Inoue[1] . With the dipeptide cyclo-phenylalanine-histidine as chiral catalyst in a reaction between benzaldehyde

and hydrogen cyanide he obtained R-mandelonitrile (enantiomeric excess 97%) in almost quantitative yield (Figure 1.1).

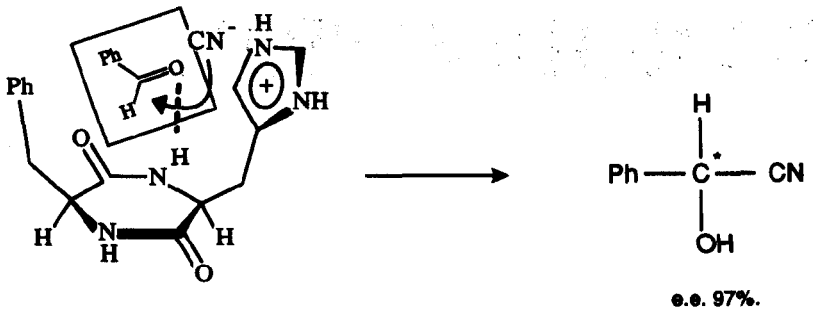

Figure 1.1 Reaction between benzaldehyde and hydrogen cyanide, proposed model for the transition state.

For at least two reasons such studies are intriguing. Firstly, detailed knowledge of the mechanism of catalytic stereoselective syntheses is fundamental to understanding the essentials of recognition processes at a molecular level and the mechanistic rules which govern these. Secondly, this mechanistic knowledge is essential for optimizing existing asymmetric routes or designing new ones. In particular, this area of endeavor has wide-ranging practical applications for the chemical, agrochemical, and pharmaceutical industries.

Both in our laboratory[2] and elsewhere[3] many successful applications have been made of cinchona and ephedra alkaloids as chiral organic catalysts in stereoselective syntheses. In contrast to the large amount of experimental data, much less is known about the mechanism of action of these alkaloids and their derivatives. Therefore, we have carried out a detailed conformational study on cinchona and ephedra alkaloids.

In chapter one we will briefly introduce the cinchona and ephedra alkaloids, and we will establish some notions regarding stereoselective synthesis. In chapter two the results will be given of a conformational analysis using molecular mechanics calculations on cinchona and ephedra alkaloids. This knowledge of the preferred conformations of cinchona alkaloids in the gas phase has been used to study their conformational behavior in solution. These results are obtained with a NMR study, and are presented in chapter three. In chapter four a study of conformational changes caused by cinchona alkaloid-substrate interactions is described. The results are used to discuss some mechanistic aspects of the asymmetric Michael addition between aromatic thiols and α,β-unsaturated ketones. A quantum mechanical analysis on the conformational behavior of cinchona and ephedra alkaloids is presented in chapter 5. An attempt is made to rationalize in detail the experimentally obtained conformational data. Finally, in chapter 6 we will give the preliminary results of improved catalyst design. Comparison of results obtained with cinchona and ephedra alkaloids as chiral catalysts in a Michael addition between aromatic thiols and conjugated ketones will be used as basis for discussion and outlook.

1.2 CINCHONA AND EPHEDRA ALKALOIDS

1.2.1 The Alkaloids

The alkaloids are a large class of naturally occurring amines[4]. Sertuner[5] isolated the first alkaloid, morphine, in pure form (1805). He described morphine as basic, salt-forming and ammonia-like, and used the term 'organic alkali'. The term alkaloid, or 'alkali-like', was first proposed by Meissner[6] (1819). Basic organic nitrogen compounds of (chiefly) plant origin are in general classified as alkaloids. Many alkaloids are marked by a noticeable biological activity in humans. Already long before the isolation of the first pure compound they were used as medicines and poisons. The alkaloids have provided our society with some potent pharma-

ceutical agents, but they are also involved in severe social problems (e.g. cocaine, LSD, heroin, see Figure 1.2).

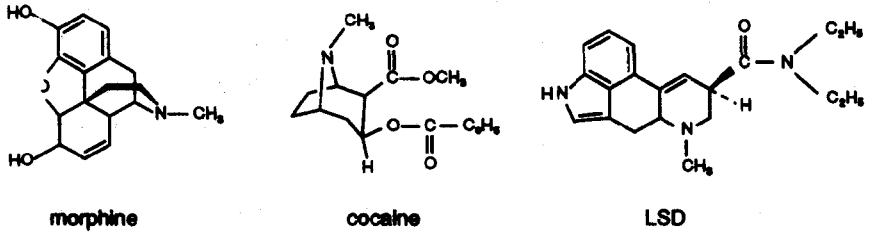

Figure 1.2 The structures of the alkaloids morphine, cocaine, and LSD.

Because of the complexity of the compounds and for historical reasons, the nomenclature of alkaloids has not been systematized. The two commonly used systems classify alkaloids either according to the plant genera in which they occur, or on the basis of similarity of molecular structure. On the latter basis, alkaloids are usually organized in families with similar types of heterocyclic rings.

1.2.2 The Cinchona Alkaloids

The cinchona alkaloids[7] form the first class of alkaloids that we have studied with regard to the conformational behavior. In this section we will briefly introduce their history, use, and structures.

The cinchona alkaloids consist of thirty members, divided into eight major alkaloids, nine minor alkaloids and thirteen lesser known alkaloids. The structures of the eight major cinchona alkaloids are depicted in Figure 1.3. The four best known cinchona alkaloids, quinine, cinchonidine, quinidine, and cinchonine are found in the bark of several species of Cinchona and Remeijia trees, indigenous to the eastern slopes of the Andes (South-America). Quinine and

cinchonine were the first cinchona alkaloids to be isolated in pure form (Pelletier and Caventou[8] ,1820). It took almost another hundred years before Rabe[9] elucidated the molecular structure (1907). The determination of the absolute configuration has been the subject of an intensive study. Prelog and Hafliger[10] established the absolute configuration correctly (1950). They concluded that the C_8 and C_9 carbons of the cinchona alkaloids have an erythro arrangement, whereas the epi- bases exist as threo pairs. The history of classical structural elucidation of the cinchona alkaloids ended in 1967, when their structures were definitely established with X-ray crystallography[11] .

The cinchona alkaloids have a rich history. The Indians of South-America were probably the first who used powdered bark of the Cinchona trees. In the beginning of the seventeenth century the Europeans became aware of the *medicinal qualities* of cinchona bark. Especially after the discovery of its action against malaria, the major component of cinchona bark, quinine, was soon to be found among the most used drugs[12] . As a consequence of the importance of quinine for the treatment of malaria the South American Cinchona trees were threatened by extinction in the nineteenth century.

The use of cinchona alkaloids as *chiral auxiliaries* is also characterized by a long tradition. The first resolution ever made was carried out with quinicine and cinchonicine[13] , which are derivatives of quinine and cinchonine, respectively.
Since then, about 25% of all resolutions have been carried out with these natural bases[14] . In addition, many applications of the cinchona alkaloids have been found as *chiral catalysts* in stereoselective syntheses.

The structures, configurations, and carbon numbering of the eight major cinchona alkaloids are given in Figure 1.3. It can be seen from this Figure that the alkaloids consist of two relatively rigid ring structures, an aromatic quinoline ring and an aliphatic quinuclidine ring. These two ring systems are connected by two carbon-carbon single bonds. Konigs[15] (1906) proposed the name quinuclidine for the bicyclic system 1-aza-bicyclo-[2,2,2]-octane.

Cinchona alkaloids contain five stereocenters (C_3, C_4, C_8, C_9, and N_1), but they differ from each other in configuration only at C_8 and C_9. As a result, cinchona

alkaloids are pair-wise related. For example, although structurally similar, quinine and quinidine form a diastereomeric pair. Quinine and quinidine are sometimes called 'pseudo-enantiomers' for reasons emphasized in Figure 1.3. This pseudo-enantiomeric relationship is also reflected in their behavior as chiral catalysts or resolving agents. For example, when an asymmetric reaction catalyzed by quinine yields predominantly product with R configuration, then product with S configuration will be formed in excess when quinidine is used as catalyst. However, the enantiomeric excesses in both reactions will almost always differ[16].

The last structural aspect that will be discussed here are the two tertiary nitrogen atoms, N_1 and $N_{1'}$. The pKa value in water of the bridgehead quinuclidine nitrogen N_1 is about three pKa units larger than that of the quinoline nitrogen $N_{1'}$[17]. Therefore the quinuclidine nitrogen is responsible for the basic character of cinchona alkaloids. The quinuclidine nitrogen also plays a key role, as we will see in chapter 4, when cinchona alkaloids are used as chiral ligands.

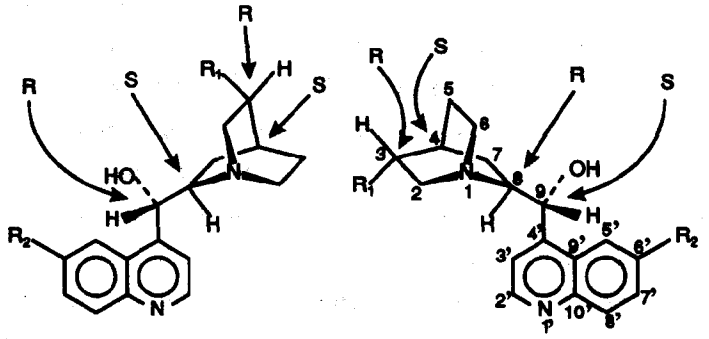

	R_1	R_2
quinine	C_2H_3	OCH_3
cinchonidine	C_2H_3	H
dihydroquinine	C_2H_5	OCH_3
dihydrocinchonidine	C_2H_5	H

	R_1	R_2
quinidine	C_2H_3	OCH_3
cinchonine	C_2H_3	H
dihydroquinidine	C_2H_5	OCH_3
dihydrocinchonine	C_2H_5	H

Figure 1.3 The structures, numbering, and absolute configuration of the eight major cinchona alkaloids.

1.2.3 The Ephedra Alkaloids

The ephedra alkaloids[18] form the second class of alkaloids that we have studied with regard to the conformational behavior. In this section we will briefly introduce them.

The herb called Ma Huang has been used in China for some five thousand years in the treatment of a variety of afflictions. Ma Huang is the best known source of ephedrine. Nagai[19] (1887) isolated the first pure basic substance from this Chinese herb and called it ephedrine.

In 1924 a revolutionary renewal of the interest in ephedrine started with the publication of the papers of Chen and Schmidt on Ma Huang[20]. These authors recorded the similarity of the physiological action of ephedrine and adrenaline. Since then an enormous volume of literature on the chemistry and pharmacology of ephedrine and related natural alkaloids has accumulated[21].

Ephedra forms the largest genus of the family Gnetaceae. Plants of this genus contain six optically active alkaloids. Their structures are depicted in Figure 1.4, in which the two stereocenters, C_7 and C_8, are marked with an asterisk. The two major ephedra alkaloids, (-)-ephedrine (A) and (+)-pseudoephedrine (B), form a diastereoisomeric pair. They differ only in configuration with respect to the carbinol function (C_7); (-)-ephedrine has an erythro configuration and (+)-pseudoephedrine a threo configuration. It has been shown that (-)-norephedrine (C) and (-)-N-methylephedrine (D) are derived from (-)-ephedrine, whereas the two other naturally occurring ephedra alkaloids, (+)-norpseudoephedrine (E) and (+)-N-methylpseudoephedrine (F), are similarly related to (+)-pseudoephedrine[22]. Of the many syntheses of (-)-ephedrine and (+)-pseudoephedrine, the ones shown in Scheme 1.1 are of commercial interest. The synthesis depicted in Scheme 1.1A was developed by Nagai[22] (1929). Condensation of benzaldehyde with nitroethane in the presence of potassium carbonate yields a stereoisomeric mixture of nitroalcohols (1). Reduction gives a mixture of norephedrine and norpseudoephedrine (2), which can be separated by crystallization into racemic norephedrine

and norpseudoephedrine. Methylation of norephedrine yields ephedrine (3), which can be resolved into the optically antipodes without difficulty.

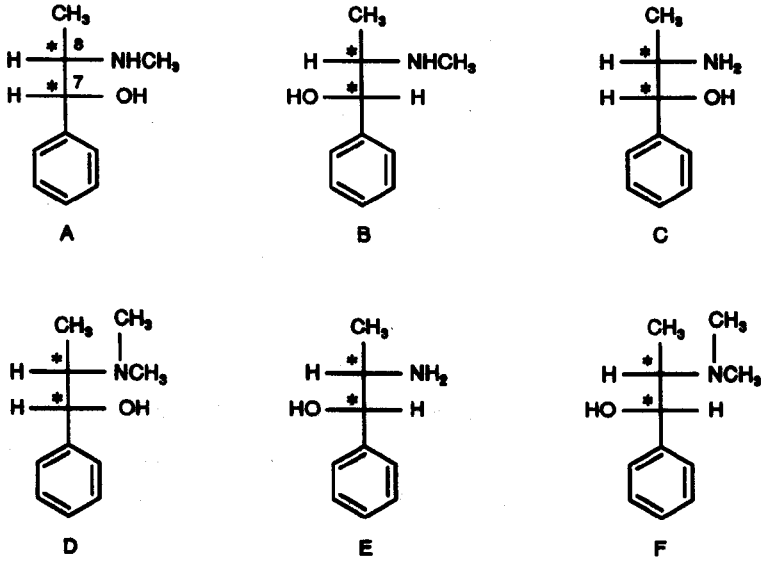

Figure 1.4. The six ephedra alkaloids (Fisher projections). A=(-)-ephedrine, B=(+)-pseudoephedrine, C=(-)-norephedrine, D=(-)-N-methylephedrine, E=(+)-norpseudoephedrine, F=(+)-N-methylpseudoephedrine.

The synthesis depicted in Scheme 1.1B illustrates that interest in ephedra alkaloids did not stop in the early days of our century. This reaction scheme was developed recently (1988) and involves the action of the enzyme oxynitrilase[23]. In the first step benzaldehyde is converted into (R)-mandelonitrile (4) (e.e.>95%). After protection of the hydroxy group by silylation, a Grignard reaction gives an intermediate iminium complex (5). This iminium complex can be converted to ephedrine in two different ways. The first route is by acid hydrolysis, followed by a reductive amination. The second involves a reduction with $NaBH_4$. Desilylation takes place on reaction with HF in acetonitrile. This procedure results in formation of one stereoisomer (1R, 2S) in high optical purity (>95%).

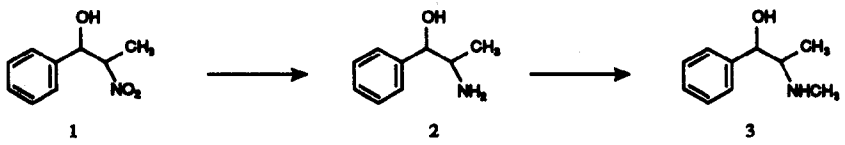

Scheme 1.1A

Synthesis of ephedrine developed in 1929 by Nagai[22].

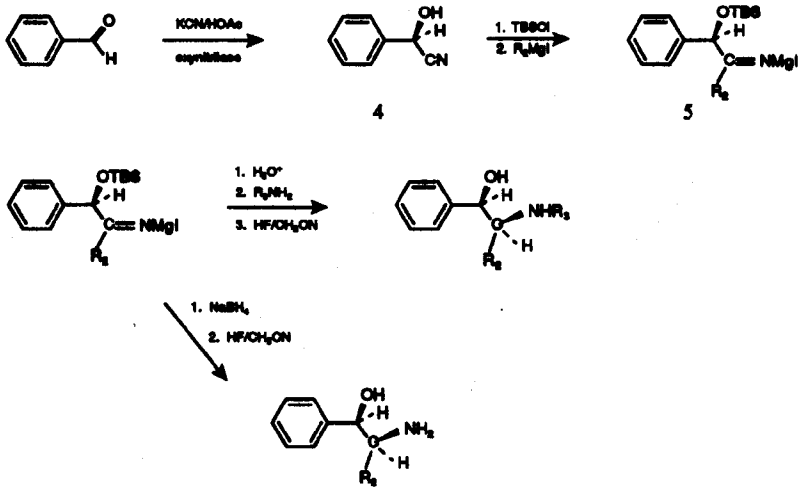

Scheme 1.1B

Synthesis of ephedrine developed in 1988 by van der Gen[23].

1.3 CHIRALITY

Chirality comes in many guises in Nature, ranging from the level of quanta and the parity violation in the weak interaction (e.g. the intrinsic left-handedness of the neutrino) to an apparent excess of left-handed galaxies[24] . Many organic compounds that occur in Nature are *chiral* (a term coined by Kelvin from the Greek word *khair*, meaning hand). Chiral compounds lack reflection symmetry, meaning that they are not identical with their mirror images. The relationship between the left and right hand is the same as that shown by any molecule which has a nonsuperimposable mirror image. Early in the nineteenth century[25] (1815) it was discovered that many natural compounds are able to rotate the plane of polarization of plane polarized light. An explanation for this optical activity on a molecular level was provided later. Pasteur[26] made the first important step by recognizing that the optical activity is caused by an asymmetric ordering of the atoms in the molecule. In 1874 this concept was refined by Van 't Hoff[27] and LeBel[28] . They independently proposed a theory in which they related the optical activity to a tetrahedral constitution of the carbon atom. To appreciate the contributions of these chemists it is important to realize that their articles appeared in a time when even the existence of atoms and molecules was questioned openly by many scientists.

Most chiral compounds occur in Nature as only (or mainly) one enantiomer[29] or diastereomer[30] . We have already mentioned the reason for this in section 1.1. In the synthesis of the majority of natural compounds enzymes are involved; these are capable of producing optically pure compounds from achiral starting materials in a highly efficient and specific manner. The high specificity of enzymes is crucial, since in principle *stereoisomers* have different physical properties in a chiral (natural) environment. Probably one of the most cited examples to demonstrate the dramatic consequences of this difference in properties is thalidomide, better known by its commercial name softenon (Figure 1.5). As a result of synthetic methods available in the early 1960s and lack of knowledge the two enantiomers of thalidomide were present in equal proportions (*racemic*

mixture) in the manufactured drug. This racemic mixture of thalidomide was used in the beginning of the sixties as a powerful tranquilliser; later it had to be withdrawn from the market because of association with fetal abnormalities. The (S)-enantiomer is now held solely responsible for the teratogenic effects of this drug[31] , whereas the (R)-enantiomer possesses the desired therapeutic effect. Softenon is not an isolated case; there are many examples that show the importance of the use of enantiomerically pure drugs.

The different behavior of enantiomers in living systems is the great stimulus for current interest in stereochemistry[32] and (in particular) stereoselective synthesis.[33]

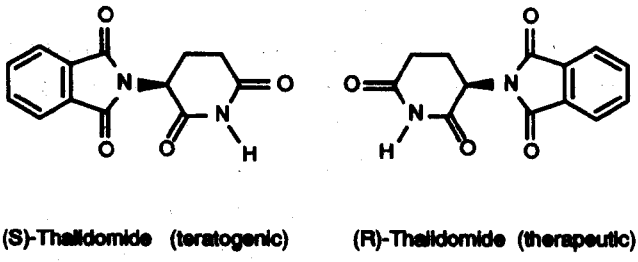

Figure 1.5 The structures of (R) and (S)-Thalidomide (Softenon).

1.4 ROUTES TO OPTICALLY PURE COMPOUNDS

We shall now describe some techniques by which stereoisomers can be obtained in optically pure form. The methods can be divided into three main categories: resolution, isolation, and stereoselective synthesis.

The oldest way to achieve this aim is by *resolution*. The first example was given by Pasteur[34] (1848), who resolved racemic sodium ammonium tartrate by separation of enantiomorphic crystals. A more general approach to the resolution of racemates is preferential crystallization of diastereomeric salts or covalently bonded diastereomeric derivatives[35] . Numerous examples exist of separations of enantiomers, in particular on industrial scale, by crystallization of diastereomeric salts. Resolution via chromatographic techniques is also a well known route to optically pure compounds. As a recent accomplishment one could mention the chromatographic separation of enantiomers employing quinine and quinidine impregnated supports[36] . Kinetic resolution[37] forms another important route for separation of enantiomers. This method is based upon the difference in reaction rates between enantiomers with a chiral reagent. The result is enrichment in starting material or product. Scheme 1.2 shows an example of kinetic resolution developed in our laboratory using cinchona alkaloids as the chiral reagent. The addition of 0.5 equivalent of thiophenol to racemic 5-methoxy-2(5H)-furanone in the presence of a catalytic amount of cinchonidine yielded butenolide A and (4S,5S)-B[38] . The thiol adduct B can easily be reconverted into butenolide. Butenolide A could be isolated in 40%, with an e.e. of 13%. This resolution experiment is still under investigation in the Feringa group, and optimizations have resulted already in an increase of the e.e. up to 80%[39] .

A serious disadvantage in obtaining pure enantiomers by resolution is that, with few exceptions, 50% of the racemic compound is lost as the unwanted enantiomer.

The second way to obtain optically pure compounds is provided by Nature itself. *Isolation* from natural sources forms an important route to enantiomerically pure compounds. Well known examples are amino acids, carbohydrates, alkaloids,

steroids, carboxylic acids, etc[40] . These molecules are often the starting materials in the synthesis of other chiral products[41] , but sometimes they are used directly. The cinchona alkaloids are an example; they are used, in many cases without modification, as drugs, resolving agents, and chiral catalysts.

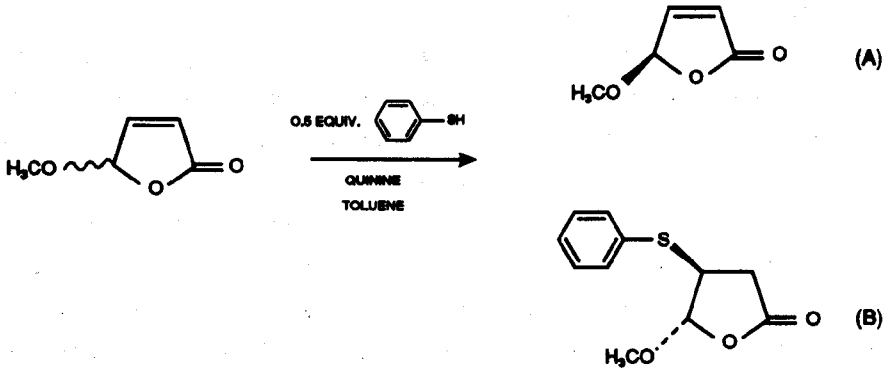

Scheme 1.2.

In principle, *stereoselective synthesis* is the method of choice to obtain optically pure compounds. Starting from achiral molecules the selective creation of the preferred stereoisomer can in principle be achieved in 100% conversion. Morrison and Mosher[42] have provided the most generally used definition of stereoselective synthesis. They use the term asymmetric synthesis and define it as: "A reaction in which an achiral unit in an ensemble of substrate molecules is converted by a reactant into a chiral unit in such a manner that the stereoisomeric products are produced in unequal amounts. This is to say an asymmetric synthesis is a process which converts a prochiral unit into a chiral unit, so that unequal amounts of stereoisomeric products result". Reactant in this definition includes, besides the usual chemical reagents, also solvents, catalysts, and physical forces. It should be noted that, according to this definition, the products of an asymmetric synthesis

are not necessarily optically active. For instance, formation of racemic diastereoisomers in unequal amounts is also called asymmetric synthesis.

Izumi[43] proposed to use the term stereoselective synthesis instead of asymmetric synthesis, because the products need not necessarily be asymmetric. Asymmetric means lack of *all* symmetry elements, whereas lack of reflection symmetry is a sufficient condition for chirality. Therefore the term stereoselective is nowadays preferred by most authors.

In principle, a stereoselective synthesis yields unequal amounts of stereoisomers. This is because stereoisomeric products are formed via different diastereomeric transition states. Stereoselective synthesis can be divided into *diastereoselective* and *enantioselective* synthesis. In a diastereoselective synthesis the starting molecule already possesses a stereogenic center, as well as a prostereogenic center. During the reaction the prostereogenic center is converted into another stereogenic center. This will lead to the formation of diastereomeric products. If the attack on the prostereogenic center is the rate determining step of a kinetically controlled process, the ratio of distribution between both diastereomers will depend on the difference in activation energy ($\Delta\Delta G$) between both transition states.

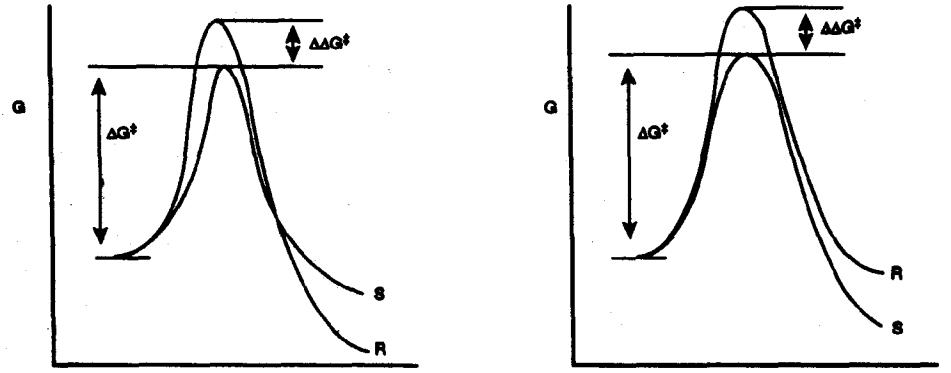

Figure 1.6 Gibbs free energy profiles for a diastereoselective process.

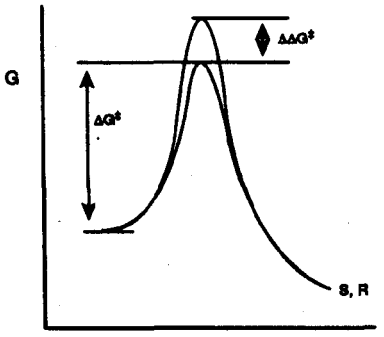

Figure 1.7 Gibbs free energy profile for an enantiomeric process.

Figure 1.6 shows the free-energy profiles for a stereoselective synthesis leading to diastereoisomers. An enantioselective synthesis will lead to the formation of enantiomeric products. This process is even more attractive, because now the chirality can be introduced by an external source, e.g. solvent, or ligand. A further advantage is that sometimes catalytic quantities of the external chiral source (a chiral catalyst) are sufficient to yield products in high enantiomeric excess (e.e.). The e.e. is usually expressed in percentage enantiomeric excess (% e.e.) given by 100% x (R-S)/(R+S). The free-energy profile of an enantioselective process is depicted in Figure 1.7. From the relationship between $\Delta\Delta G$ and % e.e., shown in Figure 1.8, it follows that energy differences of only >2 kcal/mol are sufficient for high inductions[44].

But chemists are not easily satisfied. Detailed mechanistic information on enantioselective syntheses is rare and successful development of an enantioselective process is still chiefly a matter of trial and error. Although the practical virtues of the above mentioned methods could hardly be overstated, recently even more appealing methods to obtain optically pure enantiomers have begun to attract

attention, namely *stereoselective autocatalysis*, and what is called *chiral amplification*. Stereoselective autocatalysis is defined as a process in which a chiral reaction product forms the catalyst for its own formation from achiral reactants. The most promising method in asymmetric synthesis may be asymmetric amplification, which is defined as an asymmetric reaction giving in high e.e.'s product with chiral auxiliary of low e.e's. Kagan[45] described the first examples, asymmetric oxidation of methyl *p*-tolyl sulfide and epoxidation of geraniol in the presence of various chiral titanium complexes. The reaction depicted in Scheme 1.3 has recently been developed by Oguni[46] . Ethylation of benzaldehyde with diethylzinc yielded (R)-1-phenylpropanol with an e.e. of 90% in the presence of a chiral β-aminoalcohol of 20% e.e. as catalyst.

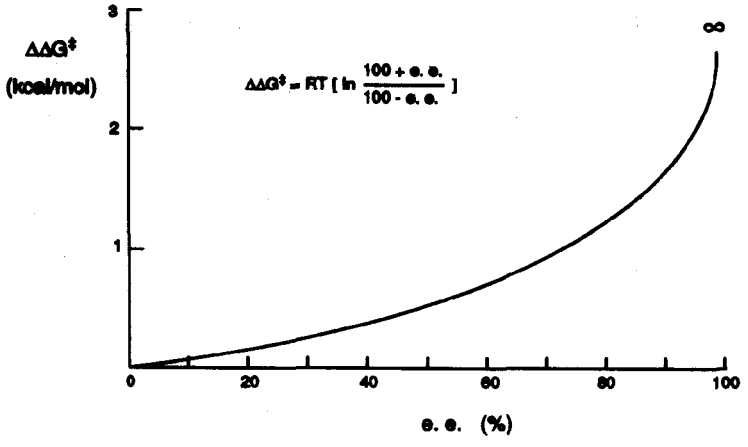

Figure 1. 8 The relationship between % e. e. and Gibbs free energy at 20°C.

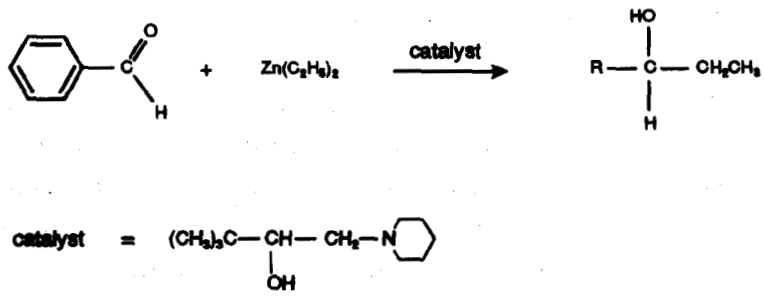

Scheme 1.3.

The discussion of the role of autocatalysis as initiator of chirality in Nature started in 1953[47] , however, pertinent experiments have been described only sporadically[48] . Recently Alberts and Wijnberg presented the first convincing evidence for an enantioselective autocatalytic reaction[49] . They prepared the titanium-alkoxide of (+)-1-phenylpropanol-1-1d and used it as catalyst in the reaction between diethylzinc and benzaldehyde (Scheme 1.4). This led to 1-phenylpropanol-1 in an enantiomeric excess of 32%.

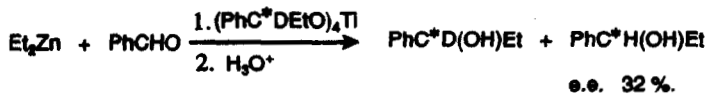

Scheme 1.4

1.5 INCENTIVE FOR THIS THESIS AND AIM

As has been outlined in the previous sections the synthesis of enantiomerically pure compounds is both a challenging and an important area of research. The different behavior of enantiomers in living systems is one of the major reasons.

As a result of rapid developments in biotechnology, enzymes will become ever more important tools for obtaining many optically pure compounds. Notwithstanding this increasing use of enzymes, the number of examples of successful enantiomeric processes, in which the chiral molecules are formed by organic catalysts, is rising. Unfortunately, some organic- and biochemists misjudge these developments as being competitive to their *own* methods. In fact both bio- and organic chemists, working in the field of stereoselective synthesis, examine the same phenomena, chiral recognition and discrimination, merely from different perspectives. In Scheme 1.5 just one (of the many) examples is depicted to demonstrate how closely the enzymatic and organic methods are associated.

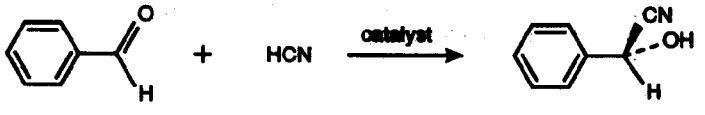

catalyst = enzyme D-hydroxynitrilase : e.e 94%.
= cyclo-(S)-phenylalanyl-(S)-histidine : e.e 97%

Scheme 1. 5. Conversion of benzaldehyde to mandelonitrile. Optically active mandelonitrile can be obtained in high e.e using an organic chiral catalyst or an enzyme.

In the Wijnberg group many successful applications of cinchona alkaloids as chiral catalysts have been found. In scheme 1.7 characteristic examples are given[50]. To exemplify the broad scope of cinchona and ephedra alkaloids as chiral catalysts scheme 1.6 shows some examples from other groups[51].

These molecules provide a particularly cogent illustration of how closely biochemistry and organic chemistry are allied. In the early decades of this century organic chemists were called upon to establish the structures of these complex molecules found in the study of plants. This structural work provided one of the underpinnings of organic chemistry, particularly with regard to the development of spectroscopic methods and synthetic methodology. There is an appropriate scientific symmetry that the applications of these alkaloids begins now at the close of the twentieth century to complement independent developments from biochemistry, specifically the possibilities for applications of enzymes.

Thus cinchona and ephedra alkaloids have been applied successfully in carbon-carbon, carbon-sulfur, carbon-selenium, and carbon-phosphorous bond formation, as chiral phase-transfer catalysts, and as chiral ligands. Their role in medicine is firmly established. Furthermore, examples where cinchona alkaloids are used as chiral resolving agents are countless. In all these examples of the use of the alkaloids, their ability for intimate interaction, discrimination and recognition are crucial to their success. Studies of complexes (acid-base pairs) between these alkaloids and the molecules they interact with by crystallographic and NMR methods give a picture of ground state interactions. Mechanistic studies of catalytic asymmetric reactions should provide insight into the (subtle) steric and electronic interactions in the transition state. The chiral catalyst plays a key role, for it both activates and orients the substrate molecules. Therefore detailed knowledge of the conformational behavior of the catalysts is of utmost importance in explaining their mechanism of action in all these fundamental and interesting phenomena.

In this thesis we will present the results of a conformational study on cinchona and ephedra alkaloids. Because of the availability of a great number of experimental data in our laboratory on cinchona alkaloids, most attention has been focussed on these alkaloids. The salient features of ground state conformations of cinchona alkaloids, their N-protonated forms, as well as an osmium tetraoxide-alkaloid complex will be described in detail, using a combined molecular modelling, NMR and X-ray analysis. The influence of different substituents at the

benzylic carbon C_9 and the influence of solvent on the conformation will also be described, and thus a picture of the conformational behavior of cinchona alkaloids and the relevance to stereoselective reactions will be presented. Finally, comparison of results obtained with cinchona and ephedra alkaloids as chiral catalysts in a Michael addition between aromatic thiols and conjugated cyclohexenone will be used as basis for discussion of the design of chiral catalysts.

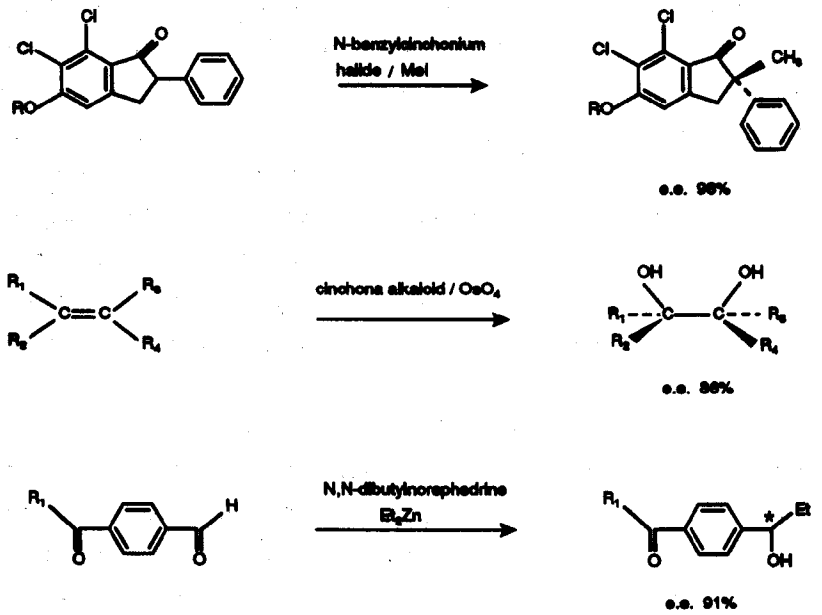

scheme 1.6 Examples of cinchona and ephedra alkaloid catalyzed asymmetric reaction developed in other laboraties.

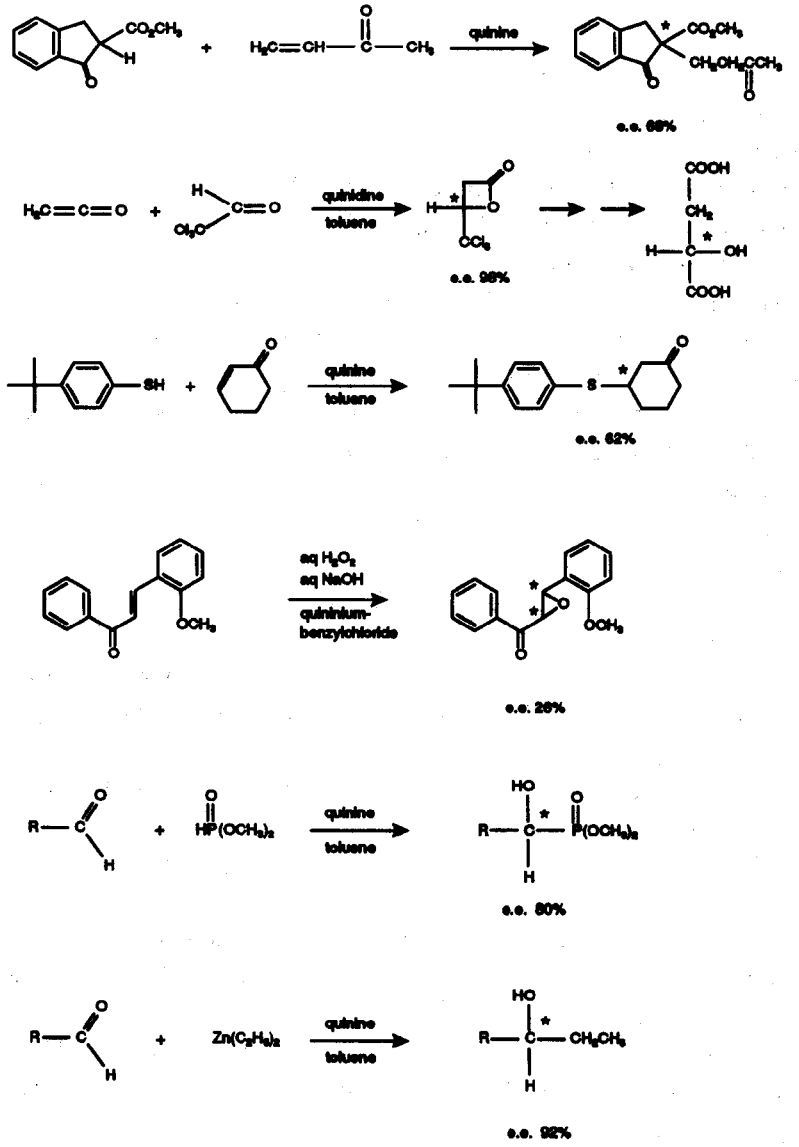

scheme 1.7 Examples of cinchona alkaloid catalyzed asymmetric reaction developed in the Wijnberg group.

1.6 REFERENCES

1. Inoue, *J. Org. Chem.* **1990**, *55*, 181.
2. see for example:
   Wijnberg, H. *Top. Stereochem.* **1986**, *16*, 87.
   Wijnberg, H.; Helder, R. *Tetrahedron Lett.* **1975**, 4057.
   Hummelen, J. C.; Wijnberg, H. *J. Org. Chem.* **1979**, *44* , 2238.
   Marsman, B.; Wijnberg, H. *J. Org. Chem.* **1979**, *44*, 2312.
   Pluim, H.; Wijnberg, H. *J. Org. Chem.* **1980**, *45*, 2498.
   Hiemstra, H.; Wijnberg, H. *J. Am. Chem. Soc.* **1981**, *103*, 417.
   Staring, A. G. J.; Wijnberg, H. *J. Am. Chem. Soc.* **1982**, *104*, 166.
   Staring, A. G. J.;Wijnberg, H. *J. Chem. Soc. Chem. Commun.* **1984**, 1181.
   Wijnberg, H.; Smaardijk, A. A. *Tetrahedron Lett.* **1983**, *24*, 5899.
3. Hughes, D. L.; Dolling, U. H.; Ryan, K. M.; Schoenewaldt, E. F.; Grabowski, E. J. J. *J. Org. Chem.* **1987**, *52*, 4745.
   Brzostowska, M.; Gawronski, J. *Monath. fur Chem.* **1984**, *115*, 1373.
   Soai, K.; Watanabe, M.; Koyano, M. *J. Chem. Soc. Chem. Commun.* **1989**, 534.
   Trost, B. M.; Shuey, C. D.; Dininno, Jr. F. *J. Am. Chem. Soc.* **1979**, *101*, 1284.
   Dolling, U. H.; Davis, P.; Grabowski, E. J. J. *J. Am. Chem. Soc.* **1984**, *106*, 446.
   Jacobsen, E. J.; Marko, I.; Mungall, W. S.; Schroder, G; Sharpless, K. B *J. Am. Chem. Soc.* **1988**, *110*, 1968.
   Wai, J. S. M.; Marko, I.; Svendsen, J. S.; Finn, M. G.; Jacobsen, E. N.; Sharpless, K. B. *J. Am. Chem. Soc.* **1989**, *111*, 1123.
   the following review articles describe many additional examples:
   Kagan, H. B.; Fiaud, J. C. in *Topics in Stereochemistry*, Vol. 10, E. L. Eliel and N. L. Allinger, Eds, Wiley, New York, 1978, p. 175.
   Pearce, R. in *Catalysis*, Vol. 2, The Chemical Society, London, 1978.
   Morrison, J. D.; Mosher, H. S. *Asymmetric Organic Reactions*, Prentice Hall, Englewood Cliffs, N. J., 1971.
4. Solomon, W. in *Chemistry of the Alkaloids*, Ed. S. W. Pelletier, van Nostrand Reinhold Company, New York, 1970.
   Dalton, D. R. *The Alkaloids*, Dekker Inc., New York, 1979.
   Brossi, A.; Pecherer, B. *Chemistry of the Alkaloids*, Ed. S. W. Pelletier, van Nostrand Reinhold Company, New York, 1970.

Footnote Cont. Next Page

Footnote 5 Cont.

5. Pelletier S. W. in *Chemistry of the Alkaloids*, Ed. S. W. Pelletier, Van Nostrand Reinhold Company, New York, 1970, p. 4.
6. Pelletier, S. W. in *Chemistry of the Alkaloids*, Ed. S. W. Pelletier, van Nostrand Reinhold Company, New York, 1970, p. 1.
7. Dalton, D. R. *The Alkaloids*, Dekker Inc., New York, 1979, p. 508.
   Solomon, W. In *Chemistry of the Alkaloids*, Ed. S. W. Pelletier, Van Nostrand Reinhold Company, New York, 1970, p. 301.
8. Pelletier, P. J.; Caventou, J. B. *Ann. Chim. Phys.* 1820, *15*, 289.
9. Rabe, P. *Chem. Ber.* 1907, *40*, 3655.
10. Prelog, V.; Hafliger, O. *Helv. Chim. Acta* 1950, *33*, 2021.
11. Carter, O. L.; McPhail, A. T.; Sim, G. A. *J. Chem. Soc. A*, 1967, 365.
12. Goodman, L. S.; Gilman, A. G. *The Pharmacological Basis of Therapeutics*, 7th ed.; McMillan Publishing Co.: New York, 1985, p.756, 1041.
13. Pasteur, M. L. *Acad. Sci.* 1853, *37*,110.
14. Wijnberg, H. *Topics in Stereochem.* 1986, *16*, 87.
15. Konigs, W. *Ann. Chem.*, 1906, *347*, 143.
16. For example, quinine derivatives employed as chiral catalysts in the catalytic asymmetric osmylation of olefins always gave a lower e.e (about 10%) than the corresponding quinidine derivatives. Similarly, cinchonine gave higher e.e. than cinchonidine when employed in the Michael addition of thiols to enones (Hiemstra, H.; Wijnberg, H. *J. Am. Chem. Soc.* 1981, *103*, 417).
17. Kolthoff, J. *Biochem. Z.*, 1925, *162*, 289.
18. Brossi, A.; Pecherer, B. In *Chemistry of the Alkaloids*, Ed. S. W. Pelletier, Van Nostrand Reinhold Company, New York, 1970, p. 24.
19. Nagai, W. N. *Pharm. Ztg.*, 1887, *32*, 700.
20. Chen, K. K.; Schmidt, C. F. *Proc. Soc. Exptl. Biol. Med.*, 1924, *21*, 351.
    Chen, K. K.; Schmidt, C. F. *J. Pharmacol.*, 1924, *24*, 339.
    Chen, K. K.; Schmidt, C. F. *J. Am. Med. Assoc.*, 1926, *87*, 836.
    Chen, K. K.; Schmidt, C. F. *Medicine*, 1930, *9*, 1.
21. see for example:
    Freudenberg *J. Am. Chem. Soc.*, 1932, *54*, 234.
    Witkop, Foltz, *J. Am. Chem. Soc.*, 1957, *79*, 197.
    Drudi-Baracco, *Compt. Rend. Soc. Biol.*, 1964, *158*, 259.
    Fodor, *Recent Develop. Chem. Nat. Carbon Compounds*, 1965, *1*, 15-160.

22. Nagai, W. N.; Kanao, S. *Ann. Chem.*, 1929, *470*, 157.
23. Brussee, J.; Roos, E. C.; van der Gen, A. *Tetrahedron Lett.* 1988, *29*, 4485.
24. Gardner, M. The Ambidextrous Universe, New York, Penquin Books, 1982.
    Mason, S. Biomolecular Handedness from Pasteur to Parity Non-Conservation, *Nouv. J. Chim.* 1986, *10*, 739.
    Mason, S. The Origin of Chirality in Nature, *Trends Pharmacol. Sci.*, 1986, *7*, 20.
    Pagels, H. R. The Cosmic Code, New York, Penquin Books, 1986.
25. Biot, J. B. *Bull. Soc. Chim. Fr.*, 1815, 190.
26. Pasteur, M. L. *Ann. Chim. et Phys.*, 1848, *24*, 442.
    Pasteur, M. L. *Ann. Chim. et Phys.*, 1850, *28*, 56.
27. Van 't Hoff, J. H. *Voorstel tot uitbreiding der tegenwoordig in de scheikunde gebruikte structuur formules in de ruimte; benevens een daarmee samenhangende opmerking omtrent het verband tussen optisch aktief vermogen en chemische constitutie van organische verbindingen*, Utrecht, 1874.
    Van 't Hoff, J. H. *Bull. Soc. Chim. Fr.*, 1875, *23*, 295.
    Van 't Hoff, J. H. *La Chimie dans l'Espace*, Rotterdam, 1875.
28. LeBel, J. A. *Bull. Soc. Chim. Fr.*, 1874, *22*, 337.
29. For definitions of stereochemical concepts used in this thesis see e.g.:
    Mislow, K. *Introduction to Stereochemistry*, Benjamin, Menlo Park, Cal. 1965.
    Testa, B. *Principles of Organic Stereochemistry*, Studies in Organic Chemistry, Vol.6, Marcel Dekker Inc., New York, N. Y. 1979.
30. Bondy, S. C.; Harrigton, M. E. *Science*, 1979, *203*, 1243.
    Bently, R. *Molecular Asymmetry in Biology*, Vol. 1,2, Academic Press, New York, N. Y. 1969.
    Bently, R. In *Applications of biochemical systems in Organic Chemistry*, Part 1, Chapter 5, Jones, J. B., Ed., Wiley and Sons, New York, 1976.
31. Merck Index, Tenth Edition, Merck & Co. Inc., Rahway 1983, p. 1324.
    Blaschke, G.; Kraft, H. P.; Fickentscher, K.; Kohler, F. *Arzneim. Forsch. Drug Res.*, 1979, *29*, 1640.
32. Eliel, E. L.; Allinger, N. L. *Topics in Stereochemistry*, Ed. Wiley and Sons, New York, 1967-1984, Vol. 1-15.
    Kocovsky, P.; Furecek, F.; Hajicek J. *Synthesis of Natural Products:*

Footnote Cont. Next Page

Footnote 32 Cont.

Problems of Stereoselectivity, Eds., CRC Press, Boca Raton, Florida, 1986, Vol 1,2.

Mislow, K.; Siegel, J. *J. Am. Chem. Soc.* 1984, *106*, 3319.

33. Enders D.; Hoffmann, R. W. *Chemie in unserer Zeit*, 1985, *6*, 177.

Morrison, J. D. *Asymmetric synthesis*, Ed., Academic Press, New York, N. Y., 1983-1984, Vol. 1-5.

Brown, J. M.; Davies, S. G. *Nature* 1989, *342*, 631.

Evans, D. A.; Chapman, K. T.; Bisaha, J. *J. Am. Chem. Soc.* 1988, *110*, 1238.

Gao, Y. *J. Am. Chem. Soc.* 1987, *109*, 5765.

Fleet, G. W.; Ransden, N. G.; Witty, D. R. *Tetrahedron* 1989, *45*, 327.

34. Pasteur, M. L. *Ann. Chim. et Phys.* 1848, *24*, 442.

35. Jacques, J.; Collet, A.; Wilen, S. H. *Enantiomers, Racemates and Resolution*, Wiley and Sons, New York, 1981.

Wilen, S. H. *Tables of Resolving Agents and Optical Resolution*, Eliel, E. L., Ed., University of Notre Dame Press, Notre Dame, Indiana, 1972.

Wilen, S. H. *Top, Stereochem.*, 1971, *6*, 107.

Newman, P. *Optical Resolution Procedures for Chemical Compounds*, Optical Resolution Information Center, Manhattan College, New York, N. Y., 1980-1984, Vol. 1-3.

Toda, F.; Tanoka, K. *Chem. Lett.* 1983, 661.

36. Salvador, P.; Rosini, C.; Pini, D.; Bertucci, C.; Altemua, P.; Uccello-Baretta, G.; Raffaelli, A. *Tetrahedron*, 1987, *43*, 4969.

37. Meyers, A. I.; Kamata, K. *J. Am. Chem. Soc.* 1976, *98*, 2290.

38. Feringa, B. L.; de Lange, B. *Tetrahedron* 1988, *44*, 7213.

39. Feringa, B. L. personal communication.

40. See: Martens, J. *Topics in Current Chemistry*, Springer Verlag, Berlin, 1984, Vol 125, p. 165-246 and references therein.

41. Hannessian, S. *Total Synthesis of Natural Products: The 'Chiron' Approach*, Pergamon Press Ltd., Oxford, 1983.

42. Morrison, J. D.; Mosher, H. S. *Asymmetric Organic Reactions*, Prentice-Hall, Englewood Cliffs, New York, N. Y., 1971.

43. Izumi, Y.; Tai, A. *Stereodifferentiating Reactions*, Academic Press, New York, 1977.

Izumi, Y. *Angew. Chem., Int. Ed. Engl.*, 1971, *10*, 871.

44. Prelog, V.; Wilhelm, M. *Helv. Chim. Acta*, 1954, *37*, 1634.
45. Puchot, C.; Samual, O.; Dunach, E.; Zhao, S.; Agami, C.; Kagan, H. B. *J. Am. Chem. Soc.* 1986, *108*, 2353.
46. Oguni, N.; Matsuda, Y.; Kaneko, T. *J. Am. Chem. Soc.* 1988, *110*, 7877.
47. Frank, F. C. *Biochim. Biophys. Acta*, 1953, *11*, 459.
48. For a thorough discussion of asymmetric autocatalysis see:
Menge, W. M. P. B. *Asymmetric Autocatalysis*, Ph. D. Thesis, Groningen, 1989.
49. Alberts. A.; Wijnberg, H. *J. Am. Chem. Soc.* 1989, *111*, 7265.
50. The examples given in scheme 1.7 are taken from reference 2.
51. The examples of scheme 1.6 are from:
Jacobsen, E. N.; Marko, I; Mungall, W. S.; Schroder, G.; Sharpless, K. B. *J. Am. Chem. Soc.* 1988, *110*, 1968.
Dolling, U-H.; Davis, P.; Grabowski, E. J. J. *J. Am. Chem. Soc.* 1984, *106*, 446.
Hughes, D. L.; Dolling, U-H.; Ryan, K. M.; Schoenewaldt, E. F.; Grabowski, E. J. J. *J. Org. Chem.* 1987, *52*, 4745.
Soai, K.; Watanabe, M.; Koyano, M. *J. Chem. Soc. Chem. Commun.* 1989, 534.

2

MOLECULAR MECHANICS CALCULATIONS

2.1 INTRODUCTION

In this chapter we will describe a conformational analysis of cinchona (2.3) and ephedra alkaloids (2.4), as well as a rigid fitting study between both classes of alkaloids (2.5). All results have been obtained using molecular mechanics calculations. Before we turn to the discussion of the outcomes we will introduce molecular mechanics calculations briefly (2.2).

From a technical point of view the past forty years have been characterized by order of magnitude changes in computer speed, size and cost. These developments, together with great chemical scientific input, are the cause of the recent birth of a new approach (tool) to chemical research; computer aided molecular design

(CAMD), or molecular modelling. With high resolution workstations, often connected to mainframe computers, complex molecular images can be visualized, manipulated and analyzed in an interactive manner, and potential molecular conformations can be evaluated by energy optimizations. In a short time molecular modelling has developed into an exciting area of chemistry. In a growing number of cases it is now possible to compete with trial and error experimental techniques.

A major criticism on the computational approach is that the calculations apply to hypothetical motionless molecules in vacuum. Indeed, the actual reaction medium is very different. It involves effects such as entropy, the population of vibrational energy levels, solvation, and aggregation. These alone are enough to determine the course of the reaction or to direct recognition between molecules. To attack these problems new computational approaches are being developed[1] . Nowadays not only static properties of a single molecule can be studied, but also dynamical calculations on multiple interacting molecules are part of the scope of computational chemistry. The progress in molecular modelling research and applications is described in several recent texts and reviews[2] .

Energy calculations play a key role in many facets of molecular modelling. The preferred conformation(s) of a molecule in solution or in the solid state can be determined by NMR spectroscopy and X-ray crystallography, respectively. However with these techniques only the most preferred molecular conformation(s) are determined. To identify all conformations of potential biological or chemical interest, a computational method must be used. Traditionally, these calculations are divided into molecular mechanics (force field) and quantum-mechanical calculations. It has been amply demonstrated that force field calculations offer a promising method to obtain the 3D-structures and energies of molecules[3] . In the next section we will give a short introduction to force field calculations. In what follows a molecular mechanics study on cinchona and ephedra alkaloids will be presented. For the results of a quantum mechanical study on cinchona and ephedra alkaloids we refer the reader to chapter 5.

2.2 MOLECULAR MECHANICS CALCULATIONS

It is not our purpose to present a thorough theoretical introduction on molecular mechanics, we will attempt merely to give the reader some feeling for the subject.

Molecular mechanics was described by Burkent and Allinger[4] as a calculational method designed to give accurate a priori structures and energies for molecules. Also known by the term force field calculations, molecular mechanics is based on a simple classical-mechanical model of molecular structure in which atoms are treated as hard spheres. The interactions between the atoms in a molecule are described by a set of classical-mechanical potential functions[5] . It is important to note that these functions have little physical significance. They are parameterized to give a force field that produce satisfactory results, not necessarily for the right reasons. It is precisely this fact that makes the molecular mechanics method 'not very popular' with some purely theoretical chemists.

The energy (molecular mechanics energy, MME) of a molecule in the force field arises from deviations from the 'ideal' structure, and is approximated by a sum of energy contributions (equation 2.1).

$$MME = \Sigma E_{str} + \Sigma E_{bend} + \Sigma E_{oop} + \Sigma E_{tor} + \Sigma E_{vdw} + \Sigma E_{ele} , \qquad (2.1)$$

in which:

MME is the molecular mechanics energy.

E_{str} is the energy of a bond stretched or compressed from its natural bond length.

E_{bend} is the energy of bending bond angles from their natural values.

E_{oop} is the energy of bending an arrangement of atoms out of plane.

E_{tor} is the torsional energy due to twisting around bonds.

E_{vdw} is the energy due to van der Waals non-bonded interactions.

E_{ele} is the energy due to electrostatic interactions.

The sums extend over all bonds, bond angles, torsion angles, and non-bonded interactions between atoms not bound to each other or to a common atom (i.e., 1,4-interactions and higher). The energy, MME, thus defined, is only a measure of intramolecular strain relative to a hypothetical situation. By itself the MME has no physical meaning. As already mentioned, the force field functions contain adjustable parameters that are optimized to give the best fit of calculated and experimental data, such as geometries and heat of formations. The basic form of a molecular mechanics force field is given in equation 2.1. More sophisticated force fields may also include 1,3-nonbonded interactions, cross-interaction terms, and hydrogen-bonding interactions. Although the exact form of the potential functions depend on the force field, almost all molecular mechanics force fields use relatively simple expressions to describe the energy dependence on bond lengths, bond angles, and other terms given in equation 2.1. These can be solved very rapidly with computers and thus permit calculations on large molecules. However, in general, they are appropriate only for small changes from standard values. The results are less reliable for large deviations. The simplest force fields approximate the distortion energies to a quadratic function (equation 2.2).

$$k(x' - x)^2, \qquad (2.2)$$

in which:

k is a constant.

x is a standard value.

x' is the observed value.

Just one typical example of such a function is given by equation 2.3. It describes the energy of a bond stretched or compressed from its natural bond length.

$$E_{str} = \Sigma\ 1/2\ k_{di}(d_i - d^o_i)^2, \qquad (2.3)$$

in which the summation extends over all bonds, and where:

d_i is the length of the i_{th} bond.
$d^o{}_i$ is the equilibrium length for the i_{th} bond.
k_{di} is a bond stretching force constant.

Molecular mechanics energy minimizations involve successive iterative computations, where an initial conformation is submitted to full geometry optimization. All parameters defining the geometry of the system are modified by small increments until the overall MME reaches a local minimum on the potential surface. A minimization algorithm will stop at the first local minimum encountered, without realizing that much deeper, more stable minima may be accessible. To circumvent this problem systematic search algorithms have been developed[6]. These explore the complete conformational space of a molecule by systematic variation of all rotatable bonds. Distance geometry techniques[7] and other random sampling approaches correspondingly attempt to locate the global minimum through exploration of the allowed conformations. We refer the reader to the standard literature on molecular mechanics calculations[8] for further details about the appearance of the different force fields and optimization methods, and we will finish this introduction with a short historical overview.

The early history of molecular mechanics has been reviewed several times[9]. The two force fields most widely used in the 1970s were Allinger's MM1[10], and the EAS force field, developed by Engler, Andose and Schleyer[11]. These force fields gave reasonably good predictions regarding the structures and energy differences for a wide variety of hydrocarbon molecules[12]. For molecules containing hetero atoms the results were far less reliable[13]. These improved with the introduction of the MM2 force field[14] in 1977. None of these force fields could be successfully applied to molecules containing conjugated systems. In these cases it was necessary to include some type of quantum mechanical calculation on the π-system. MMP1[15], and later MMP2[16], have been developed to accommodate conjugated systems. The first step in these programs is a molecular orbital (MO) calculation on the conjugated system only. The resulting bond orders are used to modify the force field for the conjugated system. The program then takes as input

the normal force field for those parts of the molecule that are not involved in the conjugated system, and the modified force field is used for the delocalized bonds. These steps are usually repeated several times during an optimization of a geometry.

In the 1980s the main efforts have been optimization and extension of the force fields[17] and also the incorporation of these force fields into 'user-friendly' molecular modelling software[18]. Recently, the optimization efforts led to the introduction of the MM3 force field[19].

2.3 MOLECULAR MECHANICS ANALYSIS ON CINCHONA ALKALOIDS

2.3.1 Introduction

Before we discuss the outcome of our molecular mechanics analysis on cinchona alkaloids, we will briefly summarize some earlier obtained conformational facets of cinchona alkaloids.

The cinchona alkaloids are composed of two relatively rigid ring systems, an aromatic quinoline ring and an aliphatic bicyclic quinuclidine ring, both connected to a hydroxyl bearing carbon atom. In the past, several studies have been addressed to the conformations of quinine and quinidine, the general result being that the C_8-C_9 and C_4'-C_9 bonds (see Figure 2.1) are considered the most important factors that determine the overall conformation. Hiemstra and Wijnberg[20] have carried out a thorough study on the asymmetric Michael addition, catalyzed by cinchona alkaloids, between aromatic thiols and conjugated cyclic ketones. They proposed that in the most stable conformation of quinine the largest substituent at C_9 -the quinuclidine ring- is oriented on one side of the quinoline ring, whereas H_8 and the hydroxyl group are on the other side. In this study conformation A of quinine (Figure 2.2) is therefore regarded as the conformation of lowest energy.

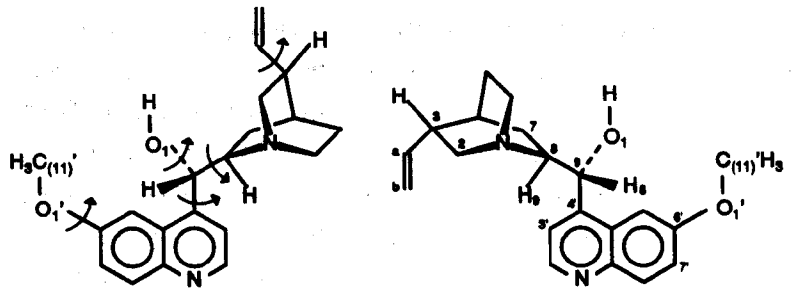

Figure 2.1 The structures of quinine (left) and quinidine (right). The five rotatable bonds are defined by the arrows (left) and the atom numbers which define the corresponding torsions are given (right).

However, conformation B was estimated to be about equally favorable. In previous studies by Prelog and Meurling conformation A was also considered to be the most favorable[21] . All six possible rotamers with respect to the C4'-C9 bond for the erythro alkaloids of the quinine series are depicted in Figure 2.2.

Hiemstra and Wijnberg have also considered the conformation with respect to the other carbon-carbon bond that connects both ring systems, the C_9-C_8 bond. The three Newman projections with respect to the C_9-C_8 bond for the erythro alkaloids of the quinine series are shown in Figure 2.3. Based on ^3J H_8H_9 coupling constants and inspection of space filling models, they argued that most probably both conformations G and I (see Figure 2.3) occur, with conformation I as the preferred one. In case of conformation I a ^3J H_8H_9 of 1-3 Hz is expected, based on a torsion angle $H_8C_9C_8H_9$ of about 75°, whereas for conformation G a ^3J H_8H_9 of about 9.5 Hz is expected. The ^{1}H NMR spectrum of quinine in $CDCl_3$ revealed a ^3J H_8H_9 of 4.0 Hz. Because inspection of space filling models showed that conformation H is unlikely, they concluded that conformation I is the minimum energy conformation.

The C_4'-C_9 and C_9-C_8 bonds are directly connected to each other. In the discussion given above the preferred conformations were considered separately per bond. In principle, at least six conformations with respect to the C_9-C_8 bond are possible. In each of the three rotamers depicted in Figure 2.3, the quinoline ring can either be oriented towards the bicyclic system or away from it. Therefore, more than only one conformation is in accordance with the $^3J\ H_8H_9$ data.

The importance of cinchona alkaloid catalyzed reactions (see chapter 1), coupled with our desire to understand the factors that determine the asymmetric induction, led us to extend this conformational study of the cinchona alkaloids. In the following sections the results obtained from a molecular mechanics analysis will be given[22].

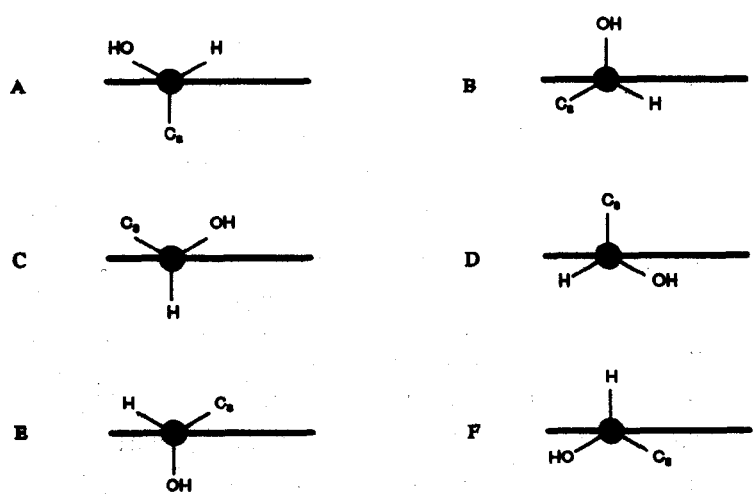

Figure 2.2 The six possible rotamers of quinine with respect to the C_4'- C_9 bond. The thick line represents the quinoline ring, perpendicular to the plane of the paper.

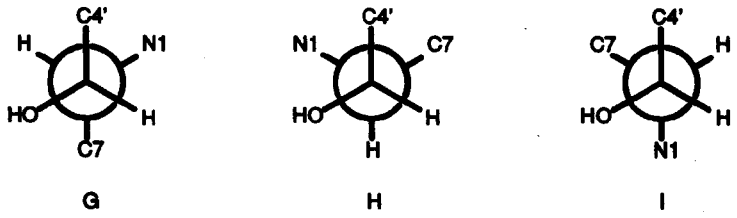

Figure 2. 3 Conformations of quinine with respect of the C_9-C_8 bond.

2.3.2 Results of Molecular Mechanics Calculations on Cinchona Alkaloids

As has been outlined above the gross conformation of the cinchona alkaloids is determined by the two torsions of the C_9-C_8 and the C_9-C_4' bonds. By using the molecular modelling program CHEMX[23] , we have investigated the conformational freedom with respect to these two bonds. Firstly, starting geometries were made for all cinchona alkaloids and derivatives that have been considered in this study. These starting geometries were constructed with the 3D-structure building facility of CHEMX, and optimized with the MMP2[24] force field. The geometries thus obtained were used as starting points for the generation of 36x36 (= 1296) different conformations by stepwise rotation of 10 degrees around both C_9-C_4' and C_9-C_8 bonds. The molecular mechanics energies (MME) were calculated for each conformation. Two examples of contour plots in which these MME's are plotted as a function of the two dihedral angles C_3'C_4'C_9C_8 and C_4'$C_9C_8C_7$ on the x- and y-axis are given in Figures 2.4 and 2.5 for quinine and quinidine, respectively. The minimum energy regions are easily recognized from these plots. We have chosen three conformations at random from each minimum

energy region, and these were optimized using the MMP2 and MMX[25] force fields.

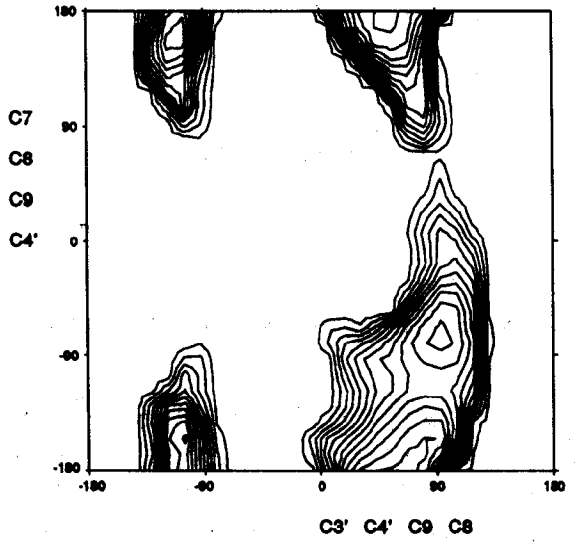

Figure 2.4 Contour plot of the MME as a function of the torsion angles C3'C4'C9C8 and C4'C9C8C7 of quinine. The energy spacing between the contours is 2 kcal/mol.

As was expected, the conformations chosen from the same minimum energy region ended up being exactly identical after optimization. In this way three different minimum energy conformations with respect to the $C_3'C_4'C_9C_8$ and $C_4'C_9C_8C_7$ dihedral angles were obtained for quinine and four minimum energy conformations for quinidine.

We have used these three optimized geometries of quinine and four of quinidine to investigate the orientations of the vinyl, hydroxy and methoxy substituents. For each substituent 72 orientations were generated by stepwise rotation of 5 degrees

around the bond that holds the group in question (see Figure 2.1). The MME was calculated for each conformation thus generated.

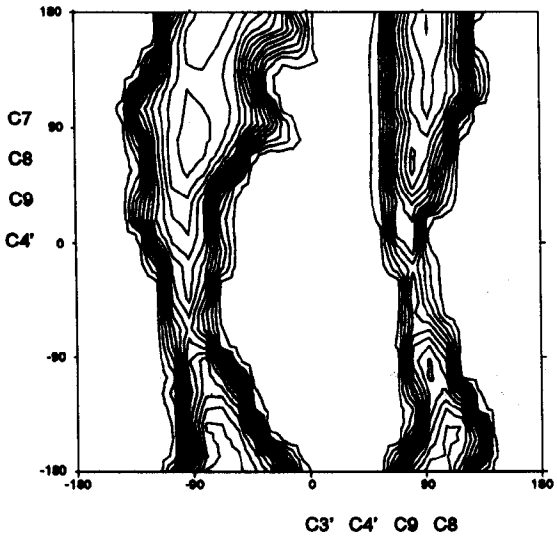

Figure 2.5 Contour plot of the MME as a function of the torsion angles C3'C4'C9C8 and C4'C9C8C7 of quinidine. The energy spacing between the contours is 2 kcal/mol.

Figure 2.6 shows the resulting energy plot, in which the MME is plotted against the torsion angle that determines the orientation of the methoxy group for one of the optimized geometries of quinine. From this plot it follows that the molecular mechanics approach predicts two preferred orientations for the methoxy group, both perpendicular to the quinoline ring. For the cases of the other two conformations of quinine we obtained almost identical energy plots with regard to the orientation of the methoxy group.

Correspondingly, Figures 2.7 and 2.8 show the energy plots obtained for the hydroxy and vinyl group of quinine, respectively. For quinidine similar energy plots were obtained for the orientations of the three substituents.

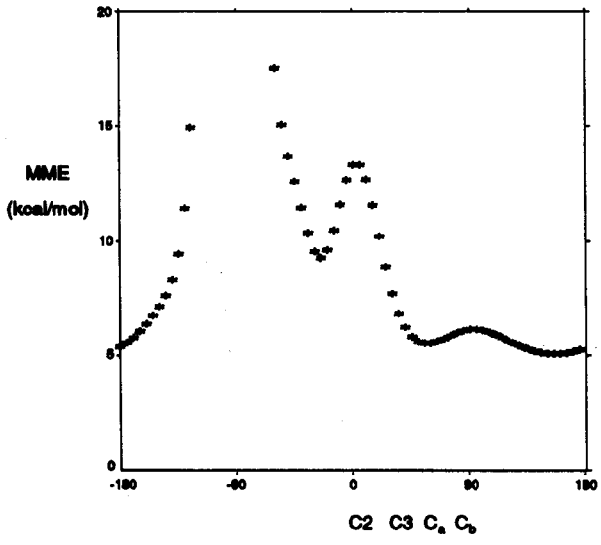

Figure 2.8 Energy plot. The torsion angle $C2C3C_aC_b$ is plotted as a function of the MME for one of the three calculated minimum energy conformations of quinine. C_a and C_b are the CH and CH_2 vinyl carbon atoms, respectively.

Some results of the calculations on quinine and quinidine are compiled in Table 2.1. The end result is that for quinine three minimum energy conformations have been found, two *closed* conformations, and one *open* conformation. These are depicted in Figure 2.9. The terms *open* and *closed* refer to the ability of the alkaloid to act as a catalyst and will be explained in chapters 4 and 5. In both closed conformations 1 and 2 the quinuclidine nitrogen lone pair points towards the quinoline ring, whereas in the open conformation 3 the quinuclidine nitrogen lone pair points away from the quinoline ring. The only difference between both closed conformations is the orientation of the quinoline ring with respect to the bicyclic system. In closed conformation 1 the quinoline ring is turned away from the quinuclidine ring, whereas in closed conformation 2 the quinoline ring is oriented towards the bicyclic ring.

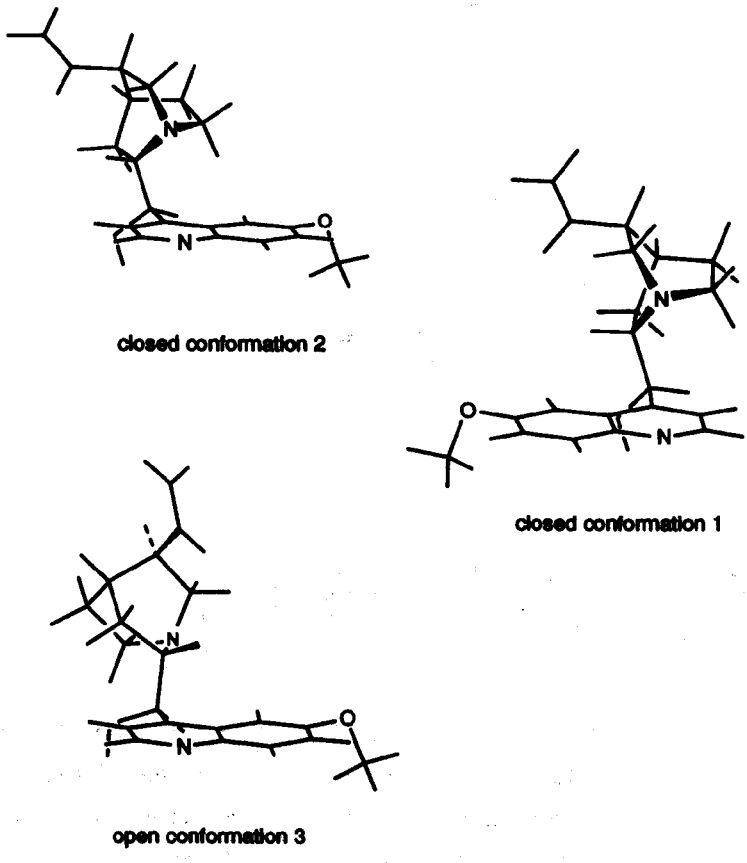

Figure 2.9 The three minimum energy conformations of quinine.

In the case of quinidine four different minimum energy conformations have been found, two closed conformations and two open conformations. These are depicted in Figure 2.10.

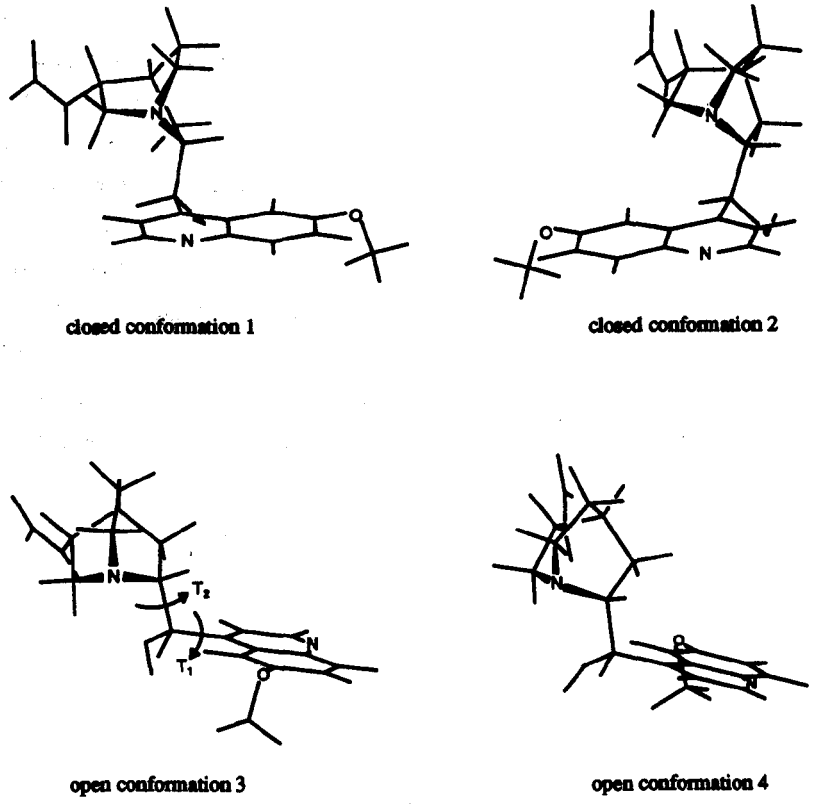

Figure 2.10 The four minimum energy conformations of quinidine.

Examination of the energy differences predicted by the MMP2 and MMX force field calculations between the different conformers (see Table 2.1) reveals that conformations 1, 2, and 3 of both quinine and quinidine are closely spaced in energy, whereas for quinidine open conformation 4 is less stable. We could not identify the equivalent of conformation 4 for quinine as a minimum energy conformation.

Since the crystal structure of quinidine is known[26], it is interesting to compare the calculated minimum energy conformations of quinidine with the geometry of the crystal structure. This comparison between a known X-ray structure and a calculated structure gives a useful indication of the accuracy of the force field for the type of compound. We have used a rigid-fitting algorithm of CHEMX for this purpose. As can be seen from Figure 2.11, one of the calculated conformations of quinidine (open conformation 3) fits almost perfectly on the geometry of the crystal structure. The only significant difference is the orientation of the methoxy group. In the crystal structure the methoxy group is oriented in the same plane as the quinoline ring, whereas in the calculated structure it is oriented perpendicularly to the quinoline ring (and thus lowering the MME as can be seen from Figure 2.6, see, however, Kollman[27] and results of our MO calculations presented in chapter 5).

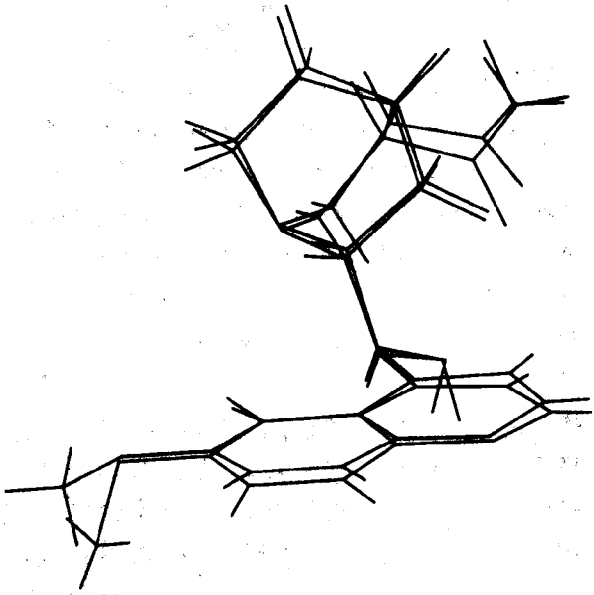

Figure 2.11 Rigid fitting plot of one of the calculated (MMP2) minimum energy conformations of quinidine (open conformation 3) and the crystal structure of quinidine.

The minimum energy conformations of some cinchona derivatives (dihydroquinine, dihydroquinidine, 9-methoxyquinidine, 9-methoxydihydroquinidine, 9-acetylquinidine, 9-acetyldihydroquinidine) were determined in the same way as described for quinine and quinidine. In the case of the quinine derivatives three minimum energy conformations have been found which are very similar to those of quinine (Figure 2.9). In the case of the quinidine derivatives four minimum energy conformations have been found for each derivative, all very similar to those of quinidine (Figure 2.10). The most important results of these calculations are compiled in Tables 2.2, 2.3, and 2.4.

This molecular mechanics analysis has revealed that:

- For quinidine and all quinidine derivatives studied here four different minimum energy conformations exist. These four conformations are very similar to those of quinidine. In all cases one of the conformations (open conformation 4) was substantially higher in energy than the other three.
- For quinine and quinine derivatives three minimum energy conformations exist, which are all closely spaced in energy.
- Results obtained with MMP2 and MMX are very similar.
- No significant effect on the global conformation of the alkaloids upon hydrogenation of the vinyl group could be observed. The molecular mechanics study on dihydroquinine, dihydroquinidine, and derivatives of these gave very similar results to those obtained for quinine and quinidine, respectively.
- The energy differences between the closed conformations 1 and 2 for all cinchona alkaloids that were considered in this study are minimal, whereas the open conformation 3 is predicted to be slightly less stable.
- The effect of the different benzylic substituents on the conformational behavior of the cinchona alkaloids is not very clear at this point. We refer the reader to chapters 3, 4, and 5, where the effects of the different benzylic substituents on the overall conformation are further investigated using NMR spectroscopy and quantum mechanical calculations.
- A rigid fitting study between the X-ray structure of quinidine and the calculated ones showed an excellent fit for one of the predicted conformations.

Table 2.1. Main results of the molecular mechanics analysis on quinine and quinidine.

	quinine			quinidine			
conformation	2	3	1	1	2	3	4
MMP2[a]	25.5	26.6	25.2	25.6	25.8	25.2	29.2
Δ energy[b]	0.3	1.4	0	0.4	0.6	0	4.0
dipole moment[c]	3.4	3.5	3.0	4.2	4.2	3.0	4.3
T_1[d]	73.9	97.2	-108.0	104.5	-71.7	-93.8	84.4
T_2[e]	59.5	159.6	48.0	-53.4	-56.5	-156.4	178.6
MMX[f]	24.5	25.8	24.6	27.9	28.5	29.1	29.0
Δ energy[b]	0	1.3	0.1	0	0.6	1.2	1.1
dipole moment[c]	2.1	1.6	2.3	4.2	4.5	2.6	4.3
T_1[d]	71.0	98.3	-111.4	104.2	-71.8	-93.0	85.0
T_2[e]	59.2	159.7	46.3	-53.2	-57.6	-155.4	-167.9
MMX[g]	42.6	43.7	42.5	43.7	44.0	44.7	45.7
Δ energy	0.1	1.2	0	0	0.3	1.0	2.0
dipole moment[c]	2.2	1.7	2.3	4.3	4.5	2.5	4.3
T_1[d]	72.2	98.8	-111.1	104.5	-71.7	-93.4	85.1
T_2[e]	59.6	159.5	45.8	-53.2	-57.5	-155.8	-167.8
MMX[h]	48.9	49.9	48.8	49.2	49.5	50.2	51.6
Δ energy[b]	0.1	1.1	0	0	0.3	1.0	2.4
dipole moment[c]	2.2	1.7	2.4	4.3	4.4	2.3	4.3
T_1[d]	72.5	99.0	-110.9	104.5	-71.4	-92.2	85.2
T_2[e]	59.8	159.8	46.0	-54.0	-57.3	-155.8	-167.9

a. Charge-charge interactions used in electrostatic potential, dielectric constant=1.5.

b. Energy differences relative to absolute minimum are given in kcal/mol

c. Dipole moment in Debye.

d. T_1 denotes the $C_3'C_4'C_9C_8$ torsional angle.

e. T_2 denotes the $C_4'C_9C_8N_1$ torsional angle.

f. dielectric constant=0.5

g. dielectric constant=1.5

h. dielectric constant=5.0

Table 2.2. Main results of the molecular mechanics analysis on dihydroquinine and dihydroquinidine.

	dihydroquinine			dihydroquinidine			
conformation	2	3	1	1	2	3	4
MMP2[a]	26.5	27.5	26.1	26.5	26.6	27.7	31.8
Δ energy[b]	0.4	1.4	0	0	0.1	1.2	5.3
dipole moment[c]	3.3	3.3	3.1	4.4	4.5	3.2	4.4
T_1[d]	72.9	99.5	-108.6	104.9	-71.5	-92.6	84.8
T_2[e]	59.4	160.4	47.7	-53.4	-56.4	-148.7	-172.4
MMX[f]	34.8	35.8	34.8	27.7	28.0	29.4	30.2
Δ energy[b]	0	1.0	0	0	0.3	1.7	2.5
dipole moment[c]	2.8	2.2	3.3	4.5	4.5	2.6	4.1
T_1[d]	70.9	98.1	-108.9	104.8	-70.3	-92.4	85.9
T_2[e]	59.1	159.4	48.9	-51.9	-55.5	-153.4	-177.3
MMX[g]	46.6	47.5	46.4	44.3	44.4	45.5	47.3
Δ energy[b]	0.2	1.1	0	0	0.1	1.2	3.0
dipole moment[c]	2.7	1.9	3.1	4.5	4.6	2.3	4.1
T_1[d]	71.7	98.3	-109.3	104.7	-70.8	-92.6	86.0
T_2[e]	59.6	160.2	48.7	-51.8	-55.5	-153.9	-177.2
MMX[h]	50.7	51.5	50.5	50.0	50.1	51.0	52.1
Δ energy[b]	0.2	1.0	0	0	0	1.0	2.1
dipole moment[c]	2.6	1.8	2.9	4.4	4.6	2.3	4.5
T_1[d]	71.6	98.3	-109.6	104.8	-70.9	-93.1	84.7
T_2[e]	59.8	160.6	48.8	-51.7	-55.7	-154.6	-169.6

a. Charge-charge interactions used in electrostatic potential, dielectric constant=1.5.

b. Energy differences relative to absolute minimum are given in kcal/mol

c. Dipole moment in Debye.

d. T_1 denotes the $C_3'C_4'C_9C_8$ torsional angle.

e. T_2 denotes the $C_4'C_9C_8N_1$ torsional angle.

f. dielectric constant=0.5

g. dielectric constant=1.5

h. dielectric constant=5.0

Table 2.3. Main results of the molecular mechanics analysis on methoxyquinidine and dihydromethoxyquinidine.

	methoxyquinidine				dihydromethoxyquinidine			
conformation	1	2	3	4	1	2	3	4
MMP2[a]	27.1	27.4	29.1	30.7	28.1	28.3	30.0	31.4
Δ energy[b]	0	0.3	2.0	3.6	0	0.2	1.9	3.3
dipole moment[c]	3.0	3.1	3.4	3.3	3.2	3.3	3.3	3.8
T_1[d]	104.5	-70.5	-92.6	85.1	104.6	-69.8	-92.8	85.1
T_2[e]	-53.0	-56.5	-156.4	-179.4	-51.5	-54.8	-155.6	-176.9
MMX[f]	-	-	-	-	24.7	24.8	26.5	29.2
energy[b]	-	-	-	-	0	0.1	1.8	4.5
dipole moment[c]	-	-	-	-	3.1	3.4	2.7	2.1
T_1[d]	-	-	-	-	106.5	-69.4	-90.7	87.7
T_2[e]	-	-	-	-	-50.5	-54.9	-152.7	-174.0
MMX[g]	44.7	44.7	46.1	48.8	45.2	44.9	46.7	49.3
Δ energy[b]	0	0	1.4	4.1	0.3	0	1.8	4.4
dipole moment[c]	3.0	3.2	2.6	1.8	3.0	3.3	2.6	2.0
T_1[d]	105.3	-69.9	-90.9	88.0	106.2	-68.9	-90.9	87.5
T_2[e]	-52.9	-56.5	-154.3	-171.6	-50.4	-54.4	-152.8	-176.8
MMX[h]	25.1	25.2	26.2	29.2	24.7	24.8	26.5	29.2
Δ energy[b]	0	0.1	1.1	4.1	0	0.1	1.8	4.5
dipole moment[c]	3.0	3.1	2.6	1.9	3.1	3.4	2.7	2.1
T_1[d]	105.7	-68.9	-90.7	88.2	106.5	-69.41	-90.7	87.7
T_2[e]	-52.9	-55.6	-154.0	-166.5	-50.5	-54.9	-152.7	-174.0

a. Charge-charge interactions used in electrostatic potential, dielectric constant=1.5.

b. Energy differences relative to absolute minimum are given in kcal/mol

c. Dipole moment in Debye.

d. T_1 denotes the $C_3'C_4'C_9C_8$ torsional angle.

e. T_2 denotes the $C_4'C_9C_8N_1$ torsional angle.

f. dielectric constant=0.5

g. dielectric constant=1.5

h. dielectric constant=5.0

Table 2.4. Main results of the molecular mechanics analysis on acetylquinidine and dihydroacetylquinidine.

	acetylquinidine				dihydroacetylquinidine			
conformation	1	2	3	4	1	2	3	4
MMP2[a]	26.7	27.1	27.1	29.2	27.5	27.8	28.0	29.9
Δ energy[b]	0	0.4	0.4	2.5	0	0.3	0.5	2.4
dipole moment[c]	3.2	2.7	6.0	2.5	3.0	2.6	6.0	2.6
T_1[d]	105.7	-65.2	-91.6	85.9	106.2	-64.6	-91.9	83.7
T_2[e]	-43.6	-42.7	-156.7	-177.4	-42.1	-41.1	-155.5	-172.8
MMX[f]	42.8	40.1	42.1	45.7	42.6	39.8	41.5	45.3
energy[b]	2.7	0	2.0	5.6	2.8	0	1.7	5.5
dipole moment[c]	4.7	5.1	4.7	5.9	3.9	5.3	5.0	6.0
T_1[d]	107.5	-63.3	-90.1	87.0	107.4	-60.7	-89.7	87.9
T_2[e]	-49.8	-50.6	-159.0	-176.1	-46.9	-49.8	-158.4	-176.7
MMX[g]	47.6	46.0	47.1	50.2	48.1	46.4	47.3	50.7
Δ energy[b]	1.6	0	1.1	4.2	1.7	0	0.9	4.3
dipole moment[c]	4.7	5.2	4.7	6.0	4.4	3.4	5.0	5.9
T_1[d]	107.5	-63.7	-89.8	87.5	107.7	-64.9	-90.3	87.7
T_2[e]	-49.8	-51.2	-158.8	-176.6	-47.4	-46.3	-158.5	-176.7
MMX[h]	49.3	48.0	48.9	51.6	50.0	48.6	49.4	51.9
Δ energy[b]	1.3	0	0.9	3.6	1.4	0	0.8	3.3
dipole moment[c]	4.7	5.3	4.8	6.0	4.6	5.4	5.0	6.3
T_1[d]	107.6	-63.6	-89.9	87.0	108.2	-63.2	-90.1	87.0
T_2[e]	-50.0	-51.5	-158.7	-176.3	-48.3	-50.4	-157.4	-175.3

a. Charge-charge interactions used in electrostatic potential, dielectric constant=1.5.

b. Energy differences relative to absolute minimum are given in kcal/mol.

c. Dipole moment in Debye.

d. T_1 denotes the $C_3'C_4'C_9C_8$ torsional angle.

e. T_2 denotes the $C_4'C_9C_8N_1$ torsional angle.

f. dielectric constant=0.5

g. dielectric constant=1.5

h. dielectric constant=5.0

2.4 MOLECULAR MECHANICS ANALYSIS ON EPHEDRA ALKALOIDS

Although the ephedra alkaloids are smaller molecules than the cinchona alkaloids, the problem of finding the minimum energy conformations is more difficult. There are three bonds (T_1, T_2, T_3) instead of two in the case of cinchona alkaloids, which determine the gross conformation of the ephedra alkaloids, and in addition a fourth bond (Ψ) determines the orientation of the hydroxy group. The torsion angles T_1, T_2, T_3, and Ψ are defined in Figure 2.12.

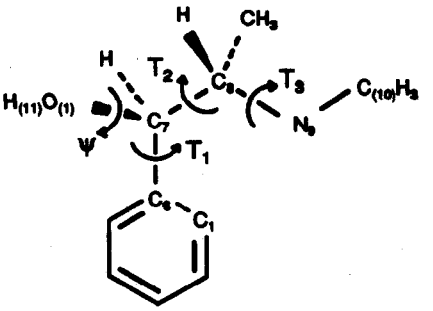

Figure 2.12 The structure and absolute configuration of (-)-ephedrine. T_1=$C_1C_6C_7C_8$, T_2=$C_8C_7C_8N_9$, T_3=$C_7C_8N_9C_{10}$, Ψ=$C_6C_7O_1H_{11}$.

We have considered only two ephedra alkaloids in this molecular mechanics study; (-)-ephedrine and (-)-N-methylephedrine. The latter was included in order to study the conformational effect of alkylation on the nitrogen.

EPHEDRINE. A starting geometry for ephedrine was constructed by a MMP2 optimization of the geometry obtained with the 3D-building routine of CHEMX. Four contour plots were calculated, each being obtained by stepwise variation of 10 degrees of two torsion angles. In the first three of these contour plots the MME

is plotted as a function of the two torsion angles T_1 and T_2, each time with a different value for T_3. Figure 2.13 shows the contour plot with T_1 and T_2 on the x- and y-axis, respectively, and with T_3=180°. In Figures 2.14 and 2.15 we have plotted the same torsion angles on both axis, but now with T_3=60° and T_3=-60°, respectively.

From these three contour plots it can be seen that there exists a distinct preference for a torsion angle T_1 of approximately 90 or -90° (which are identical for symmetry reasons). Thus the preferred conformation of ephedrine is one with the 'tail' approximately perpendicular to the phenyl ring.

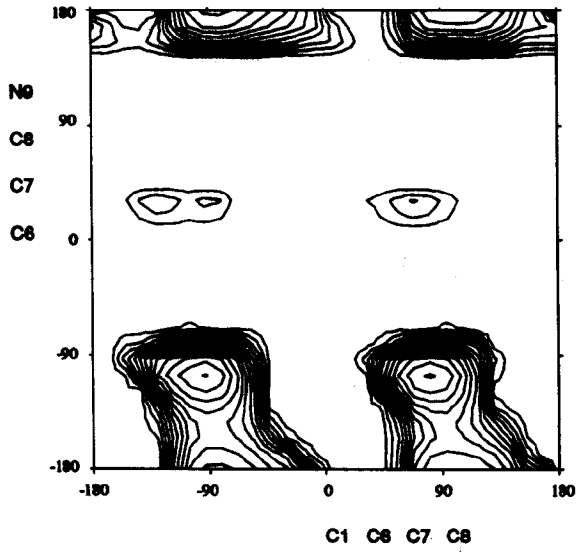

Figure 2.13 Contour plot of the MME as a function of the torsion angles C1C6C7C8 (T_1) and C6C7C8N9 (T_2) of ephedrine. The energy spacing between the contours is 2 kcal/mol

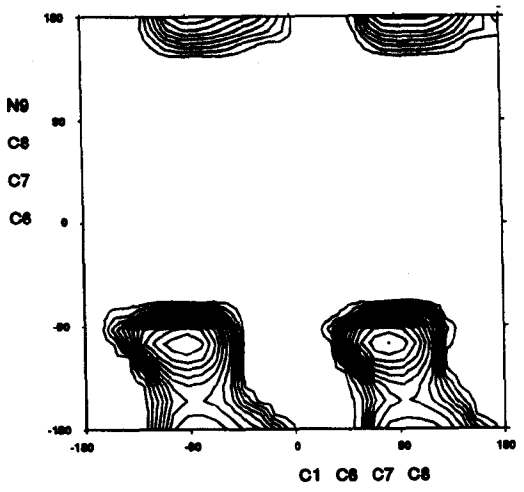

Figure 2.14 Contour plot of the MME as a function of the torsion angles C1C6C7C8 (T_1) and C6C7C8N9 (T_2) of ephedrine (T_3=60°).The energy spacing between the contours is 2 kcal/mol.

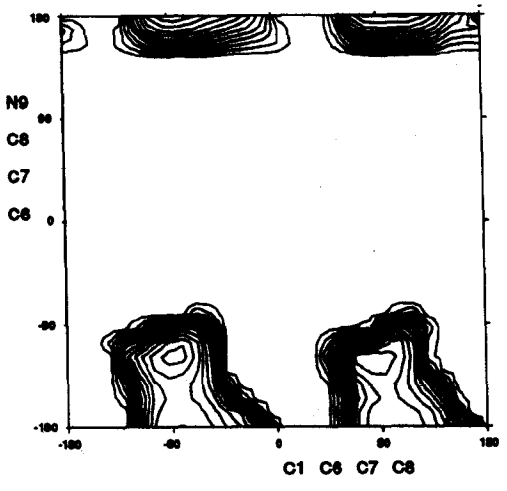

Figure 2.15 Contour plot of the MME as a function of the torsion angles C1C6C7C8 (T_1) and C6C7C8N9 (T_2) of ephedrine (T_3=-60°). The energy spacing between the contours is 2 kcal/mol.

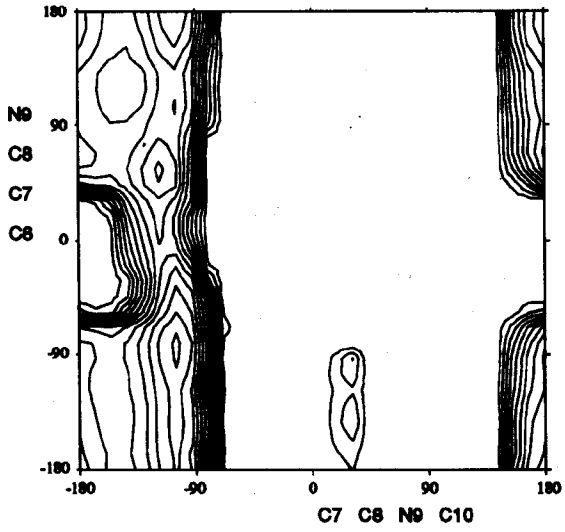

Figure 2.16 Contour plot of the MME as a function of the torsion angles C6C7C8N9 (T_2) and C7C8N9C10 (T_3) of ephedrine (T_1=90°). The energy spacing between the contours is 2 kcal/mol

This perpendicular orientation of the chain was chosen for a fourth contour plot, in which only T_2 and T_3 were varied. The resulting contour plot is given in Figure 2.16.

We have followed the same procedure as described in section 2.3.2 for the cinchona alkaloids for further optimization, the result being that finally nine minimum energy conformations were identified with respect to T_1, T_2, and T_3. Each of these nine conformations has three possible orientations for the hydroxy group (called a, b, c). Some results of the calculations are summarized in Table 2.5.

Table 2.5 Main results of the molecular mechanics analysis on (-)-ephedrine.

conformation		torsion angle T_1	T_2	T_3	Ψ	Δ energy[a]
ephedrine	-1a	-95.8	-64.1	172.1	62.1	0.4
	-1b	-97.0	-65.6	172.1	179.5	0
	-1c	-103.0	-61.0	167.3	-66.6	2.8
ephedrine	-2a	-91.1	-61.6	-77.4	60.1	0.9
	-2b	-92.1	-61.7	-77.7	178.4	0.5
	-2c	-95.7	-57.0	-83.1	-63.1	3.4
ephedrine	-3a	-91.9	-64.2	103.3	62.5	1.6
	-3b	-92.1	-64.9	101.7	177.9	0.9
	-3c	-94.5	-59.9	100.6	-57.9	3.5
ephedrine	-4a	-107.3	42.3	75.1	63.3	1.9
	-4b	-104.0	47.3	75.0	-178.8	1.2
	-4c	-120.0	42.4	68.3	-62.6	1.9
ephedrine	-5a	-102.4	52.8	-100.1	64.3	2.0
	-5b	-103.1	56.4	-98.3	-179.6	1.0
	-5c	-118.5	58.6	-85.1	-61.8	1.7
ephedrine	-6a	-104.8	49.7	165.2	66.0	3.9
	-6b	-105.2	58.0	170.8	179.6	2.2
	-6c	-117.5	57.0	172.1	-61.7	2.8
ephedrine	-7a	-76.3	176.2	176.4	62.4	2.1
	-7b	-81.0	-176.2	174.0	177.8	0.6
	-7c	-59.9	-174.5	174.1	-62.1	2.2
ephedrine	-8a	-82.8	151.3	52.5	61.8	4.5
	-8b	-84.5	166.5	53.0	178.1	2.1
	-8c	-79.2	165.3	53.2	-58.7	3.9
ephedrine	-9a	-79.2	178.2	-61.7	64.0	1.6
	-9b	-82.7	-173.3	-69.0	178.1	0.3
	-9c	-62.2	-171.3	-65.2	-60.7	1.8

[a] energy difference in kcal/mol.

$T_1=C_1C_6C_7C_8$, $T_2=C_6C_7C_8N_9$, $T_3=C_7C_8N_9C_{10}$, $\Psi=C_8C_7O_1H_{11}$.

The orientation around T_2 determines whether the overall conformation of ephedrine is gauche (the 'tail' folds back) or trans (extended conformation). Based on this definition the nine minimum energy conformations can be divided into three gauche conformations characterized by a T_2 of approximately -60°, three gauche conformations with T_2 of approximately 50°, and three trans conformations with a T_2 of approximately 180°.

As can be seen from Table 2.5 each of the nine conformers is further split up into three other ones, depending on the orientation of the hydroxy group. These three possible minima are characterized by a Ψ of respectively about 60°, -60°, and 180°. It can be concluded from Table 2.5 that the orientation of the hydroxy group is able to affect the total energy of the molecule significantly. In all cases the preferred orientation is one with a Ψ of about 180°. The energy differences relative to the nearest local minima vary from 0.4 to 1.9 kcal/mol. The preference for Ψ=180° is most distinct for the extended conformations (1.3-1.9 kcal/mol) and less for both groups of gauche conformers (0.4-0.7 kcal/mol).
The preferred conformation with respect to T_3 depends on T_2. In case of the 'gauche -60°' conformers the absolute minima are found at T_3 values of about 170°, while for the 'gauche 50°' conformers the absolute minima are found at T_3 of approximately -100°. The trans conformers attain their absolute minima at T_3 values of about -60°.

When we inspect the relative energy differences between the conformers it can be concluded that there seems to be a slight preference for the 'gauche -60' conformers.

Next we have compared the structures of all calculated minimum energy conformations with the known crystal structure of ephedrine[28] . The rigid-fitting algorithm of CHEMX has been used and as can be seen from Figure 2.17, one of the calculated minimum energy conformations (ephedrine-7) matches very well with the geometry of the crystal structure. In case of ephedrine-8 and ephedrine-9 only T_3 differs significantly from the crystal structure.

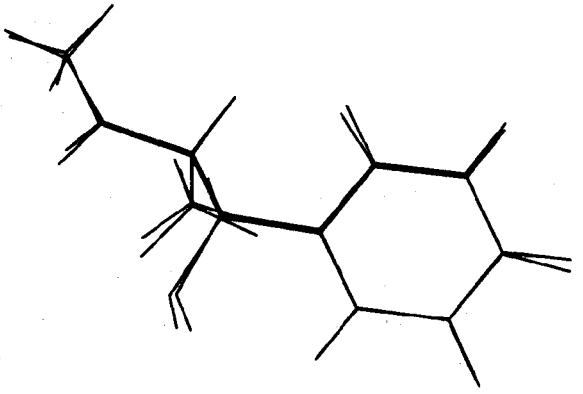

Figure 2.17 Rigid fitting between the crystal structure of ephedrine and ephedrine_7

Earlier work of Pullman[29], who carried out PCILO calculations[30] to study the conformational properties of phenylethylamines, suggests that in case of ephedrine a small preference (not quantified, but less than 1 kcal/mol) for the extended conformation exists. In his analysis a preferred torsion angle of Ψ=-60° for the hydroxy group was assumed. From the molecular mechanics calculations we carried out, another absolute minimum has been observed for the hydroxy group with a torsional angle Ψ of approximately 180°. When we compare the energy differences between Ψ=180° and -60° for the 'gauche -60°' conformers (the absolute minima in our study) and the extended ones we see that the gauche conformers are on average at least 1 kcal/mol more stabilized in case of Ψ=180°. This suggests that the results of the analysis of Pullman would be better in agreement with our results if he too had considered conformations with Ψ=180°. However, see chapter 5 in which additional MO calculations on ephedrine are presented.

N-METHYLEPHEDRINE. For the conformational analysis of N-methylephedrine a similar procedure as for ephedrine was followed. In this case we have found seven different minimum energy conformations. The most important results are summarized in Table 2.6.

Table 2.6 Main results of the molecular mechanics analysis on (-)-N-methylephedrine

		torsion angle				
conformation		T_1	T_2	T_3	Ψ	Δ energy[a]
N-methyleph.	-1a	-93.7	-60.0	-10.3	60.1	2.1
	-1b	-96.4	-56.9	-6.9	179.9	1.4
	-1c	-96.9	-58.8	-11.9	-57.4	2.3
N-methyleph.	-2a	-88.6	-61.5	-179.1	59.1	3.0
	-2b	-87.6	-65.5	-168.0	177.6	2.1
	-2c	-75.4	-69.0	152.3	-59.4	4.5
N-methyleph.	-4a	-97.1	48.0	-29.9	64.8	1.0
	-4b	-96.4	51.2	-31.2	-178.7	0.1
	-4c	-120.7	57.2	-28.3	-63.3	0.5
N-methyleph.	-5a	-114.5	56.4	163.4	65.0	1.2
	-5b	-114.1	58.5	161.6	-179.8	0.0
	-5c	-120.6	57.2	161.9	-63.3	0.5
N-methyleph.	-7a	-77.8	172.5	19.1	58.6	2.5
	-7b	-86.0	164.8	-30.4	178.2	1.6
	-7c	-86.6	162.8	-28.9	-62.1	3.6
N-methyleph.	-8a	-73.3	177.3	52.8	58.4	2.9
	-8c	-60.8	-173.0	59.4	-56.9	4.1
N-methyleph.	-9a	-78.6	174.8	-158.0	65.4	2.6
	-9b	-85.7	167.4	161.2	178.2	0.8
	-9c	-82.1	165.8	162.9	-59.6	2.9

[a] energy difference in kcal/mol.

T_1=$C_1C_6C_7C_8$, T_2=$C_6C_7C_8N_9$, T_3=$C_7C_8N_9N_{lone\ pair}$, Ψ=$C_8C_7O_1H_{11}$.

The results summarized in Table 2.6 show that the preferred orientation with respect to T_1 is the same as found for ephedrine; also a preference for a more or less perpendicular orientation of the chain with respect to the phenyl ring is observed. It should be noted, however, that the situation with respect to T_2 is different. Four instead of six gauche conformations are found and in addition three extended conformations are identified. The 'gauche 60°' conformers (N-methyleph.-4 and N-methyleph.-5) are the absolute minima. The contour plot of Figure 2.18 also indicates the preference for the gauche conformations. In this contour plot T_2 and T_3 are plotted on the x and the y-axis, respectively, with T_1=90°.

We can conclude from these results that the introduction of a methyl group on the nitrogen of ephedrine does change the conformational behavior significantly. The preference for the 'gauche -60' conformation, found for ephedrine, is turned into a preference for the 'gauche 60' conformers. The 'gauche 60' conformers resemble the closed conformation 2 of quinine. In the next section we will discuss the conformational similarities between ephedra and cinchona alkaloids further.

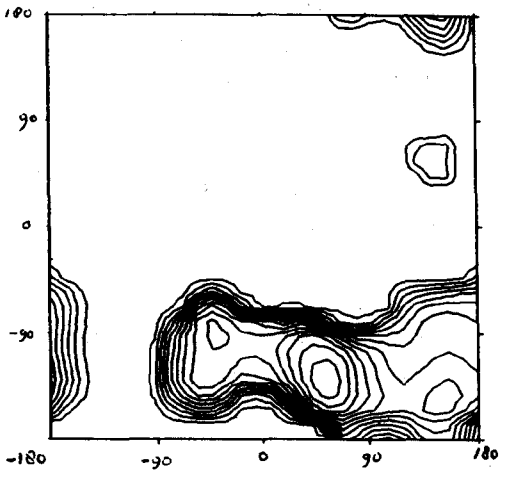

Figure 2.18 Contour plot of N-methylephedrine. On the x-axis T_2 ($C_6C_7C_8N_9$) is plotted and on the y-axis T_3 ($C_7C_8N_9C_{10}$).

2.5 RIGID FITTING BETWEEN EPHEDRA AND CINCHONA ALKALOIDS

The cinchona and ephedra alkaloids both catalyze the asymmetric Michael addition between aromatic thiols and α,β-unsaturated alkenones (see chapters 4 and 6). The stereoselectivity of this reaction, when using quinine or (-)-ephedrine as chiral catalyst, is the same and opposite to that obtained with quinidine. Both the cinchona and ephedra catalysts are β-hydroxy amines. This structural similarity may lead to mechanistic similarities, but does not explain the identical stereoselectivities of the cinchona and ephedra alkaloids. Therefore,we have compared all the calculated minimum energy conformations of quinine with those of ephedrine and N-methylephedrine. In the 'rigid fitting' plots of Figure 2.19 only two examples are given of the excellent similarities that exist between all minimum energy conformations of quinine and (N-methyl)ephedrine.

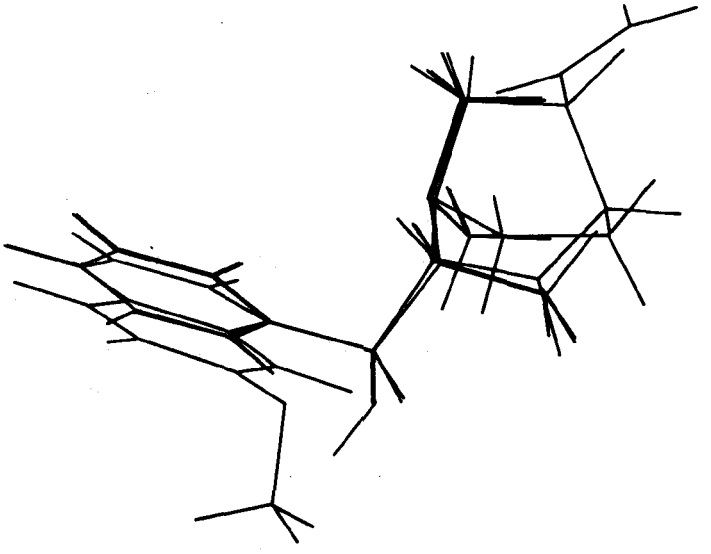

Figure 2.19A An example of a rigid fitting between quinine in the closed conformation 2 and N-methylephedrine.

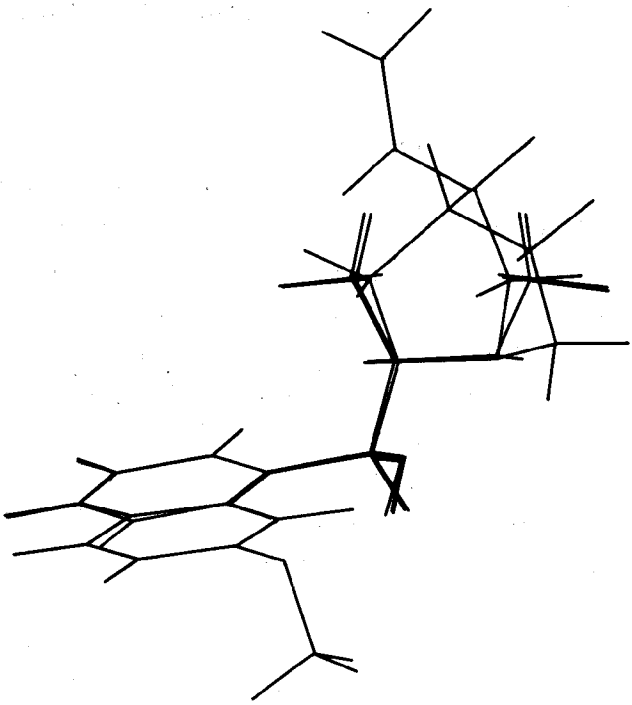

Figure 2.19B An example of a rigid fitting between quinine in the open conformation 3 and (-)-ephedrine.

The identical stereoselectivity in the Michael addition of quinine and ephedrine is much easier to understand now; all three minimum energy conformations of quinine have an equivalent minimum in case of ephedrine and N-methylephedrine. Thus both groups of alkaloids share the important β-hydroxyamino segment, as well as a very similar conformational behavior. Before we started this study we hoped to find, beside similarities, characteristic differences in conformational behavior as well. These differences might have given us helpful mechanistic information. Because of the excellent fits between all the calculated minimum energy conformations of both cinchona and ephedra alkaloids, we cannot exclude a priori any of the possible minimum energy conformations as being important in the catalytic process.

2.6 REFERENCES

1. see for example:
   Yun-Yu, S.; Lu, W.; van Gunsteren, W. F. *Molec. Simul.* 1988, *1*, 369.
   Bash, P. A.; Singh, U. C.; Brown, F. K.; Langridge, R.; Kollman, P. A. *Science* 1987, *235*, 574.
2. Cohen, N. C. *Drugs Future* 1985, *10*, 311.
   Cohen, N. C.; Blaney, J. M.; Humblet, C.; Gund, P.; Barry, D. C. *J. Med. Chem.* 1990, *33*, 883.
   Ripka, W. C. *Nature* 1986, *21*, 93.
   Burgen, A. S. V.; Roberts, G. C. K.; Tute, M. S. *Molecular Graphics and Drug Design* 1986, Topics in Molecular Pharmacology, Vol. 3, Elsevier, Amsterdam.
   Dean, P. M. *Molecular foundations of drug-receptor interaction* 1987, Cambridge University Press, Cambridge.
3. Allinger, N. L. *Adv. Org. Chem.*, 1976, *45*, 1.
   Merz, K. M.; Kollman, P. A. *J. Am. Chem. Soc.* 1989, *111*, 5649.
   Postma, J. P. M.; Berendsen, H. J. C.; Haak, J, R. *Faraday Symp.* 1982, *17*, 55.
   Colucci, W. J.; Gandour, R. D.; Mooberry, E. A. *J. Am. Chem. Soc.* 1986, *108*, 7141.
   Schneider, H. J.; Buchheit, U.; Becker, N.; Schmidt, G.; Siehl, U. *J. Am. Chem. Soc.* 1985, *107*, 7027.
   Kao, J.; Leister, D. *J. Am. Chem. Soc.* 1988, *110*, 7286.
   Wipff, G.; Weiner, P.; Kollman, P. A. *J. Am. Chem. Soc.* 1982, *104*, 3249.
   Dunitz, J. D.; Dobler, M.; Vedani, A. *J. Compt. Chem.* 1986, *7*, 701.
4. Burkent, U.; Allinger, N. L. in *Molecular Mechanics*, American Chemical Society, Washington, D. C. 1982, ACS Monograph 177.
5. see for example:
   Allinger, N. L. *Adv. Phys. Org. Chem.* 1976, *13*, 1.
   Altona, C. L.; Faber, D. H. *Top. Curr. Chem.* 1974, *45*, 1.
   Engler, E. M.; Andose, J. D.; Schleyer, P. v. R. *J. Am. Chem. Soc.* 1973, *95*, 8005.
   Bartell, L. S. *J. Am. Chem. Soc.* 1977, *99*, 3279.
   White, D. N. J. *Mol. Struct. Diffr. Methods* 1978, *6*, 38.
6. Dammkoehler, R. A.; Darasek, S. F.; Berkely Shands, E. F. *J. Comput.-Aided Mol. Des.* 1989, *3*, 3.

Footnote Cont. Next Page

Footnote 6 Cont.

Motoc, I.; Dammkoehler, R. A.; Marshall, G. R. *Mathematical and Computational Concepts in Chemistry* Trinajstic, N., Ed.; Horwood, Ltd., Chichester, 1986, p.222.

7. Crippen, G. M. *Distance Geometry and Conformational Calculations* Bawden, D., Ed.; Research Studies Press (Wiley), New York, 1981.
   Crippen, G. M.; Havel, T. F. *Distance Geometry and Molecular Conformation* Bawden, D., Ed.; Research Studies PRess (Wiley), New York, 1988.
8. Clark, T. *A Handbook of Computational Chemistry* J. Wiley and Sons, New York, 1985.
   Burkent, U.; Allinger, N. L. *Molecular Mechanics* American Chemical Society, ACS Monograph 177, Washington D. C., 1982.
   Press, W. H.; Flannery, B. P.; Teukolsky, S. A.; Vetterling, W. T. in *The Art of Scientific Computing*, Cambridge Univ. Press, 1986.
9. Burkert, U.; Allinger, N. L. 'Molecular Mechanics', ACS Monograph 177, American Chemical Society, Washington, D. C., 1982.
   William, J. E.; Stang, P.; Schleyer, P. V. R. *Ann. Rev. Phys. Chem.* 1968, *19*, 591.
   Allinger, N. L. *Adv. Phys. Org. Chem. 1976, 13*, 1.
10. Wertz, D. H.; Allinger, N. L. *Tetrahedron* 1974, *30*, 1576.
11. Engler, E. M.; Andose, J. D.; Schleyer, P. V. R. *J. Am. Chem. Soc.* 1973, *95*, 8005.
12. Altona, C.; Faber, D. H. *Top. Curr. Chem.* 1974, *45*, 1.
    Allinger, N. L. *Adv. Phys. Org. Chem.* 1976, *13*, 1.
    White, D. N. J.; Bovill, M. *J. Chem. Soc. Perkin Trans.* 2, 1977, 1610.
    Warshel, A. *Mod. Theor. Chem.* 1978, *7*, 133.
    Bartell, L. S. *J. Am. Chem. Soc.* 1977, *99*, 3279.
    Fitzwater, S.; Bartell, L. S. *J. Am. Chem. Soc.* 1976, *98*, 5107.
13. Allinger, N. L. *Adv. Phys. Org. Chem.*1976, *13*, 1.
14. Allinger, N. L. *J. Am. Chem. Soc.* 1977, *99*, 8127.
    QCPE, 1980, *12*, 395.
15. Allinger, N. L.; Sprague, J. T. *J. Am. Chem. Soc.* 1973, *95*, 3893.
    QCPE, 1976, *11*, 318.
16. Allinger, N. L. *J. Am. Chem. Soc.* 1977, *99*, 8127.
    Sprague, J. T.; Tai, J. C.; Yuh, Y.; Allinger, N. L. *J. Comput. Chem.* 1987, *8*, 581.

17. see for example:
Allinger, N. L.; Pathiaseril, A. *J. Comput. Chem.* 1987, *8*, 1225.
Bowen, J. P.; Pathiaseril, A.; Profeta, S.; Allinger, N. L. *J. Org. Chem.* 1987, *52*, 5162.
Bowen, J. P.; Allinger, N. L. *J. Org. Chem.* 1987, *52*, 2937.
Allinger, N. L.; Kok, R. A.; Imam, M. R. *J. Comput. Chem* 1988, *9*, 591.
Bowen, J. P.; Reddy, V. V.; Patterson, D. G.; Allinger, N. L. *J. Org. Chem.* 1988, *53*, 5471.
18. AMBER, Weiner, S. P.; Kollman, P. A.; Case, D. A.; Singh, U. C.; Ghio, C.; Alagona, G.; Profeta, S.; Weiner, P. *J. Am. Chem. Soc.* 1984, *106*, 765.
Weiner, P.; Kollman, P. *J. Comp. Chem.* 1981, *2*, 287.
CHEMX, developed and distributed by Chemical Design Ltd., Oxford, England.
GROMOS, van Gunsteren, W. F.; Berendsen, H. J. C. *Groningen Molecular Simulation (GROMOS) Library manual*, BIOMOS, Nijenborgh 16, Groningen, The Netherlands.
19. Allinger, N. L.; Lii, J. H. *J. Comput. Chem.* 1987, *8*, 1146.
Lii, J. H.; Allinger, N. L. *J. Am. Chem. Soc.* 1989, *111*, 8576.
Lii, J. H.; Allinger, N. L. *J. Am. Chem. Soc.* 1989, *111*, 8566.
Allinger, N. L.; Yuh, Y. H.; Lii, J. H. *J. Am. Chem. Soc.* 1989, *111*, 8551.
Allinger, N. L.; Geise, H. J.; Pyckhout, W.; Paquette, L.A.; Gallucci, J. C. *J. Am. Chem. Soc.* 1989, *111*, 1106.
20. Hiemstra, H.; Wijnberg, H. *J. Am. Chem. Soc.* 1981, *103*, 417.
21. Prelog, V.; Wilhelm, H. *Helv. Chim. Acta* 1954, *37*, 1634.
Meurling, L. *Chem. Scr.* 1975, *7*, 90.
22. The results presented here are partly published already:
Dijkstra, G. D. H.; Kellogg, R. M.; Wijnberg, H. *Recl. Trav. Chim. Pays-Bas* 1989, *108*, 195.
Dijkstra, G. D. H.; Kellogg, R. M.; Wijnberg, H.; Svendsen, J. S.; Marko, I.; Sharpless, K. B. *J. Am. Chem. Soc.* 1989, *111*, 8069.
23. CHEMX, developed and distributed by Chemical Design Ltd., Oxford, England.
24. QCPE Program 95/400. Allinger Force Field Molecular Mechanics Calculations, Ed. N. L. allinger, Dept. of Chem., Univ. of Georgia, Athens, Georgia 30602.

25. MMX, derived from MM2 (QCPE 395) with MMP1 pi subroutines (QCPE 318) incorporated for delocalized pi-electron systems, N. L. Allinger, Dept. of Chem., Univ. of Georgia, written by Y. H. Yuh.
26. Kashino, S.; Haisa, M. *Acta Cryst. Sect. C*, 1983, *39*, 310.
27. Spellmeyer, D. C.; Grootenhuis, P. D. J.; Miller, M. D.; Kuyper, L.; Kollman, P. A. *J. Am. Chem. Soc.*, submitted.
28. Bergin, R. *Acta Cryst. Sect. B* 1971, *27*, 381.
29. Pullman, B.; Coubeils, J. L.; Couriere, Ph.; Gervois, J. P. *J. Med. Chem.* 1971, *15*, 17.
30. PCILO3, QCPE Program 462, Pertubative Configuration Interaction, Ed. Roman Boca, Dept. of Inorg. Chem. Slovak Techn. Univ. Bratislava, Czechoslovakia.

3

CONFORMATIONAL ANALYSIS OF CINCHONA ALKALOIDS IN SOLUTION

3.1 INTRODUCTION

In this chapter we will present a detailed conformational analysis of cinchona alkaloids in solution[1]. The results have been obtained by using several Nuclear Magnetic Resonance (NMR) techniques. Firstly, we will briefly introduce NMR (3.1). After that, the assignments of the ^{1}H NMR spectra of various cinchona alkaloids are discussed (3.2.1). With all chemical shifts in hand we turn to the conformational assignments of the alkaloids in different solvents (3.2.2). The conformational aspects of the quinuclidine ring are discussed separately (3.2.3). Results of the study presented in this chapter are used to discuss detailed mechanistic aspects of the asymmetric Michael addition between aromatic thiols and α,β-unsaturated alkenones. These results together with additional NMR data will be presented in chapter 4.

High-resolution NMR and two-dimensional NMR spectroscopy have become extremely powerful tools in studies of the conformation of molecules in solution. The development of high resolution NMR spectrometers started in the 1950's. The fast progress of NMR since then is clear from Table 3.1.

Nuclear resonances are influenced by a number of weak interactions between nuclei and the electrons of molecules, between nuclei within the molecule, and between nuclei in neighbouring molecules. These multiple NMR interactions permit one, for example, to probe molecular structures, or to measure proton-proton distances in a molecule or between different molecules. Thus conformations of molecules in solution can be examined, or information on interactions between molecules can be obtained. We refer the reader to the standard text books on modern NMR techniques for theoretical details and description of the many available NMR methods[2].

In recent years NMR spectroscopy has undergone a particularly revolutionary change. The main reasons are the development of accurate superconducting magnets and application of pulse techniques, together with the introduction of computers and development of special pulse sequences. These advances have made it possible to study intimate details of processes on a molecular level. Typi-

cal examples are conformational studies on oligosacharides, peptides, proteins, surfactant aggregates, or conformational changes of macrocycles induced by complexation[3].

TABLE 3.1 SHORT HISTORICAL OVERVIEW OF NMR.[4]

1946	Bloch and Purcell demonstrated NMR experimentally[5].
1952	Nobel prize Bloch and Purcell.
1953	First structural analysis by Bloch, Anderson, and Arnold.
	30 HMz ^{1}H NMR spectrometer commercially available.
1954	40 HMz ^{1}H NMR spectrometer.
1957	^{13}C NMR spectroscopy introduced by Lauterbur[6].
1958	60 HMz NMR spectrometer.
1961	100 MHz NMR spectrometer.
1966	220 MHz ^{1}H NMR spectrometer. Field of 5.15 Tesla with a super conducting solenoid.
1967	Fourier transform NMR introduced by Ernst[7].
1971	300 HMz ^{1}H NMR spectrometer.
1976	2D NMR introduced by Ernst and Freeman.
1978	Experimental 600 MHz NMR.
1979	Commercially available 500 MHz NMR spectrometers.
	Introduction of multipulse NMR techniques on commercially available apparatus.
1988	3D NMR techniques are introduced[8].

3.2 NMR ANALYSIS ON CINCHONA ALKALOIDS

The general structure of cinchona alkaloids consists of two relatively rigid ring structures, an aromatic quinoline ring and an aliphatic quinuclidine ring. In Figure

3.1 the structures and proton numbering of the cinchona alkaloids and derivatives that we have considered in this study are given. The major cinchona alkaloids only differ in configuration at C_9 and C_8 (for carbon numbering see Figure 1.3, page 6). Quinine and all quinine analogs have the R, S configuration at C_9 and C_8, respectively, whereas for quinidine and quinidine analogs the configuration at C_9 and C_8 is opposite (S, R)[9] . The configurations of the other three stereocenters, C_3, C_4, and N_1 are identical in both series. Quinine and quinidine are sometimes referred to as pseudoenantiomers.

Most cinchona alkaloids may differ structurally at three positions; a methoxy group is present or absent at C_6' of the quinoline ring (R_2); a vinyl or ethyl group is substituted at C_3 of the quinuclidine ring (R_1); and different substituents can be introduced at C_9 (R_3, R_4) (Figure 3.1).

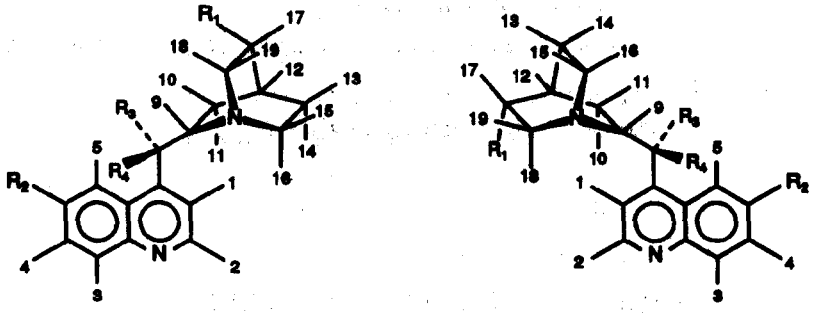

	R_1	R_2	R_3	R_4
quinine	C_2H_5	OCH_3	OH	H
cinchonidine	C_2H_5	H	OH	H
dihydroquinine	C_2H_5	OCH_3	OH	H
dihydrocinchonidine	C_2H_5	H	OH	H
epiquinine	C_2H_5	OCH_3	H	OH
benzoylquinine	C_2H_5	OCH_3	Bz	H
(p-Cl)- benzoyldihydroquinine	C_2H_5	OCH_3	pClBz	H
chloroquinine	C_2H_5	OCH_3	Cl	H
deoxycinchonidine	C_2H_5	H	H	H

	R_1	R_2	R_3	R_4
quinidine	C_2H_5	OCH_3	OH	H
cinchonine	C_2H_5	H	OH	H
dihydroquinidine	C_2H_5	OCH_3	OH	H
dihydrocinchonine	C_2H_5	H	OH	H
epi quinidine	C_2H_5	OCH_3	H	OH
epidihydroquinidine	C_2H_5	OCH_3	H	OH
(p-Cl)-benzoyldihydroquinidine	C_2H_5	OCH_3	pClBz	H
acetyldihydroquinidine	C_2H_5	OCH_3	Ac	H
(dimethylcarbamoyl)dihydroquinidine	C_2H_5	OCH_3	$CONMe_2$	H
methoxydihydroquinidine	C_2H_5	OCH_3	OCH_3	H

Figure 3.1. The structures and proton numbering of the cinchona alkaloids that have been considered in the NMR study.

For the conformational study of the cinchona alkaloids in solution we have used several NMR techniques: COrrelation SpectroscopY (COSY), Nuclear Overhauser Enhancement Spectroscopy (NOESY)[10], NOE-Difference[11], and vicinal *J*-couplings. The COSY experiments were necessary for the assignments of the ^{1}H NMR spectra of the cinchona alkaloids. With NOESY and NOE-difference spectra we were able to determine the conformation(s) of the alkaloids. These NOE measurements provide a way to extract information about the dipolar coupling, which can be related to interatomic distances and molecular motion[12]. The vicinal *J*-couplings provided additional conformational information.

The results of the molecular mechanics study, described in chapter 2, proved to be very helpful for the interpretation of the NOESY spectra. From this study we already know that cinchona alkaloids can in principle adopt four different conformations; two closed conformations in which the quinuclidine nitrogen points towards the quinoline ring, and two open conformations in which the quinuclidine nitrogen points away from the quinoline ring. These four conformations are characterized by specific distances between protons of the quinoline ring and protons of the quinuclidine ring. In the following section we will report the interpretation of the ^{1}H NMR spectra of the cinchona alkaloids in various solvents.

3.2.1 Assignment of ^{1}H NMR Spectra of Cinchona Alkaloids

All cinchona alkaloids have complex ^{1}H NMR spectra. The spectra of the quinidines and quinines were very different, but, not unexpectedly, most of the quinidine spectra, as well as the quinine spectra, were mutually similar. The assignments for (*p*-chlorobenzoyl)dihydroquinidine (*p*-ClBzDHQD) and deoxy-

cinchonidine (Figure 3.1) will serve here as a model for all quinidine and quinine derivatives, respectively[13].

(*p*-Chlorobenzoyl)dihydroquinidine (*p*-ClBzDHQD). The chemical shift assignments of *p*-ClBzDHQD in chloroform-d_1 are presented in Table 3.2. The hydrogens in the quinoline ring could be assigned straightforwardly. The H_1 and H_2 hydrogens are located as doublets at δ 7.40 and δ 8.75, respectively, and their identity is verified by an ortho coupling of 4.6 Hz. The H_3 proton appears as a doublet at δ 8.02 with an ortho coupling of 9.2 Hz to H_4 at δ 7.39. In addition, H_4 is coupled to H_5 at δ 7.45 through a meta coupling of 2.6 Hz. The assignment of the protons in the quinuclidine ring was a more challenging task. The benzylic hydrogen H_8 is apparent as a doublet at δ 6.72 with a vicinal coupling of 7.5 Hz to H_9 at δ 3.38. The COSY spectrum reveals that H_9 is coupled with the vicinal protons H_{10} and H_{11} at δ 1.85 and δ 1.55. These two signals showed similar NOE effect upon irradiation of H_9, rendering their relative assignment impossible by this strategy. Irradiation of H_9 gave rise to an additional NOE at δ 2.79, which was assigned to the closest methylene proton H_{16}. This proton yields a strong NOE at δ 1.56 and a weaker enhancement at δ 1.46. These two signals were assigned to H_{14} and H_{13}, respectively. The former gives the strongest NOE due to its cis relationship with H_{16}. The H_{16} proton is coupled with the geminal proton H_{15} at δ 2.70 and displays a strong vicinal coupling to H_{14} and a weak coupling to H_{13}. On the other hand, H_{15} has a strong coupling to both H_{14} and H_{13}. The two remaining unassigned protons α to the quinuclidine nitrogen, H_{18} and H_{19}, observed as multiplets at δ 2.68 and δ 2.85, are both coupled with H_{17} at δ 1.45. The signal at δ 2.85 showed a strong NOE to H_{17} and was assigned to the cis proton H_{19}, thereby locating H_{18} at δ 2.68. The two methylene hydrogens in the ethyl group, H_{20}, could be assigned to the δ 1.45 absorption due to their coupling with the three hydrogens, H_{21}, of the methyl group. The H_{20} protons showed a small NOE with the signal at δ 1.85, which then could be assigned to H_{10}, located at the same side of the quinuclidine ring. This resolves the ambiguity of the H_{10}, H_{11} assignment (vide supra). The remaining unassigned proton in the quinuclidine

ring, H_{12}, is observed as a narrow multiplet at δ 1.75, with only minute couplings to the other protons.

^1H NMR spectra of *p*-ClBzDHQD were also recorded in CD_3COCD_3, CD_3CN, $C_6D_5CD_3$, and CD_2Cl_2. The chemical shift assignments in these solvents were obtained by similar reasoning as described above and are summarized in Table 3.2.

Deoxycinchonidine. The ^1H NMR spectra of the quinines are different from those of the quinidines. The aromatic hydrogens, however, show close resemblance between the two groups of alkaloids. Figure 3.2 shows a 300 MHz ^1H NMR spectrum of deoxycinchonidine in C_6D_6.

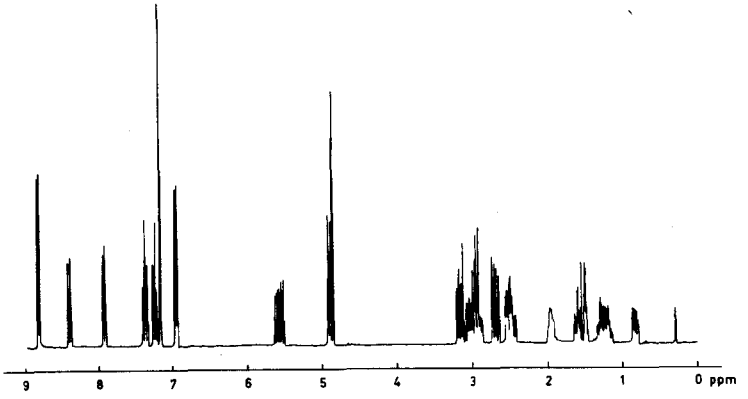

Figure 3.2 300 MHz ^1H NMR spectrum of deoxycinchonidine in C_6D_6.

The chemical shift assignments of deoxycinchonidine in C_6D_6 are presented in Table 3.3. We refer to Figure 3.3 for the proton numbering of deoxycinchonidine. The aromatic H_1 and H_2 hydrogens are located as doublets at δ 6.93 and δ 8.81, respectively, with an ortho coupling of 4.3 Hz. The H_3 proton appears as a doublet at δ 8.39 with an ortho coupling of 8.5 Hz to H_4, which appears as a multiplet at δ 7.37. As a result of a meta fine coupling of 0.9 Hz the doublet of H_3 is further split by H_6 (H_6 hydrogen replaces the quinoline methoxy group), which appears as a multiplet at δ 7.24. H_5 at δ 7.93 appears as a doublet, owing to an ortho coupling of 8.4 Hz with H_6. In addition, a fine coupling of 0.9 Hz was observed, due to a meta coupling with H_4. The vinyl proton H_{20} appears as a multiplet at δ 5.58 and both vinyl protons H_{21} and H_{22} as a multiplet at δ 4.90. The assignments of the quinuclidine protons were less straightforward. The benzylic C_9 carbon is substituted with two hydrogens. We will call the hydrogen which replaces the hydroxy group in case of cinchonidine H_{8b}, the other benzylic hydrogen will be called H_{8a}. Both H_{8a} and H_{8b} appear as multiplets of four lines at δ 3.15 and δ 2.69, respectively. The geminal H_{8a}-H_{8b} coupling is 7.8 Hz. In addition H_{8a} and H_{8b} have vicinal couplings with H_9 at δ 3.03 of 6.6 Hz and 7.4 Hz, respectively. The COSY spectrum reveals that H_9 is coupled with the vicinal protons H_{10} and H_{11} at δ 1.60 and δ 0.83. Because of the stronger NOE between H_9-H_{10} than between H_9-H_{11}, the cis hydrogen H_{10} could be assigned to δ 1.60, thereby locating the trans hydrogen H_{11} at δ 0.83. Irradiation of H_9 yielded a NOE at δ 2.51, which was assigned to the nearest methylene proton H_{18}. This proton yields a strong NOE at δ 2.95 and a weaker enhancement at δ 1.94. These two signals were assigned to H_{19} and H_{17}, respectively, the former giving the strongest NOE due to its geminal relationship with H_{18}. The NOE between H_{18}-H_{20} supports the H_{18} assignment. The strong NOE between H_{19}-H_{17}, owing to their cis relationship, is also in accordance with the assignments thus far. H_{17} shows two upfield NOE's at δ 1.48 and δ 1.18, which were assigned to H_{12} and H_{13}, respectively. Due to the geminal H_{13}-H_{14} relationship the strong NOE at δ 1.29 has been assigned to H_{14}. Because of both cis relationships H_{13}-H_{15} and H_{14}-H_{16}, revealed by strong NOE's, H_{15} could be assigned to δ 2.46 and H_{16} to δ 2.89.

The W-couplings between H_9-H_{15} and between H_{10}-H_{13}, revealed by the COSY spectrum, support the assignments.
We have also recorded the ^1H NMR spectrum of deoxycinchonidine in $CDCl_3$. The chemical shift were obtained in a similar manner and are given in Table 3.3.

Assignments of ^1H NMR Spectra of other Quinine and Quinidine Derivatives. The ^1H NMR chemical shift assignments for quinine (Q), quinidine (QD), dihydroquinine (DHQ), dihydroquinidine (DHQD), methoxydihydroquinidine (MeDHQD), acetyldihydroquinidine (AcDHQD), (dimethylcarbamoyl)dihydroquinidine (DMeCDHQD), (*p*-chlorobenzoyl)dihydroquinine (*p*-ClBzDHQ), benzylquinine (BzQ), and chloroquinine (ClQ) were obtained in a similar manner as described for *p*ClBzDHQD and deoxycinchonidine and are presented in Tables 3.4, 3.5, and 3.6.

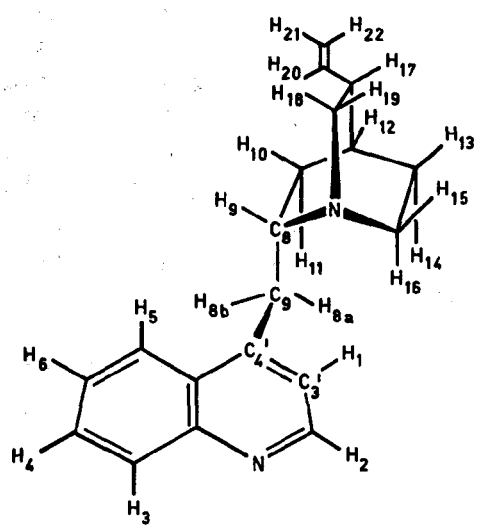

Figure 3.3 Structure and proton numbering of deoxycinchonidine.

Table 3.2 ^{1}H NMR chemical shifts (in ppm) with a precision of 0.03 ppm for *p*-ClBzDHQD. Spectra recorded at 20°C, in the indicated solvents at an alkaloid concentration of 0.02 M.

Proton	$CDCl_3$	CD_3COCD_3	CD_3CN	$C_6D_5CD_3$	CD_2Cl_2
1	7.40	7.59	7.48	7.24	7.42
2	8.75	8.68	8.65	8.73	8.69
3	8.02	7.96	7.94	8.15	7.99
4	7.39	7.39	7.37	7.20	7.36
5	7.45	7.66	7.58	7.64	7.51
8	6.72	6.73	6.59	6.99	6.61
9	3.38	3.56	3.48	3.27	3.43
10	1.85	1.90	1.80	1.82	1.82
11	1.55	1.5-1.6	1.4-1.7	1.3-1.4	1.45-1.75
12	1.75	1.73	1.71	1.33	1.74
13	1.46	1.5-1.6	1.4-1.7	1.18*	1.45-1.75
14	1.56	1.5-1.6	1.4-1.7	1.28*	1.45-1.75
15	2.70	2.69*	2.5-2.9	2.42	2.60-2.80
16	2.79	2.85	2.5-2.9	2.58	2.60-2.80
17	1.45	1.5-1.6	1.4-1.7	1.10	1.45-1.75
18	2.68	2.60*	2.5-2.9	2.6-2.7	2.60-2.80
19	2.85	2.85	2.5-2.9	2.6-2.7	2.90
20	1.45	1.5-1.6	1.4-1.7	1.32	1.47
21	0.92	0.87	1.11	0.77	0.95
OMe	3.95	4.00	3.96	3.57	3.90
R-gr	7.46	7.59	7.51	6.98	7.46
	8.05	8.14	8.04	7.85	8.02

* assignments may be reversed.

Table 3.3 ^1H NMR chemical shifts in ppm from internal TMS with precision of 0.03 ppm for deoxycinchonidine in C_6D_6 and $CDCl_3$ at 20°C.

proton	C_6D_6	$CDCl_3$
1	6.93	7.27
2	8.81	8.80
3	8.39	8.11
4	7.37	7.69
5	7.93	8.05
6	7.24	7.56
8a	3.15	3.40
8b	2.69	3.07
9	3.03	3.20
10	1.60	1.81
11	0.83	1.16
12	1.48	1.75
13	1.18	1.65
14	1.29	1.58
15	2.46	2.78
16	2.89	3.20
17	1.94	2.26
18	2.51	2.67
19	2.95	3.20
20	5.58	5.78
21	4.9	4.90

Table 3.4 ^1H NMR chemical shifts (in ppm) from internal TMS with precision of 0.03 ppm for a series of alkaloid derivatives. Spectra at 20°C, and an alkaloid concentrations of 0.02M.

proton	A	B	C	D	E	F
1	7.48	7.50	7.37	7.34	7.26	7.31
2	8.54	8.70	8.58	8.48	8.50	8.71
3	7.89	8.00	8.17	8.07	7.90	8.24
4	7.24	7.35	7.18	7.14	7.26	7.22
5	7.20	7.24	7.45	7.39	7.17	7.32
6	-	-	-	-	-	-
8	5.60	5.50	5.48	5.43	5.52	5.08
9	3.06	3.09	3.15	3.09	3.04	2.89
10	1.30-1.45	1.66	1.85	1.82	1.96	0.96
11	1.62-1.80	1.60	1.54	1.42	1.06	2.11
12	1.62-1.80	1.80	1.63	1.60	1.66	1.54
13	1.62-1.80	1.52	1.68	1.68	1.3-1.55	1.12
14	1.30-1.45	1.66	1.22	1.23	1.3-1.55	1.12
15	2.61	2.64	2.50	2.48	2.65-3.05	2.46
16	3.53	3.38	3.48	3.48	2.65-3.05	2.60
17	1.30-1.45	2.26	1.98	1.96	1.3-1.55	1.98
18	2.35	3.16	2.54	2.50	2.65-3.05	3.37
19	3.03	2.69	2.89	2.88	2.65-3.05	2.79
20	1.19	5.77	5.52	5.48	1.43	6.14
21	0.77	4.93	4.83	4.81	0.85	5.05
OMe	3.83	3.85	3.54	3.57	3.81	3.52
R-gr	4.96	5.02	4.27	4.55	5.15	5.44

A=Dihydroquinine (DHQ) in $CDCl_3$, B=Quinine (Q) in $CDCl_3$, C=Quinine (Q) in C_6D_6, D=Quinine (Q) in $C_6D_5CD_3$, E=Dihydroquinidine (DHQD) in $CDCl_3$, F=Quinidine (QD) in C_6D_6.

Table 3.5 ^1H NMR chemical shifts (in ppm) from internal TMS standard with precision of 0.03 ppm for several alkaloids in the indicated solvents at 20°C.

proton	A	B	C	D	E
1	7.38	7.43	7.43	7.55	7.43
2	8.62	8.76	8.83	8.62	8.72
3	7.98	8.04	8.13	7.96	8.02
4	7.35	7.37	7.47	7.42	7.38
5	7.44	7.30	7.54	7.60	7.53
8	4.86	5.01	6.42	6.79	6.75
9	3.05	2.7-3.1	3.38	3.45	3.49
10	1.88	1.97	2.00	1.84	1.95
11	1.35-1.60	1.13	1.50	1.84	1.73
12	1.69	1.68	1.89	1.84	1.89
13	1.35-1.60	1.35-1.55	1.55-1.75	1.58	1.58
14	1.35-1.60	1.35-1.55	1.55-1.75	1.84	1.80
15	2.6-2.9	2.7-3.1	2.8-3.0	2.64	2.72
16	2.6-2.9	2.7-3.1	2.8-3.0	3.23	3.21
17	1.35-1.60	1.35-1.55	1.55-1.75	2.31	2.30
18	2.6-2.9	2.7-3.1	2.8-3.0	2.71	2.66
19	2.6-2.9	2.7-3.1	3.10	3.04	3.09
20	1.35-1.60	1.47	1.64	5.80	5.84
21	0.92	0.91	1.06	4.90	5.00
OMe	3.96	3.94	4.10	4.00	3.98
R-gr	3.26	3.31	2.30	8.12	8.10
				7.62	7.59
				7.45	7.51

A=Methoxydihydroquinidine (MeDHQD) in CD_2Cl_2, B=Methoxydihydro-quinidine (MeDHQD) in $CDCl_3$, C=Acetyldihydroquinidine (AcDHQD) in $CDCl_3$, D=Benzylquinine (BzQ) in CD_3OD, E=Benzylquinine (BzQ) in $CDCl_3$.

Table 3.6 ^{1}H NMR chemical shifts in ppm from internal TMS with precision of 0.03 ppm for some alkaloids in the indicated solvents at 20°C.

proton	A	B	C	D
1	7.20-7.58	6.95-7.12	7.34	7.40
2	8.77	8.70	8.74	8.72
3	8.06	8.26	8.00	8.02
4	7.41	7.21	7.35	7.38
5	7.20-7.58	7.40-7.60	7.46	7.49
8	5.30-5.60	5.26-5.56	6.43	6.72
9	3.42-3.70	3.40-3.60	3.29	3.47
10	1.55	1.27	1.81	1.63
11	0.70	0.43	1.55	1.88
12	1.66	1.27	1.73	1.85
13	1.55	1.08	1.45	1.76
14	1.55	1.08	1.50*	1.51
15	2.90	2.57	2.70*	2.67
16	3.22	3.02	2.70*	3.17
17	2.30	1.92	1.50*	1.50
18	2.90	2.38	2.70*	2.37
19	3.39	3.10	2.90	3.06
20	5.80	5.59	1.38	1.35
21	5.00	4.90	0.90	0.85
OMe	3.97	3.36	3.95	3.97
R-gr			2.89	7.44
			3.03	8.03

A=Chloroquinine (ClQ) in $CDCl_3$, B=chloroquinine (ClQ) in C_6D_6, C=Dimethylcarba-moyldihydroquinidine (DMeCDHQD) in $CDCl_3$, D=*p*-Chlorobenzoyldihydro-quinine (*p*-ClBzDHQ) in $CDCl_3$.

* Assignments may be reversed.

Assignments of ^{1}H NMR Spectra of Epicinchona Alkaloid Derivatives. The ^{1}H NMR chemical shift assignments for epidihydroquinidine (epiDHQD), epiquinidine (epiQD) and epiquinine (epiQ) were also obtained in a similar manner as described above. They are presented in Table 3.7.

Table 3.7 ^{1}H NMR chemical shifts in ppm from internal TMS with precision of 0.03 ppm in $CDCl_3$ for the epi-alkaloids at 20°C.

proton	A	B	C
1	7.40	7.42	7.27
2	8.69	8.70	8.60
3	7.98	7.98	7.92
4	7.32	7.31	7.25
5	7.59	7.53	7.56
8	5.02	5.08	4.92
9	2.8-3.0	2.9	2.95-3.05
10	1.20	1.27	0.79
11	0.95	0.95	1.29
12	1.54	1.63	1.54
13	1.28-1.50	1.5	1.4
14	1.28-1.50	1.5	1.4
15	2.8-3.0	2.9	2.61-2.67
16	2.8-3.0	2.9	2.95-3.15
17	1.28-1.50	2.28	2.15
18	2.57	2.9	2.61-2.67
19	2.8-3.0	2.9	2.95-3.15
20	1.28-1.50	5.86	5.58
21	0.84	5.05	4.83
OMe	3.88	3.87	3.77
OH	4.78	4.77	4.8

A=Epidihydroquinidine (epiDHQD), B=Epiquinidine (epiQD), C=Epiquinine (epiQ).

3.2.2 Conformational Assignments of Cinchona Alkaloids

The gross conformation of the cinchona alkaloids is determined by the torsions about the C_8-C_9 and C_9-C_4' bonds. The strategy has been to use inter-ring NOE's in order to establish the overall conformation. These inter-ring NOE's between quinoline hydrogens and quinuclidine hydrogens are important, because they reveal the spatial relationship between both rings and thus the overall conformation of the alkaloid. NOESY and NOE-difference spectra have been recorded to obtain these inter-ring NOE's. A typical example of a NOESY spectrum of quinidine is depicted in Figure 3.4.

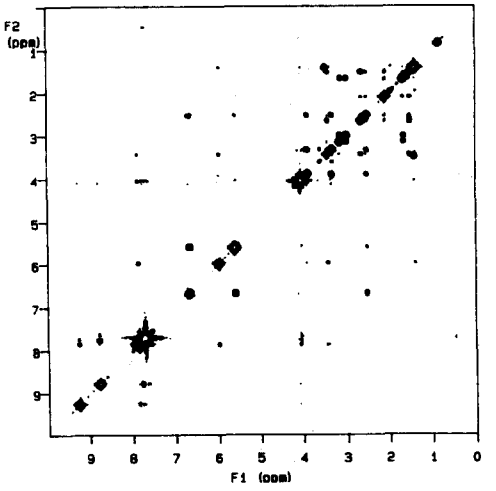

Figure 3.4 500 MHz NOESY spectrum of quinidine in C_6D_6.

The results of the molecular mechanics study, described in chapter two, proved to be very helpful for the interpretation of the spectra. Figures 3.5 and 3.6 show schematic drawings of the closed conformation 2 and open conformation 3 of

quinidine and quinine derivatives, respectively, as predicted by the molecular mechanics analysis. In these Figures the arrows mark the hydrogens between which inter-ring NOE's are expected for that particular conformation.

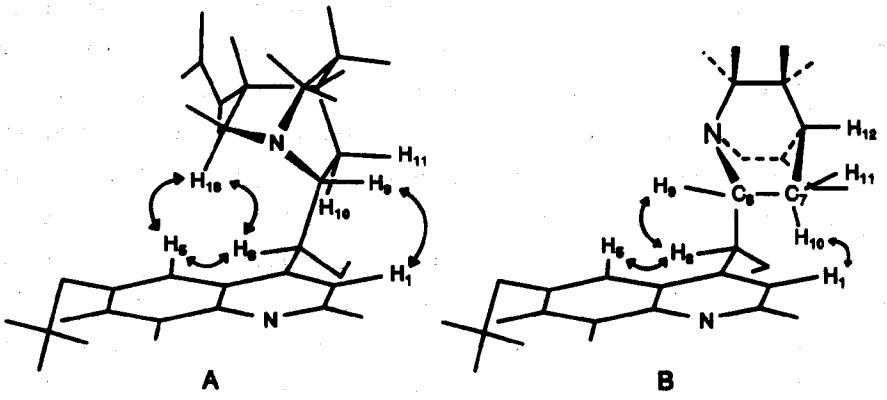

closed conformation 2 open conformation 3

Figure 3.5 Schematic drawing showing (a) the closed conformation 2 and (b) the open conformation 3 of quinidine.

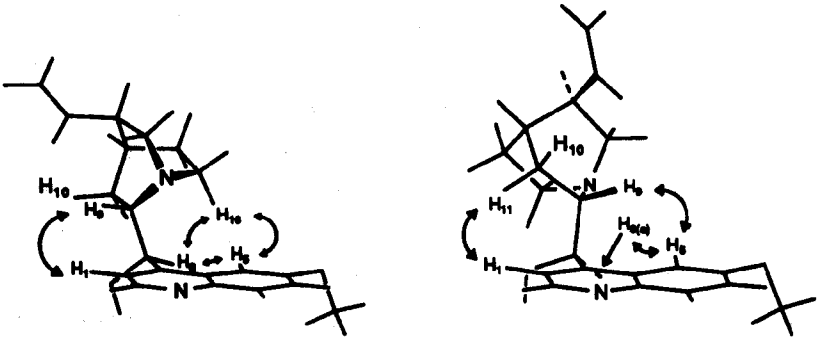

closed conformation 2 open conformation 3

Figure 3.6 Schematic drawing showing (left) the closed conformation 2 and (right) the open conformation 3 of quinine.

Conformational assignment of deoxycinchonidine in C_6D_6 and $CDCl_3$

With the complete assignments of all hydrogens of deoxycinchonidine in hand, we next investigated the conformational behavior of this alkaloid in C_6D_6 and $CDCl_3$. The existence of closed conformation 2 in C_6D_6 could be excluded, because no NOE is observed between H_{16}-H_5 (Figure 3.6). We realize that the absence of an Overhauser enhancement is a negative experiment and not a strong structural argument. However, we know from the conformational analysis of ester derivatives of quinine (described in the next paragraph) that in case of closed conformation 2 a strong NOE is indeed present between H_{16}-H_5. Based on the same argument also open conformation 4 could be excluded, because no NOE was found between H_5 and H_{11}. From the epi-cinchona alkaloids (which adopt this open conformation 4) we know that a strong NOE is present between H_5 and H_{11} in case of the open conformation 4. On the other hand, the NOE's observed between H_{11}-H_1, H_9-H_5, H_{16}-H_{8a}, H_{8a}-H_5, and H_{8b}-H_{11} (Figure 3.6) indicate that open conformation 3 must be present. But NOE's between H_{8b}-H_5, H_9-H_5, H_{8a}-H_{11}, and H_{16}-H_1 were also found. These are all in accordance with closed conformation 1. Thus both open conformation 3 as well as closed conformation 1 are present at the same time in solution. On the NMR time scale these two conformers exchange rapidly, because only an averaged ^1H NMR spectrum is recorded at 25°C. In Figure 3.7A the trace of the NOESY spectrum, which shows the NOE interactions with H_5, is depicted. The enhancement marked 8A is due to a NOE between H_5-H_{8a} in the open conformation 3, and the one marked 8B is due to a NOE between H_5-H_{8b} in the closed conformation 1. We know from the molecular mechanics analysis (chapter 2) that the interatomic H_5-H_{8a} distance in the open conformation 3 and the H_5-H_{8b} distance in the closed conformation 1 are approximately the same (about 2.1 A). Thus integration of both enhancements 8A and 8B gives an approximate estimation of the ratio of distribution between both conformers. In Figures 3.7B and 3.7C the traces of hydrogens H_{8a} and H_{8b} are shown. In case of the H_{8a} trace a relatively large NOE with H_5 and a smaller one with H_1 are observed, whereas in case of the H_{8b} trace both H_{8b}-H_5 and H_{8b}-H_1 enhancements are of the same order of magnitude. From the integration of these

NOE traces we conclude that the ratio between open conformation 3 and closed conformation 1 is approximately 60/40.

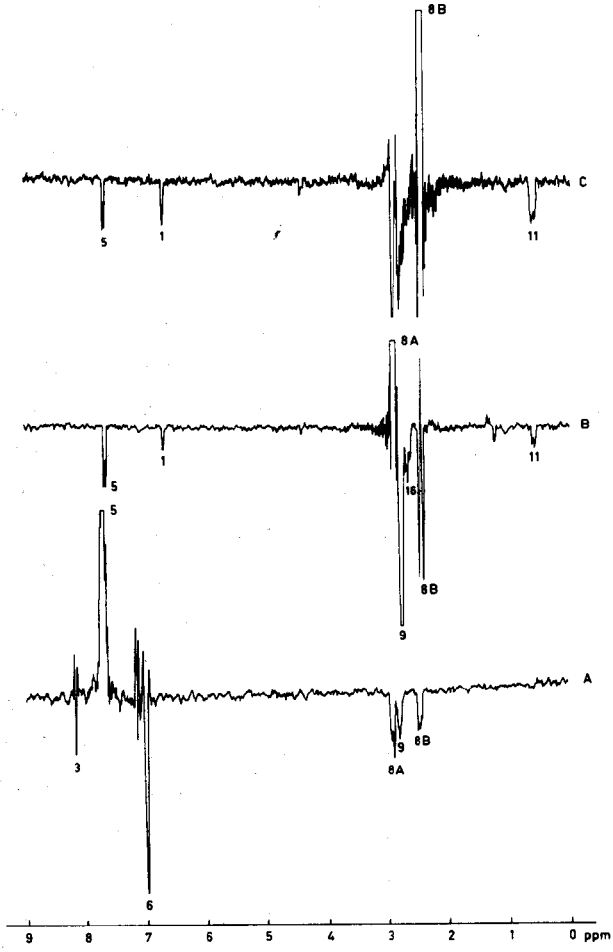

Figure 3.7 Traces of the NOESY spectrum of deoxycinchonidine in C_6D_6. A=H_5 trace, B=H_{8a} trace, and C=H_{8b} trace.

^{1}H NMR and NOESY spectra of deoxycinchonidine have also been recorded in $CDCl_3$. Because of complete overlap in the ^{1}H NMR of protons H_9 and H_{16} the presence of conformations 2 and 4 could not been excluded, but because of NOE's between H_1-H_{8a}, H_1-H_{8b}, H_5-H_{8a}, H_5-H_{8b}, and H_1-H_{11} we conclude that also in $CDCl_3$ a mixture of conformers is present, which must include conformers 1 and 3. Low temperature experiments at -20°C and -60°C in $CDCl_3$ did not alter the ^{1}H NMR spectra; no line broadening has been observed, and averaged spectra were still recorded. Thus even at -60°C it was not possible to freeze out the different conformers. This is indicative of a fast exchange between the different conformations on the NMR time scale and thus of a low energy barrier.

Conformational assignment of *p*-CLBzDHQD in $CDCl_3$

With the complete assignments of the hydrogens of *p*-ClBzDHQD in hand, its conformation was investigated. The presence of NOE's in $CDCl_3$ between H_5, H_8 and H_{18} suggests that these three nuclei are in close spatial proximity (see Figure 3.5). An additional, but weaker inter-ring NOE was observed between H_9 and H_1. These interactions are only possible in an alkaloid conformation in which the quinuclidine nitrogen lone pair points over the quinoline ring. This suggests an alkaloid structure in which the $C_3'C_4'C_9C_8$ dihedral angle is close to -90°, and the $H_8C_9C_8H_9$ dihedral angle approaches an anti conformation (this conformation resembles closed conformation 2). The most apparent indication of the $H_8C_9C_8H_9$ dihedral angle was obtained from the ^3J H_8H_9 coupling constant of 7.5 Hz. By application of the Altona equation[14] this angle is estimated to be 155°. This is in good agreement with the conformation suggested by the NOE interactions. From the additional appearance of NOE's between H_1-H_{11}, H_8-H_9, and between H_{16} with the ortho protons of the benzoyl moiety, we conclude that also the open conformation 3 occurs. Based on integration of NOE traces as outlined above for deoxycinchonidine we conclude that open conformation 3 occurs to the extent of about 30% in $CDCl_3$.

The ^{1}H NMR spectra of *p*-ClBzDHQD were also measured in acetone-d_6, acetonitrile-d_3, dichloromethane-d_2, and toluene-d_8. The chemical shifts have been compiled (Table 3.2). The results reveal that, with the exception of toluene-d_8, there are only small differences in the chemical shifts. Furthermore, the coupling constants ^3J H_8H_9 were in the range of 7.5-8.6 Hz, with one exception, in toluene-d_8, in which a coupling constant of 6.8 Hz was measured.

These results suggest that there are only small variations in the equilibrium between conformers 2 and 3 in chloroform-d_1, acetone-d_6, acetonitrile-d_3 and dichloromethane-d_2. The ^3J H_8H_9 coupling in toluene-d_8 implies that the equilibrium between closed conformation 2 and open conformation 3 shifts slightly in favor of open conformation 3. From NOESY spectra of an ester derivative of quinine (benzoylquinine) in CD_3OD it follows that in this polar solvent the equilibrium between both conformers 2 and 3 is shifted even further in favor of the open conformation 3. This is also reflected by a decrease of the ^3J H_8H_9 coupling constant from 7.5 Hz in $CDCl_3$ to 5.1 Hz in CD_3OD.

In an attempt to substantiate further the conformation of *p*-ClBzDHQD, a single X-ray diffraction analysis has been undertaken. This X-ray analysis showed that the alkaloid in the solid state exists in a closed conformation (Figure 3.8). All essential features of the closed conformation 2 in solution, as discussed above, are present in the solid state. This is particularly evident for the important dihedral angles, $C_3'C_4'C_9C_8$ and $H_8C_9C_8H_9$, which are approximately -86° and 170° in the crystal structure, closely resembling the corresponding angles of -90° and 155°, suggested by the NMR experiments of the alkaloid in solution. Furthermore, the X-ray analysis revealed that H_5, H_8, and H_{18}, are positioned in a close spatial arrangement, with internuclear distances of 2.23 (H_5, H_8), 2.41 (H_5, H_{18}), and 2.24 A (H_8, H_{18}). This is in agreement with the strong NOE observed between these nuclei. The weaker NOE observed between H_1 and H_9 is reflected by a longer internuclear distance of 2.89 A.

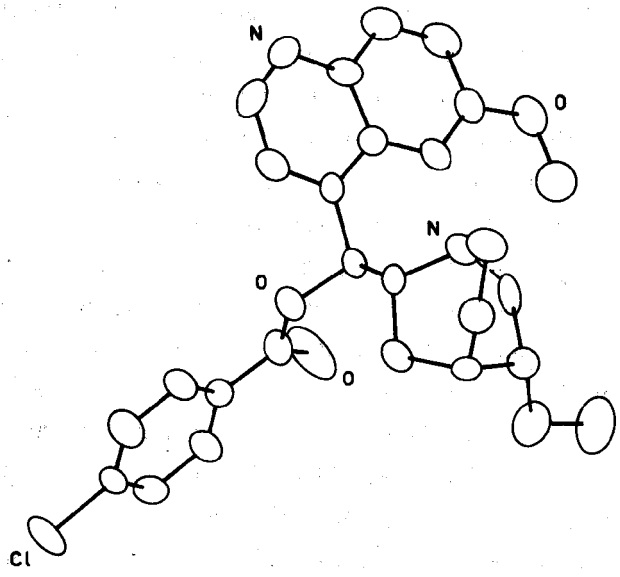

Figure 3.8 X-Ray crystal structure of (*p*-chlorobenzoyl)dihydroquinidine.

Conformational Assignments of Other Quinidine Derivatives. The ^{1}H NMR spectra of (dimethylcarbamoyl)dihydroquinidine and acetyldihydroquinidine are very similar to that of (*p*-chlorobenzoyl)dihydroquinidine (see Table 3.2). The ^{1}H NMR spectra of quinidine, dihydroquinidine, and methoxydihydroquinidine showed several differences relative to the ester derivatives. In the ester derivatives of quinidine and dihydroquinidine H_{11} appeared between δ 1.50 and δ 1.55, whereas in the methoxy and hydroxy substituted quinidines H_{11} appeared at δ 1.13 and δ 1.06, respectively. Furthermore, the ^3J H_8H_9 coupling constant for the ester derivatives in $CDCl_3$ are between 7.5 and 8.3 Hz, but for the methoxy and hydroxy substituted quinidines this coupling constant decreases to 3.9 and 3.5 Hz,

respectively. This suggests that the torsion angle $H_8C_9C_8H_9$ is very different from those of the quinidine esters. Application of the Altona equation gives a torsion angle $H_8C_9C_8H_9$ of either close to 120°, indicating an eclipsed conformation, or approximately 60°, indicative of a staggered conformation. In order to resolve this ambiguity, NOESY spectra and NOE difference experiments were undertaken. Based on arguments as outlined above we will only discuss the main results.

The *hydroxy cinchona alkaloids* (quinine, quinidine, cinchonine, cinchonidine) predominantly adopt the open conformation 3, but some conformational freedom of the quinuclidine ring is revealed by small NOE's between H_9-H_1 and H_8-H_{11} in case of quinine and cinchonidine and between H_9-H_1 and H_8-H_{10} in case of quinidine and cinchonine. These NOE's are characteristic for closed conformation 2. However, a NOE between H_{16}-H_5 (quinine, cinchonidine) or H_{18}-H_5 (quinidine, cinchonine) was never observed. It is therefore concluded that the hydroxy cinchona alkaloids exist at least for more than 90% in open conformation 3, wherein some conformational freedom of the quinuclidine ring exists.

The *methoxy cinchona alkaloids* predominantly adopt the open conformation 3 and to a lesser amount the closed conformation 2 in $CDCl_3$. However, in CD_2Cl_2 the closed conformation 2 is found in excess. Thus now the distinct preference for the open conformation 3, seen for the hydroxy alkaloids, has vanished. In solvents like $CDCl_3$ and CD_3OD the open conformer 3 is still predominant, but in the 'non-coordinating' solvent CD_2Cl_2 it is the closed conformer 2 which is in excess. These observations are also reflected in the ^1H NMR spectra of the methoxy derivatives. In the ^1H NMR of methoxydihydroquinidine in $CDCl_3$ H_{11} appears at δ 1.13, whereas in CD_2Cl_2 H_{11} is found at δ 1.50, and this change in chemical shift was accompanied by a substantial increase in $^3J_{H_8H_9}$ from 3.9 to 6.6 Hz.

Chloroquinine adopts for at least 90% the closed conformation 2 in C_6D_6, $CDCl_3$, and CD_3OD. The presence of small amounts of the open conformer 3 are revealed, however, by a very weak NOE between H_1-H_{11}. This weak enhancement could only be detected by selective irradiation of hydrogen H_1.

There is still another interesting feature regarding the proton spectra of chloroquinine; all protons in the ^1H NMR spectra of the cinchona alkaloids

discussed so far appear as sharp absorptions (a typical example is shown in Figure 3.2). But in case of chloroquinine in C_6D_6 and in $CDCl_3$ the hydrogens H_1, H_5, H_8, and H_9 appear as broad lines, whereas all other protons are observed as sharp absorptions. It follows from Figures 3.9 and 3.10 that this is caused by coalescence. Figure 3.9 shows the absorption of the benzylic hydrogen H_9 at 20, 30, 40, and 50°C, respectively, in $CDCl_3$. In Figure 3.10 the absorptions of both quinoline protons H_1 and H_5 are depicted at 20 and 70°C in C_6D_6. These observations indicate that the energy barrier between closed conformer 2 and open conformer 3 is increased to such a height that at room temperature averaged spectra are no longer recorded. Also note that we have observed these phenomena only for the cinchona derivatives substituted at C_9 with Cl.

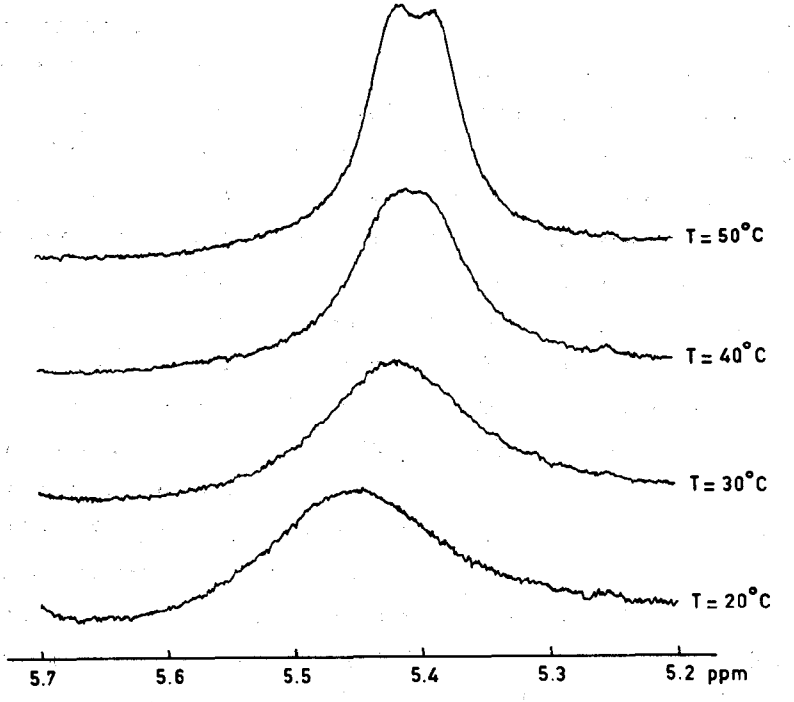

Figure 3.9 ^1H NMR spectra of chloroquinine at different temperatures. Absorptions of H_9 at 20, 30, 40, and 50°C in $CDCl_3$.

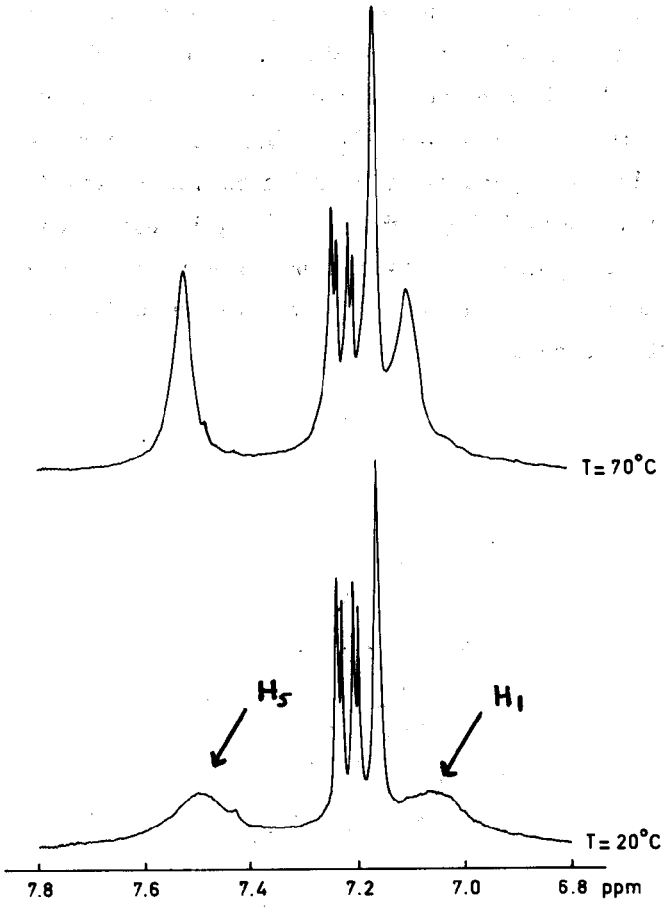

Figure 3.10 ^{1}H NMR spectra of chloroquinine at different temperatures. Absorptions of H_1 and H_5 at 20 and 70°C in C_6D_6.

NOESY spectra of *epidihydroquinidine* and *epiquinidine* revealed inter-ring NOE's between H_8, H_{18}, H_{10}, and H_5 (see Figure 3.11). These NOE's indicate that epiquinidines have an open conformation. This conformation differs, however, from the open conformation 3, which was observed for the cinchona alkaloids discussed thus far. The open conformation of the epi derivatives resembles the open conformation 4, predicted by the molecular mechanics calculations on the quinidines. The ^3J H_8H_9 coupling constant of 10.1 Hz of epidihydroquinidine corresponds to the anti arrangement of H_8 and H_9, as expected in this conformation. Based on the same arguments, we found that the open conformation 4 is also preferred by epiquinine in $CDCl_3$. In this case a ^3J H_8H_9 coupling constant of 9.9 Hz was found, once again corresponding to an anti relationship between H_8 and H_9. NOE's between H_{11}, H_5, and H_8 and between H_9-H_1 complete the conformational assignment.

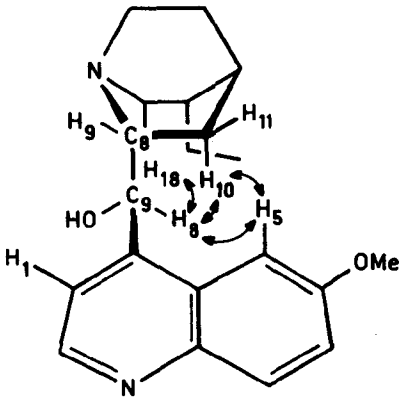

Figure 3.11 Schematic drawing of the open conformation 4 of epi(dihydro)-quinidine.

3.2.3. Conformation of the Quinuclidine Ring

There is still another conformational feature of the cinchona alkaloids that has not yet been discussed, namely the conformation of the quinuclidine ring. It is highly unlikely that the quinuclidine ring will have its methylene groups opposed to form an unfavoured all-eclipsed conformation. Rather, the steric strain will be reduced by a twist in the quinuclidine ring, allowing the methylene groups to approach staggered conformations. This twist can take place in two different directions, either to form a right-handed or left-handed screw (viewed from the quinuclidine nitrogen atom along the pseudo C_3 symmetry axis). We were interested to see if the pseudoenantiomeric relationship between the quinidines and quinines is also reflected in the direction of the twist in the quinuclidine ring.

The twist in the quinuclidine ring gives rise to differences in dihedral angles of the vicinal hydrogens and should, hence, be reflected in differences in the vicinal coupling constants. Because most of the signals of the quinuclidine hydrogens in the ^{1}H NMR spectrum of(*p*-chlorobenzoyl)dihydroquinine are well resolved, all vicinal coupling constants could be obtained, either directly from the spectrum or estimated by computer simulations of the spin systems involved. The magnitude of the twist is not necessarily the same in all bonds, and thus the C_5-C_6 bond was addressed first. For the proton and carbon numbering we refer to Figures 3.12 and 3.13, respectively. The vicinal couplings between H_{16} and H_{13} and between H_{16} and H_{14} are 6.1 and 10.3 Hz, respectively, corresponding to dihedral angles of -135 and -15°. This suggests a left-handed twist of approximately 15° in the C_5-C_6 bond. The direction and size of this twist is supported by the ^3J $H_{15}H_{13}$ coupling constant of 10.3 Hz corresponding to a dihedral angle of 15°. The ^3J $H_{15}H_{14}$ coupling constant was harder to assess directly from the spectrum, but computer simulation showed that this coupling is between 3.5 and 4 Hz, which also is in accordance with the left handed-twist (Figure 3.12).

Similarly, the torsional angle of the C_7-C_8 bond was obtained from the couplings of H_9 with both H_{10} and H_{11}. These couplings were both 7.7 Hz, which corresponds to dihedral angles of 20° for the H_9H_{10} and 140° for the H_9H_{11}

dihedrals. These angles show that the C_7-C_8 bond is twisted approximately 20° in a left-handed screw.

Finally, the torsional angle of the C_2-C_3 bond was obtained from the couplings between H_{17} and the vicinal protons H_{18} and H_{19}, which were 3.3 (-115°) and 9.8 Hz (-10°), respectively. These couplings indicate a C_2-C_3 torsion of approximately 10° to form a left-handed screw.

These results clearly show that the quinuclidine ring of (*p*-chlorobenzoyl)-dihydroquinine is twisted as a left-handed screw (Figure 3.12) and that the twist is largest in the C_7-C_8 bond, less in the C_5-C_6 bond, and least in the C_2-C_3 bond. A similar twist of the quinuclidine ring is observed with the molecular mechanics calculations of the dihydroquinines (chapter 2).

The twist was also investigated for (*p*-chlorobenzoyl)dihydroquinidine, but due to severe overlap of several signals in the spectrum, not all vicinal couplings could be obtained. The couplings available proved, however, to be sufficient to determine the twist of the quinuclidine ring. The spectrum in toluene-d_8 revealed that $^3J\ H_{15}H_{13}$ is 9.7 Hz, corresponding to a dihedral angle of 20°. $^3J\ H_{15}H_{14}$ is 7.8 Hz, corresponding to a dihedral of 140°. The analogous vicinal couplings with H_{16} were derived by computer simulations, yielding a coupling constant of 9-10 Hz for $^3J\ H_{16}H_{14}$, and a coupling constant of 1-2 Hz for $^3J\ H_{16}H_{13}$. The corresponding dihedral angles obtained by the Altona equation were 20 and -110°, respectively, establishing a right-handed screw of the quinuclidine ring with a torsional angle of 20° in the C_5-C_6 bond (Figure 3.12). The H_9 couplings to both H_{10} and H_{11} are 8.9 Hz, in accordance with dihedral angles of 145° for the H_9H_{10} dihedral and 25° for the H_9H_{11} dihedral, suggesting a right-handed twist of about 25° of the C_7-C_8 bond. Similarly, the $^3J\ H_{17}H_{19}$ coupling of 7.7 Hz suggests a torsional angle of 20° in the C_2-C_3 bond, also in accordance with the right-handed twist.

These results show that the quinuclidine ring has a right-handed twist, the twist being largest in the C_7-C_8 bond, and smaller in the C_2-C_3 and C_5-C_6 bonds (Figures 3.12 and 3.13). The right-handed twist in (*p*-chlorobenzoyl)dihydro-quinidine was also observed with the molecular mechanics calculations (chapter 2), as

well as in the X-ray structure (Figure 3.8), where the $N_1C_8C_7C_4$ dihedral angle is 22.2°, the $N_1C_6C_5C_4$ angle is 17.6°, and the $N_1C_2C_3C_4$ angle is 19.6°. This is all in excellent agreement with the angles obtained from the NMR study.

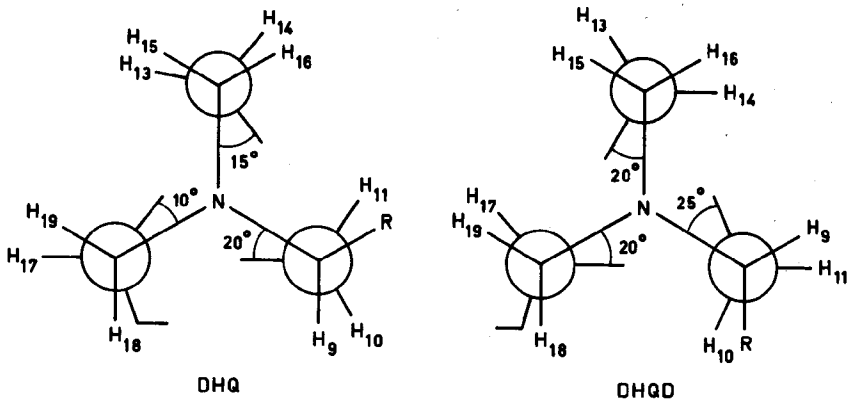

Figure 3.12 Schematic drawing of the quinuclidine ring of (left) (*p*-chlorobenzoyl)-dihydroquinine and (right) (*p*-chlorobenzoyl)dihydroquinidine.

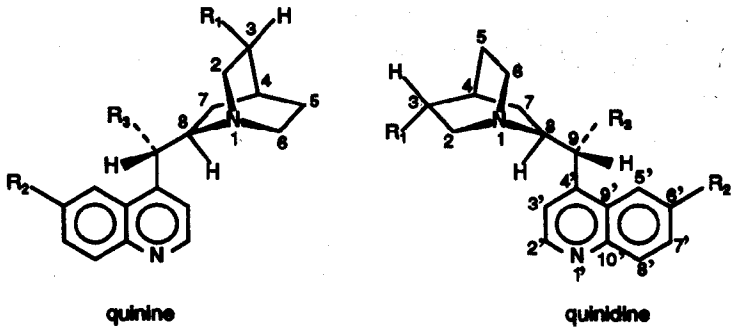

Figure 3.13 The structures and carbon numbering of quinine and quinidine derivatives.

3.3 EXPERIMENTAL PART

The NOESY and COSY spectra were measured as 0.05-0.1 M solutions in a 5 mm NMR tube. In case of the NOESY spectra the oxygen was removed by freeze-pump-thaw cycles and the NMR tubes were sealed under reduced pressure. All spectra (^{1}H NMR, COSY, NOE-diff., and NOESY) were recorded using a Varian VXR-300 and VXR-500 spectrometer at 20°C. For each NOESY spectrum between 512 and 1024 FID's of between 1024 and 2048 data points each were collected. The spectral width was chosen as narrow as possible (about 3000 Hz). Corrections with weighting functions (mostly shifted sine bells[15]) were used before Fourier transformations in the t_2 and t_1 dimensions. All NOESY spectra were recorded in phase sensitive mode[16].

3.4 REFERENCES

---

1. Parts of the work described here have already been published:
   Dijkstra, G. D. H.; Kellogg, R. M.; Wijnberg, H. *Recl. Trav. Chim. Pays-Bas* 1989, *108*, 195.
   Dijkstra, G. D. H.; Kellogg, R. M.; Wijnberg, H. ; Svendsen, J. S.; Marko, I.; Sharpless, K. B. *J. Am. Chem. Soc.* 1989, *111*, 8069.
   Dijkstra, G. D. H.; Kellogg, R. M.; Wijnberg, H. *J. Org. Chem.* 1990, *55*, 6121.
2. See for example:
   Derome, A. E. Modern NMR Techniques for Chemistry Research, Pergamon Press, Oxford, 1987.
3. See for example:
   Eliason, B.; Larsson, K. M.; Kowaleski, J. *J. Phys. Chem.* 1985, *89*, 258.
   Stover, H. D.; Delville, A.; Detellier, C. *J. Am. Chem. Soc.* 1985, *107*, 4167.
   Kintzinger, J. -P.; Lehn, J. -M. *J. Am. Chem. Soc.* 1974, *96*, 3313.
   Schmidt, E.; Tremillon, J. M.; Kintzinger, J. -D.; Popov, A. I. *J. Am. Chem. Soc.* 1983, *105*, 7563.
   Dijkstra, G. D. H.; Kruizinga, W. K.; Kellogg, R. M. *J. Org. Chem.* 1987, *52*,

Footnote Cont. Next Page

Footnote 3 Cont.

4230.

Ragnothama, S *J. Magn. Reson.* 1984, *57*, 294.

Bush, C. A.; Yun, Z. -Y.; Rao, B. N. N. *J. Am. Chem. Soc.* 1986, *108*, 6168.

Rao, B. N. N.; Dua, V. K.; Bush, C. A. *Biopolymers* 1985, *24*, 2207.

Montelione, G. T.; Hughes, P.; Clardy, J.; Scheraga, H. A. *J. Am. Chem. Soc.* 1986, *108*, 6765.

Kumar, A.; Wagner, G.; Ernst, R. R.; Wuthrich, K. *J. Am. Chem. Soc.* 1981, *103*, 3654.

Mirau, P. A.; Bovey, F. A. *J. Am. Chem. Soc.* 1986, *108*, 5130.

Nusselder, J. J. H.; Engberts, J. B. F. N.; Boelens, R.; Kaptein, R. *Recl. Trav. Chim. Pays-Bas* 1988, *107*, 105.

4. Table 3.1 is partly taken over from a NMR course; NMR spectroscopie, afd. Instrumentele analyse, Org. Chem. Laboratorium, Utrecht, 1984.
5. Purcell, E. M.; Torrey, H. C.; Pound, R. V. *Phys. Rev* 1946, *69*, 37.
   Bloch, F.; Rabi, I. I. *Rev. Modern Phys.* 1945, *17*, 237.
6. Lauterbur, P. C. *J. Chem. Phys.* 1957, *26*, 217.
   Lauterbur, P. C. *Ann. N. Y. Acad. Sci.* 1958, *70*, 841.
7. Ernst, R. R. *J. Magn. Reson.* 1971, *4*, 280.
8. Vuister, G. W.; Boelens, R.; Kaptein, R. *J. Magn. Reson.* 1988, *80*, 176.
   Bax, A. *Chemtracts: Anal. Phys. Chem.* 1989, *1*, 215.
9. Prelog concluded that for cinchona alkaloids the C_9 and C_8 carbon atoms have erythro arrangements, whereas for the epi-cinchona alkaloids a threo relationship exist:
   Prelog, V.; Hafliger, O *Helv. Chim. Acta.* 1950, *33*, 2021.
   Prelog, V. *Tetrahedron Lett.* 1964, 2037.
10. Jeener, J.; Meier, B. H.; Bachmann, D.; Ernst, R. R. *J. Chem. Phys.* 1979, *71*, 4546.
    Macura, S.; Ernst, R. R. *Mol. Phys.* 1980, *41*, 95.
11. Noggle, J. H.; Schirmer, R. E. *The Nuclear Overhauser Effect, Chemical Applications*, Academic Press, New York, 1971.
    McLachlan, S. J.;La Mar, G. N.; Sletten, E. *J. Am. Chem. Soc.* 1986, *108*, 1285.
12. Benn, R.; Gunther, H. *Angew. Chem.* 1983, *95*, 381.
    Bosch, C.; Kumar, A.; Baumann, R.; Ernst, R. R.; Wuthrich, K. *J. Magn. Reson.* 1981, *42*, 159.

13. For the assignment of quinine and quinidine as hydrochlorides in DMSO-d_6, see: Chazin, W. J.; Coolebrook, L. D. *J. Org. Chem.* **1986**, *51*, 1243.
14. Haasnoot, C. A. G.; de Leeuw, F. A. A. M.; Altona, C. *Tetrahedron* **1980**, *36*, 2387.
15. Levitt, M. H.; Radloff, C.; Ernst, R. R. *Chem. Phys. Lett.* **1985**, *114*, 435.
16. States, D. J.; Haberkorn, R. A.; Ruben, D. J. *J. Magn. Reson.* **1982**, *48*, 286.

4

CONFORMATIONAL EFFECTS OF CINCHONA ALKALOID-SUBSTRATE INTERACTIONS

4.1. INTRODUCTION

The use of cinchona alkaloids as chiral catalysts in asymmetric synthesis or as resolving agents is well established (see chapter 1). With detailed conformational information in hand, forthcoming from direct measurements in solution and in the solid state (see chapter 3), as well as from calculations (see chapter 2), we began a study of the conformational effects of alkaloid-substrate interactions. This knowledge is vital for the explanation of the function of the alkaloids in above mentioned areas. We have studied two cases; cinchona alkaloids used as chiral bases and as chiral ligands. In the first case the main interaction with the substrate is protonation of the tertiary quinuclidine nitrogen and subsequent formation of an ion pair between the protonated alkaloid and the deprotonated substrate molecule. In the second case cinchona alkaloids are used as chiral ligands. The main interaction with substrate molecules is the formation of a coordinative complex between the tertiary quinuclidine nitrogen and the metal atom of the substrate molecule.

In this chapter we report a NMR analysis of the effects of complexation (4.2) and protonation (4.3) on the conformation of the alkaloids in solution. Additional NMR data and results from a molecular dynamics study of alkaloid-aromatic thiol interactions are used to propose a transition state for the asymmetric Michael addition between aromatic thiols and conjugated alkenones (4.4).

4.2. COMPLEXATION WITH OSMIUM TETRAOXIDE

From the work of Sharpless[1] it is well known that cinchona alkaloid derivatives act as excellent chiral ligands in the asymmetric dihydroxylation reaction of olefins. The general reaction scheme is depicted in Figure 4.1. Pyridine is known to accelerate the rate of reaction of osmium tetraoxide with olefins[2]. Griffith[3] has observed that tertiary alkyl bridgehead amines, such as quinuclidine, form complexes with osmium tetraoxide which are much more stable than the corres-

ponding pyridine complex. Sharpless reasoned that replacement of these ligands with a similar chiral ligand might induce chirality in the diol product.

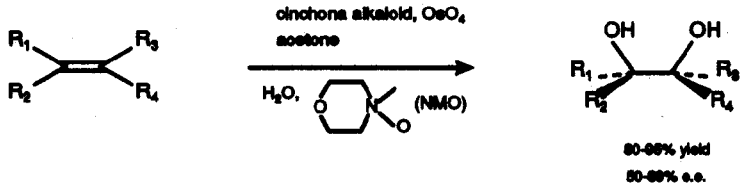

Figure 4.1 Asymmetric dihydroxylation of olefins with OsO_4 in the presence of cinchona alkaloids[1].

Thus the qualities of various cinchona alkaloid derivatives as chiral catalyst were investigated. In the first experiments stochiometric amounts of these cinchona alkaloids were used and e.e.'s up to 90% were achieved. Later the Sharpless group reported that by adding the olefin slowly to the reaction mixture higher e.e.'s and a faster reaction resulted. As a consequence, the scope of this asymmetric dihydroxylation process has been greatly enlarged and includes, besides olefins with aromatic substituents, those with simple alkyl substituents.

We have used 1-D and 2-D ^{1}H NMR techniques to study the interactions between osmium tetraoxide and (*p*-chlorobenzoyl)dihydroquinidine (1) and between osmium tetraoxide and (*p*-chlorobenzoyl)dihydroquinine (2). These two cinchona alkaloid derivatives have been applied successfully as chiral catalysts in the asymmetric dihydroxylation reaction. To be sure that complexation of osmium tetraoxide is as complete as possible before analyzing the NMR spectra of the osmium-alkaloid complexes, small amounts of osmium tetraoxide were gradually added to the alkaloid and the chemical shifts of the ortho protons of the quinuclidine nitrogen were plotted against the total osmium tetraoxide concentration. Asymptotic curves were obtained, which leveled off when maximum complexation had been reached. The NMR experiments were then performed at

this point. When osmium tetraoxide is added to a solution of 1 or 2 in $CDCl_3$, a yellow-orange complex is formed. In the ^1H NMR spectrum of this complex we could only observe averaged signals. Even by cooling down to -80°C in dichloromethane-d_2 no separate signals for complexed and uncomplexed 1 or 2 could be detected.

The formation of the osmium tetraoxide-alkaloid complex caused several changes in the ^1H NMR spectrum of 1 and 2 (see Table 4.1). These changes are partly due to direct shielding contributions of the heavy-metal oxo species. More important, however, is the reduction of the ^3J H_8H_9 coupling constant, accompanied by a large upfield shift of H_{11} in case of the quinidine derivative 2 (0.5 ppm), and of H_{10} in case of the quinine derivative 1 (0.2 ppm). The decrease of the ^3J H_8H_9 coupling constant suggests a change of the C_9-C_8 torsional angle upon complexation from an anti orientation between H_8 and H_9 to a gauche orientation. This rotation results in an open conformation 3 (see Figures 4.2 and 4.3). In the transition from the closed conformation 2 to the open conformation 3, the quinuclidine ring of 1 rotates around the C_9-C_8 bond thereby causing a change of the positions of H_{10} and H_{11} relative to the quinoline ring. In the open conformation 3 H_{11} is positioned in the shielding cone above the quinoline ring and experiences a strong upfield shift, whereas H_{10}, being in the same plane as the quinoline ring, suffers a downfield shift (in case of the quinine derivative 2 the positions of H_{10} and H_{11} are interchanged). Again, these observations suggest that the binding of osmium tetraoxide imposes a conformational change of the alkaloid from the closed conformation 2 to the open conformation 3. The conformation of (*p*-chlorobenzoyl)dihydroquinidine (1) osmium tetraoxide complex was further investigated by using NOE difference and NOESY spectra in $CDCl_3$. The presence of strong NOE's between H_8 with both H_5 and H_9 and an additional NOE between H_{10} and H_1 confirms that the osmium tetraoxide-alkaloid complex has the open conformation 3.

Table 4.1 ^1H NMR chemical shifts in ppm from internal TMS with precision of 0.03 ppm of osmium tetraoxide complexes and some cinchona alkaloids at 20°C.

proton	A	B	C	D
1	7.29	7.40	7.28	7.40
2	8.66	8.75	8.66	8.72
3	8.06	8.02	8.08	8.02
4	7.42	7.39	7.43	7.38
5	7.74	7.45	7.72	7.49
8	7.07	6.72	7.05	6.72
9	3.17	3.38	3.25	3.47
10	2.16	1.85	1.41	1.63
11	1.08	1.55	1.92	1.88
12	1.85	1.75	2.00	1.85
13	1.45-1.55	1.46	1.65	1.76
14	1.45-1.55	1.56	1.95	1.51
15	2.93	2.70	2.82	2.67
16	2.93	2.79	3.49	3.17
17	1.59	1.45	1.61	1.50
18	3.09	2.68	2.42	2.37
19	3.09	2.85	3.30	3.06
20	1.63	1.45	1.17	1.35
21	1.00	0.92	0.78	0.85
OMe	4.00	3.95	4.00	3.97
R-gr	7.49	7.46	7.51	7.44
	8.09	8.05	8.06	8.03

A=(*p*-chlorobenzoyl)dihydroquinidine + OsO_4 in $CDCl_3$.
B=(*p*-chlorobenzoyl)dihydroquinidine in $CDCl_3$.
C=(*p*-chlorobenzoyl)dihydroquinine + OsO_4 in $CDCl_3$.
D=(*p*-chlorobenzoyl)dihydroquinine in $CDCl_3$.
R-gr=*p*-chlorobenzoyl group.

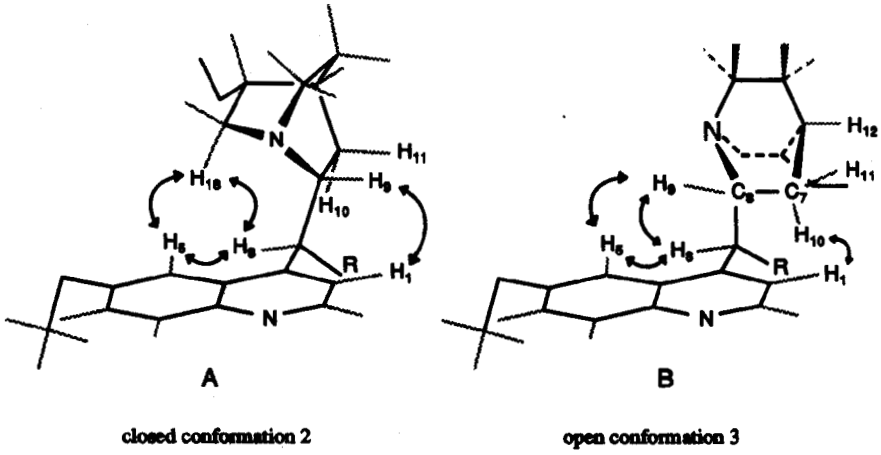

closed conformation 2 open conformation 3

Figure 4.2 Schematic drawing showing (A) the closed conformation 2 and (B) the open conformation 3 of a quinidine derivative (R=OH, OMe, p-ClBz, Cl).

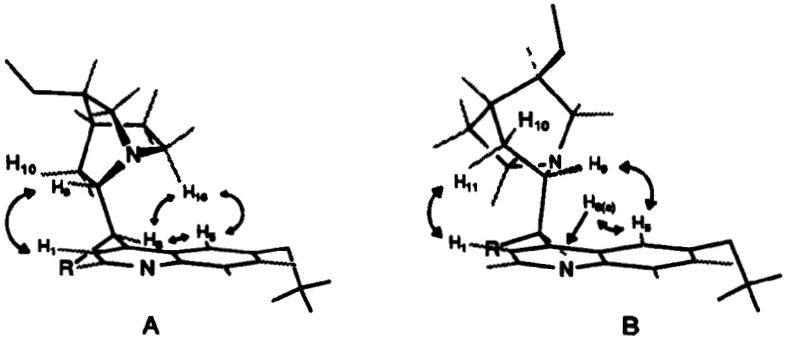

closed conformation 2 open conformation 3

Figure 4.3 Schematic drawing showing (A) the closed conformation 2 and (B) the open conformation 3 of a quinine derivative (R=OH, OMe, p-ClBz, Cl).

Similar investigations of the 2D NMR spectra of the other ester derivatives of the alkaloids (acetyldihydroquinidine, (dimethylcarbamoyl)dihydroquinidine, (*p*-

chlorobenzoyl)dihydroquinine) reveal that all these ester derivatives attain the open conformation 3 upon complexation with osmium tetraoxide. Note that the ester derivatives in absence of osmium tetraoxide possess a distinct preference for the closed conformation 2 (see chapter 3). A similar 1D- and 2D NMR analysis of the methoxy-dihydroquinidine osmium tetraoxide complex in $CDCl_3$ revealed that the initial equilibrium between closed conformation 2 and open conformation 3 is shifted completely towards the open conformer 3 upon complexation with osmium tetraoxide.

In an attempt to elucidate the mechanism of the asymmetric dihydroxylation reaction of olefins the Sharpless group recently reported a X-ray study of the coordination complex between (dimethylcarbamoyl)dihydroquinidine and osmium tetraoxide[4] . The interest in the geometry of this complex stems from kinetic evidence for a 1:1 alkaloid-osmium tetraoxide complex as the asymmetry-inducing oxidant in both the stochiometric and catalytic dihydroxylation reactions[5] . The X-ray analysis revealed the structure shown in Figure 4.4. The X-ray structure of the complex is in excellent agreement with our NMR results in solution. In the solid state the alkaloid attains the open conformation 3 and the quinuclidine nitrogen is coordinated to osmium. The geometry of the osmium tetraoxide-cinchona alkaloid complex is that of a trigonal bipyramid. Note that the conformational preference in solution and solid state of both free and complexed ester derivatives are similar. In chapter 3 (3.2.2) we have reported the X-ray of an uncomplexed ester derivative of quinidine (1). It was found in the closed conformation 2 in the crystal structure, while a NMR analysis of 1 revealed the same conformation in solution. Now, we see that complexation with osmium tetraoxide causes a conformational change to open conformation 3, both in solution and in the solid state. This knowledge of the geometry of both the free alkaloid and the alkaloid-osmium tetraoxide complex has not yet led to mechanistic insight of how chirality is transmitted to the substrate. Because the chiral centers of the alkaloid are quite remote from the oxo ligands there is so far no clear picture of the cause of enantioselectivity. This subject is currently under investigation in the Sharpless group.

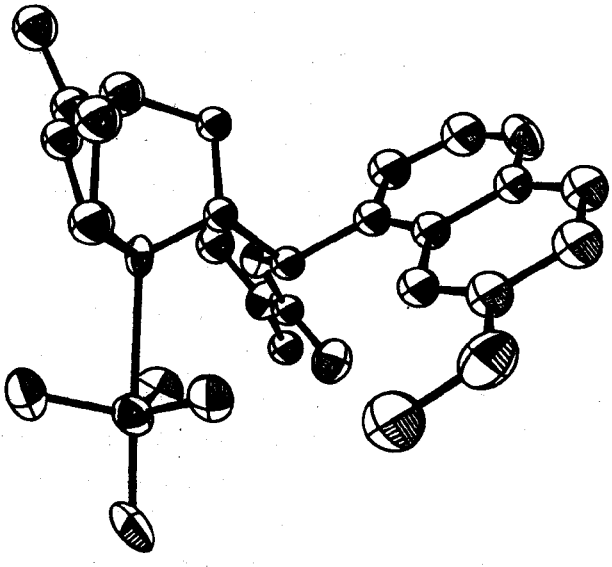

Figure 4.4 Ortep view of the osmium tetraoxide complex of (dimethylcarbamoyl)-dihydroquinidine[4].

Very recently Corey[6] has reported 'the origin of enantioselectivity in the dihydroxylation of olefins by osmium tetraoxide and cinchona derivatives'. Inspired by their mechanistic study of enantioselective vicinal dihydroxylations of olefins by a chiral 1,2-diamine complex of osmium tetraoxide[7] , they have extended their model in an attempt to encompass the cinchona alkaloid promoted reactions. In Corey's diamine-catalyzed reaction an octahedral C_2-symmetric complex of osmium tetraoxide and chiral 1,2-diamine is postulated as the reactive complex. It has been used to construct a model for a transition state assembly that provides a satisfactory explanation of the observed enantiomeric excess. The octahedral osmium complex is crucial in their model. Because the cinchona alkaloids form a trigonal bipyramidal complex with osmium tetraoxide (Figure

4.4), Corey proposed a dimerization of two such pentacoordinate species by a [2+2] cycloaddition of metal oxo linkages to an octahedral binuclear structure (Figure 4.6). According to Corey this chiral octahedral complex has very favorable three dimensional properties for enantioselective transition state formation, including possible C_2 symmetry and strong electronic and steric differentation between the three oxygens on each osmium. However, the proposed octahedral osmium complex is difficult to encompass in the mechanism proposed by Sharpless, depicted in Figure 4.5. In this mechanism the key intermediate is an osmium(VIII) trioxoglycolate complex (C), it occupies the central position at the junction between the two catalytic cycles. Although the details of chiral discrimination are not clearly explained by this mechanism, it seems more probable than Corey's idea's. Many of the events proposed in Figure 4.5 can be replicated by performing the process in a stepwise manner under stochiometric conditions. Evidence for A has been presented in this section (X-ray, NMR). Intermediates B and D have been isolated and characterized by the Sharpless group. Moreover, the reaction scheme presented in Figure 4.5 explains some crucial experimental observations, such as the increased e.e. by adding the olefin slowly to the reaction mixture, or by adding acetate ions as additive. The first catalytic cycle turns over faster and produces diol in high e.e., while the second cycle proceeds slower and exhibits low, to opposite enantiofacial selectivity. Slow addition of the olefin to the reaction mixture minimizes production of diol by the second cycle, thereby increasing the e.e. of the product. The idea is thus simply to give C sufficient time to hydrolyze so that the osmium catalyst does not get trapped into the second cycle by reacting with olefin. Increased e.e. by adding acetate ions to the reaction mixture are similarly explained, they facilitate hydrolysis of the osmate esters. All these facts are not explained by Corey's mechanism. Also the role of the amine N-oxide (NMO), which oxidizes B into C, is obscured in the Corey mechanism.

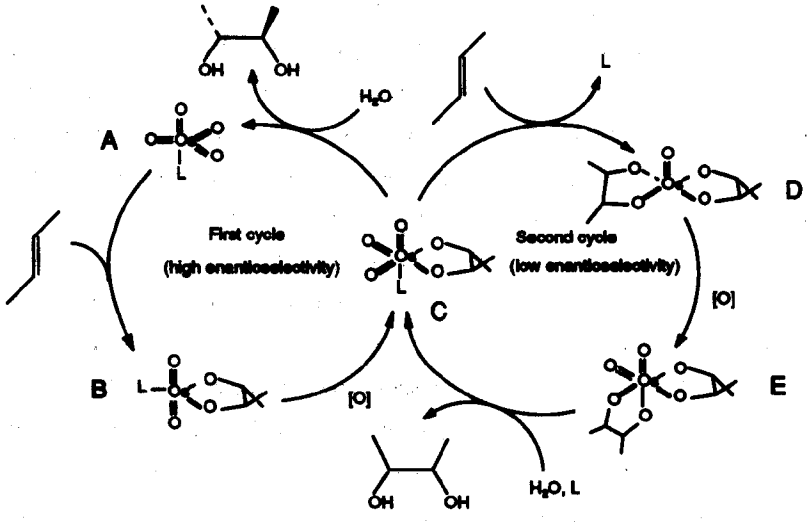

Figure 4.5 Proposed mechanism of the asymmetric dihydroxylation of olefins by Sharpless[1].

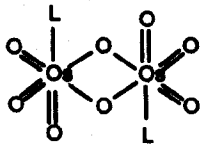

Figure 4.6 Octahedral binuclear osmium complex. L is (p-chlorobenzoyl)dihydroquinidine[6].

4.3 EFFECT OF PROTONATION ON THE CONFORMATION OF CINCHONA ALKALOIDS

In order to assess if similar conformational changes occur when the alkaloids are protonated, (*p*-chlorobenzoyl)dihydroquinidine (1) was treated with trifluoroacetic acid-d_1. To be sure that protonation is as complete as possible before analyzing the NMR spectra, small amounts of the acid were gradually added to the alkaloid and the chemical shifts of the ortho protons of the quinuclidine nitrogen were plotted against the total acid concentration. An asymptotic curve was obtained, which leveled off when maximum protonation had been reached. The NMR experiments were then performed at this point. The cinchona alkaloids contain two different basic sites, the quinoline and quinuclidine nitrogen. The quinuclidine nitrogen is the most basic one[8] . This is also apparent from the ^{1}H NMR spectrum of 1 in $CDCl_3$; it demonstrates that protonation of the first protonation step takes place on the quinuclidine nitrogen, as revealed by extensive line broadening of the α-hydrogens of the quinuclidine nitrogen, H_9, H_{15}, H_{16}, H_{18}, and H_{19} (Table 4.2). Furthermore, the ^{1}H NMR spectrum underwent several by now familiar changes: the ^3J H_8H_9 coupling constant almost disappeared, and the chemical shift of H_{11} moved 0.47 ppm upfield, all in agreement with a complete shift of the equilibrium between closed conformation 2 and open conformation 3 to the open conformation 3 (see Figure 4.2).

A similar NMR study of the conformational effects upon protonation of dihydroquinidine in $CDCl_3$ showed that in case of this hydroxy derivative no conformational transition occurs. After protonation of the quinuclidine nitrogen of dihydroquinidine it still attains the open conformation 3.

We have also investigated whether the conformational transition from the closed conformation 2 to the open conformation 3, induced by protonation, occurs in case of chloroquinine. NOESY spectra of chloroquinine with one equivalent DCl in CD_3OD revealed that no conformational transition is induced. NOE's were found between H_{11}-H_8, H_{11}-H_{14}, H_1-H_9, and H_8-H_5, but not between H_{11}-H_1 (see Figure 4.3). NOE-difference experiments with selective irradition of either H_1 or

H_{11} also did not reveal any NOE interaction between these two nuclei. The ^3J H_8H_9 coupling constant of 9.0 Hz is also in agreement with the closed conformation 2. However, the quinuclidine nitrogen experiences the presence of DCl, which follows from the upfield shifts of the α-protons of the quinuclidine nitrogen. H_9 shifts 0.98 ppm upfield, H_{16} 0.88 ppm, and H_{19} 0.52 ppm upfield, all relative to the chemical shifts of these protons in CD_3OD. In chapter 3 we have discussed the spectra of chloroquinine in C_6D_6 and $CDCl_3$ and noticed that the hydrogens H_1, H_5, H_8, and H_9 appeared as broad lines, whereas all other protons were observed as sharp lines. We argued that these observations indicate that the energy barrier between closed conformation 2 and open conformation 3 is increased to such a height that at room temperature averaged spectra are no longer recorded. On the NMR time scale conformational transitions between closed conformation 2 and open conformation 3 occur slowly. In CD_3OD, however, we do not observe this line broadening in the ^1H NMR of chloroquinine. Also after the addition of one equivalent DCl to the NMR tube all absorptions of chloroquinine appeared as sharp lines. These observations suggest that the energy barrier between closed conformation 2 and open conformation 3 decreases in the polar solvents CD_3OD and CD_3OD/DCl. Another possibility is that only conformation 2 exists in these solvents. We have demonstrated that after protonation all cinchona derivatives discussed so far are found in the open conformation 3, the only exception being the chloro derivative. This supports the strong preference of chloroquinine for the closed conformation 2.

Table 4.2. ^{1}H NMR chemical shifts in ppm from internal TMS with precision of 0.03 ppm of free and protonated *p*ClBzDHQD in $CDCl_3$ at 20°C.

proton	A	B
1	7.23	7.40
2	8.58	8.75
3	7.93	8.02
4	7.33	7.49
5	7.49	7.45
8	7.22	6.72
9	3.48	3.38
10	2.36	1.85
11	1.42	1.55
12	1.94	1.75
13	1.65-1.80	1.46
14	1.65-1.80	1.56
15	2.95-3.40	2.70
16	2.95-3.40	2.79
17	1.65-1.80	1.45
18	2.95-3.40	2.68
19	2.95-3.40	2.85
20	1.56	1.45
21	0.86	0.92
OMe	3.98	3.95
R-gr	7.40	7.46
	7.95	8.05

A=(*p*-chlorobenzoyl)dihydroquinidine + trifluoroacetic acid-d_1 in $CDCl_3$.
B=(*p*-chlorobenzoyl)dihydroquinidine in $CDCl_3$.

4.4 ASYMMETRIC MICHAEL ADDITION

4.4.1 Introduction

With this detailed conformational information on the catalysts in hand, we turned to the mechanism of the asymmetric Michael addition of aromatic thiols to conjugated cycloalkenones. These reactions under influence of a catalytic amount of cinchona or ephedra alkaloid have been studied extensively by Hiemstra[9] . The general reaction scheme is depicted in Figure 4.7. On the basis of considerable experimental data Hiemstra has proposed a model for the transition state of this reaction. This experimentally based model was derived from thorough analysis of the relationship between configuration of the major enantiomers of the products obtained, as well as a detailed examination of the kinetics of the reaction. Attempts to improve or design better alkaloid catalysts[10] revolved around this model, but were not successful.

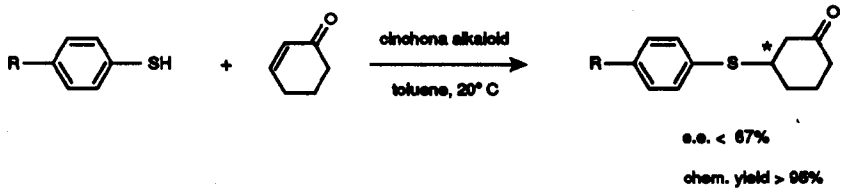

Figure 4.7 Asymmetric Michael addition between aromatic thiols and cyclohexenone.

As shown in Figure 4.8, a conformational transition of the catalyst quinine from the open conformation 3 to the closed conformation 2 was postulated on formation of an ion pair between the thiol and tertiary amine[9]. This conformational change allows the deprotonated sulfur of the benzenethiolate ion to interact with the electron cloud of the quinoline ring, giving a weak dispersion interaction. To reach

the transition state of the rate-determining step the π-orbital of the carbon double bond in 2-cyclohexenone has to approach the deprotonated sulfur. There are two possibilities, both of which are represented in Figure 4.9. Transition state A leads to product with the absolute configuration R and transition state B to product with S configuration. It was concluded that transition state A is more favorable than B because of severe steric interactions between the ring of cyclohexenone and the quinuclidine ring of quinine in transition state B. This steric repulsion is absent in transition state A. During the reaction product with R configuration is formed in excess, thus the proposed model for the transition state is in agreement with experimental results.

The importance of the cinchona alkaloid catalyzed reactions (see chapter 1), coupled with our eagerness to understand the mechanism of asymmetric inductions, induced us to extend this mechanistic study of cinchona alkaloid-substrate interactions.

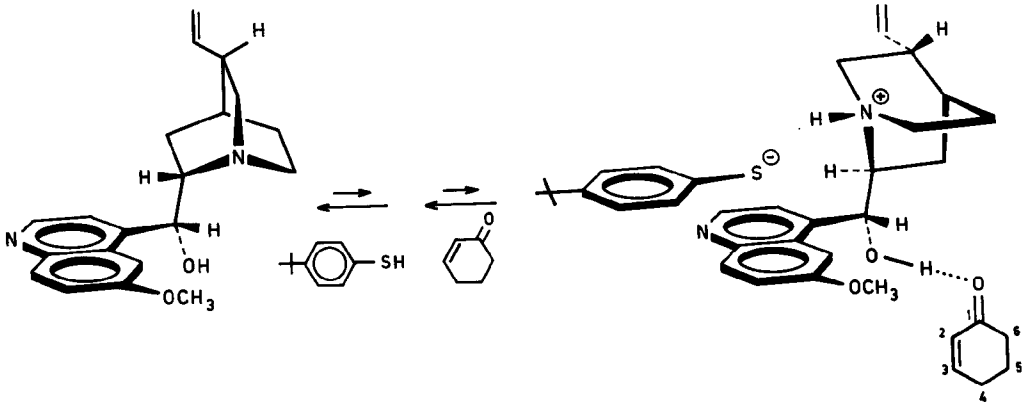

Figure 4.8 Postulated conformational transition of quinine, induced by thiol-quinine interactions on formation of an ion pair according to Hiemstra[9].

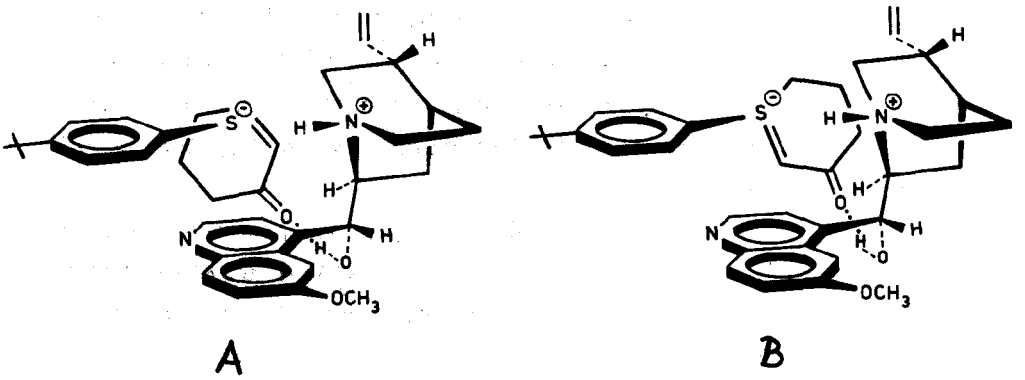

Figure 4.9 Two postulated orientations of cyclohexenone in the transition state according to Hiemstra[9]. Left, transition state A. Right transition state B.

Moreover, based on our recent knowledge (see 4.3) the proposed conformational shift of the alkaloid by Hiemstra, induced by protonation, from an open conformation 3 to a closed conformation 2 is unexpected. This conformational transition is crucial in his description of the mechanism of the asymmetric Michael addition. In the following sections we will describe the main results of an additional study of alkaloid-substrate interactions. The results have been obtained by molecular dynamics calculations (4.4.2), a molecular docking study (4.4.3), and a NMR study (4.4.4).

4.4.2 Molecular Dynamics Calculations

Molecular dynamics[11] (MD) provides a tool for studying the motions of a molecular system. The forces acting on the atoms are calculated from the first derivatives of the potential energy of the molecular system with respect to the atomic positions. By integration of Newton's equations of motion these forces can be used to calculate the dynamical properties of the system. A wide range of problems have been attacked successfully by MD, mostly involving nucleic acids[12] and proteins[13]. A great advantage of the MD method compared to a molecular mechanics energy minimization is that the presence of motional freedom allows the possibility of passing energy barriers. Thus MD searches a larger part of the configuration space and as a consequence generally ends up in a lower energy minimum than regular energy minimization techniques. A conventional energy minimization will stop at the first local minimum encountered.

All MD calculations described here were performed with the MD module of SYBYL[14] with the TRIPOS force field[15]. The Verlet method[16] is used for integration of the equations of motion. All simulations were performed at a constant temperature of 300 K, starting velocities were taken from a Boltzmann distribution and a time step of 1 fs was used. To avoid systematic oscillations and rapid changes during the constant temperature simulations a damping function (equation 4.1) was applied with a coupling constant τ=10 fs.

$$\lambda = 1 + \Delta t(T_0/T - 1)/2\tau \qquad 4.1$$

where,

Δt is time step.

T_0 is desired temperature.

T is actual temperature.

τ is coupling constant.

The temperature is gradually elevated from 0 K to the desired 300 K in time steps of 250 fs using temperature steps of 30 K.

We have taken both the open conformation 3 and closed conformation 2 of quinidine as the starting geometries in a MD study between quinidine and 4-methylbenzenethiol. The starting geometries of the alkaloid-thiol complexes were first optimized[17]. In these complexes we have deprotonated the thiol sulfur atom and protonated quinuclidine nitrogen. A formal negative charge is placed thereby on the thiol and a positive charge on quinidine. After equilibration at 300 K a 50 picosecond (ps) MD run has been calculated for both complexes. Figure 4.10 shows two resulting plots in which the distance between the thiol sulfur and the proton on the quinuclidine nitrogen is plotted as a function of time. It follows from these plots that during the simulation the thiol-alkaloid complexes remain intact. After some initial fluctuations the distances vary from 2.3 to 3.5 A and from 2.3 to 3.8 A for the closed conformation 2 and open conformation 3, respectively.

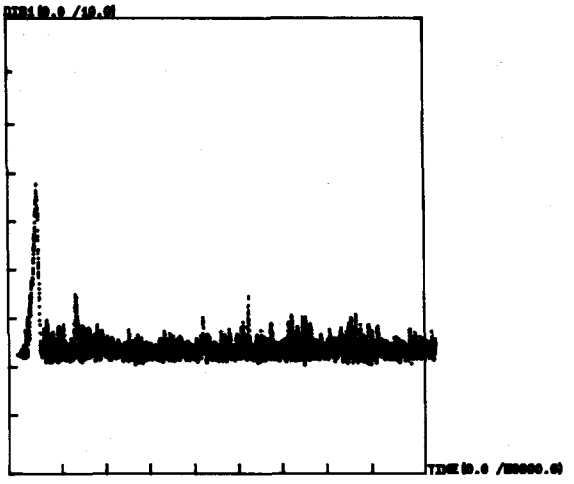

Figure 4.10A Distance between the thiol S and quinuclidine H (y-axis, from 0 to 10A) as a function of time (x-axis, from 0 to 50000 fs) for quinidine in the open conformation 3.

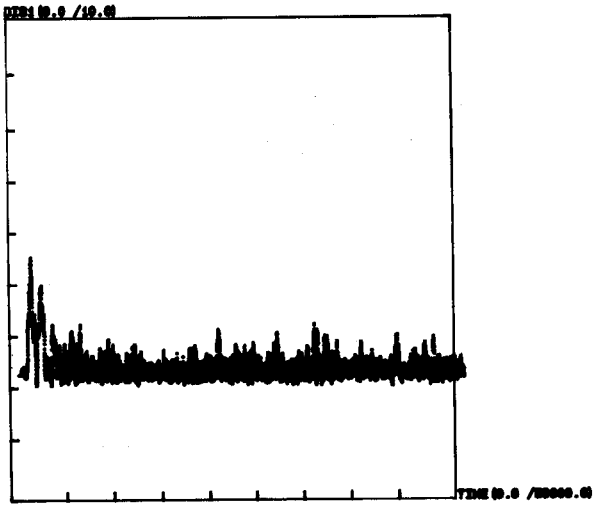

Figure 4.10B Distance between the thiol S and the proton on the quinuclidine nitrogen (y-axis, from 0 to 10A) as a function of time (x-axis, from 0 to 50000 fs) for quinidine in the closed conformation 2.

Figure 4.11 gives the potential energy of both systems as a function of time. The conformation of quinidine during the simulations is followed by monitoring the $C_3'C_4'C_9C_8$ (T_1) and $C_4'C_9C_8N_1$ (T_2) torsion angles. The resulting plots are given (respectively, Figure 4.12, and 4.13). During the simulation of quinidine with the initial open conformation 3 the average values of T_1 and T_2 are approximately -100 and 180°, respectively. These are characteristic for the open conformation 3. However, from Figure 4.13A, in which T_2 is plotted as a function of time, it can be observed that conformational changes occur to unrealistic conformations (T_2 of approximately 40°), but never to closed conformation 2.

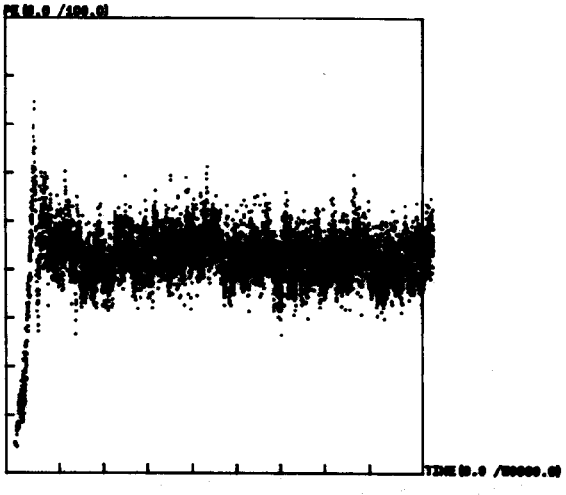

Figure 4.11A Potential energy (y-axis, from 0 to 100 kcal/mol) as a function of time (x-axis, from 0 to 50000 fs) for quinidine in the open conformation 3.

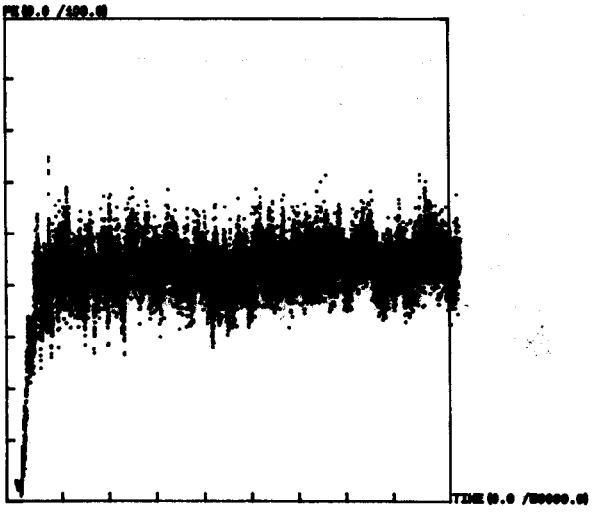

Figure 4.11B Potential energy (y-axis, from 0 to 100 kcal/mol) as a function of time (x-axis, from 0 to 50000 fs) for quinidine in the closed conformation 2.

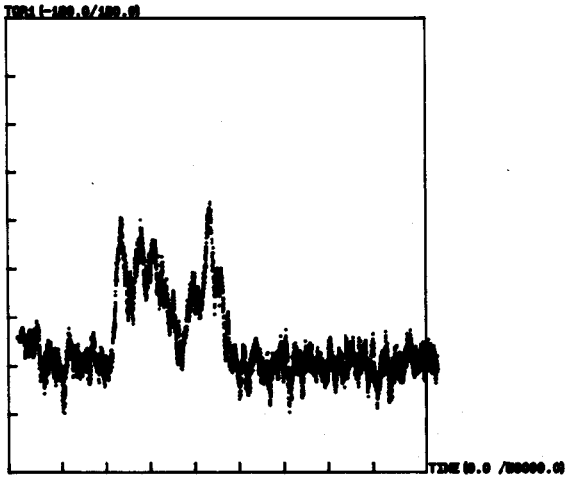

Figure 4.12A Torsion angle T_1 (y-axis, from -180 to 180°) as a function of time (x-axis, from 0 to 50000 fs) for quinidine in the open conformation 3.

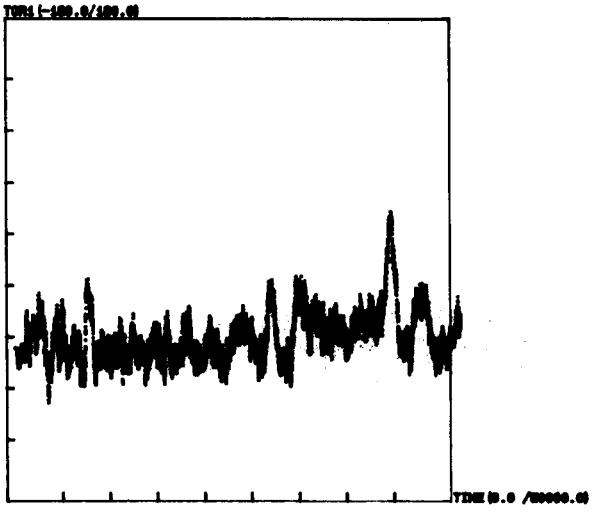

Figure 4.12B Torsion angle T_1 (y-axis, from -180 to 180°) as a function of time (x-axis, from 0 to 50000 fs) for quinidine in the closed conformation 2.

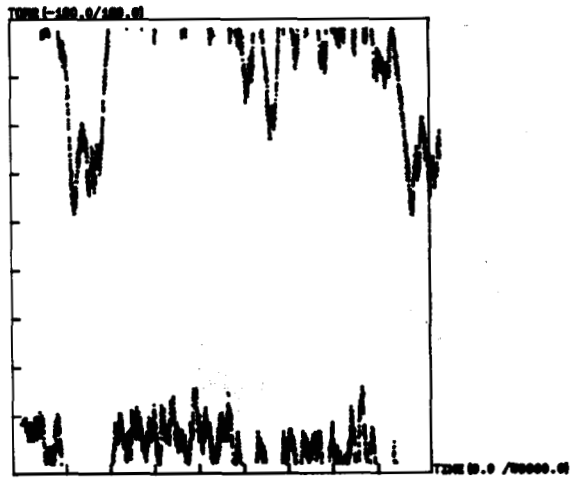

Figure 4.13A Torsion angle T_2 (y-axis, from -180 to 180°) as a function of time (x-axis, from 0 to 50000 fs) for quinidine in the open conformation 3.

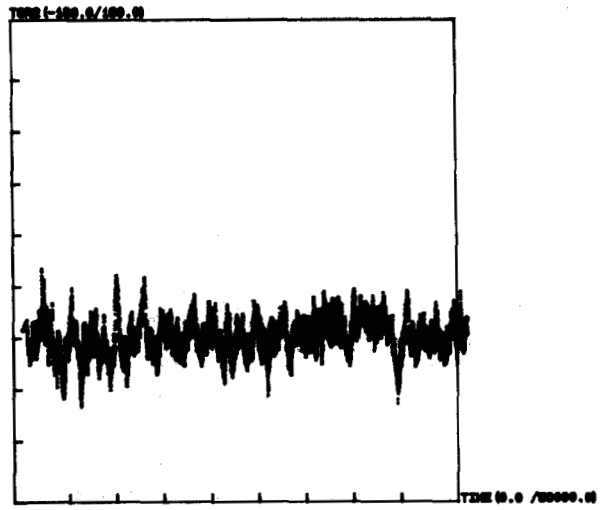

Figure 4.13B Torsion angle T_2 (y-axis, from -180 to 180°) as a function of time (x-axis, from 0 to 50000 fs) for quinidine in the closed conformation 2.

Figure 4.14 shows the distance between H_5 of the quinoline ring of the alkaloid and one of the ortho phenyl protons of the thiol as a function of time during the simulations for the open conformation 3 and closed conformation 2. In a following section we will demonstrate with a NMR study that an intermuclear NOE between these two protons exists. From Figure 4.14A it follows that the interatomic distance between both protons during the simulations is clearly larger when T_2 attains unrealistic values between approximately 40 and 160° (see Figure 4.13A). Figure 4.14B shows that the average distance between both protons is larger when the alkaloid attains a closed conformation 2.

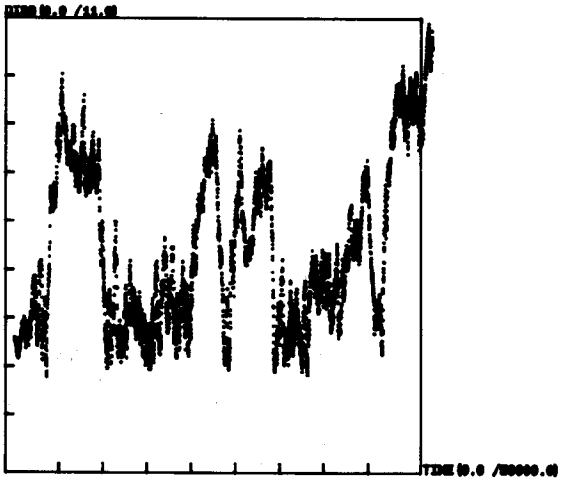

Figure 4.14A Distance between the H_5 proton (y-axis, from 0 to 11 A) of quinidine (with initial open conformation 3) and one of the ortho phenyl protons of the thiol as a function of time (x-axis, from 0 to 50000 fs).

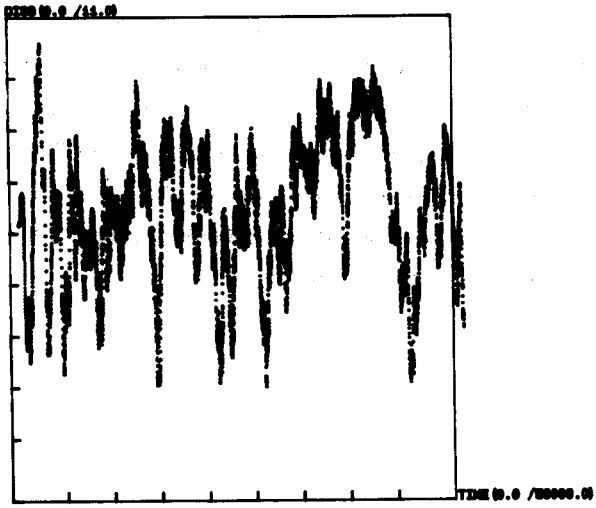

Figure 4.14B Distance between the H_5 proton (y-axis, from 0 to 11 A) of quinidine (with initial closed conformation 2) and one of the ortho phenyl protons of the thiol as a function of time (x-axis, from 0 to 50000 fs).

We conclude that these MD calculations have not given us a clear description of the alkaloid-thiol complex, in particular they did not support a discrimination between a complex with either the alkaloid in a closed or open conformation. We decided to perform an additional docking study (4.4.3) and NMR experiments (4.4.4) to elucidate the geometry of the complex.

4.4.3 Molecular Docking Study of a Quinine-Thiol Complex

We have investigated the possible orientations of thiol towards quinine with a molecular docking algorithm of CHEMX[18]. With this algorithm it is possible to simulate the motion of a structure about specified degrees of freedom relative towards another structure. We have restricted the docking study to quinine. As described already, three minimum energy conformations of quinine were predicted by the molecular mechanics calculations. One of these conformations (open conformer 3) was consistent with the NOESY data. This conformation of quinine was used as the starting conformation in a molecular docking study between quinine and 4-methylbenzenethiol. The geometry of the thiol was optimized with MMP2. To force both molecules to approach each other during the simulation, the thiol was deprotonated at the sulfur atom and quinine was protonated at the tertiary nitrogen of the bicyclic system. A formal negative charge is placed thereby on the thiol and a positive charge on quinine. At random five different starting orientations were chosen of 4-methylbenzenethiol with respect to quinine. With the algorithm just described, a molecular docking run was calculated for each of the five starting orientation. During each simulation 300 different orientations of the thiol with respect to quinine were generated. In Figure 4.15 those calculated 300 orientations of the thiol are plotted for one of the five runs. The molecular mechanics energies were calculated for all the 300 orientations and the results are summarized in Figure 4.16. On the y-axis the molecular mechanics energy is plotted and on the x-axis the distance between the sulfur of 4-methylbenzenethiol and the proton on the tertiary nitrogen of quinine. It can be seen from this plot that at the start of the calculation the distance between the two molecules is about 8 A. During the run both molecules approach; the distance decreases and simultaneously the energy decreases. The thiol tumbles into an energy well and although it still possesses much rotational and translational freedom, it no longer escapes from the well. By comparing the relative depths of these energy wells and examination of the corresponding structures of the quinine-thiol complexes the preferred orientation of the thiol towards quinine in the open conformation 3 was determined (see

Figure 4.17). As we will demonstrate in the next section, the calculated geometry of the alkaloid-thiol complex is in good accordance with a geometry that was deduced from NOESY experiments.

In the transition state the third molecule, cyclohexenone, is also involved. The same molecular docking approach was used to calculate the possible minimum energy orientations of cyclohexenone towards quinine and 4-methylbenzenethiol. We have used the results to propose two diastereomeric transition states, these will be discussed in section 4.4.4 (see Figures 4.18 and 4.19).

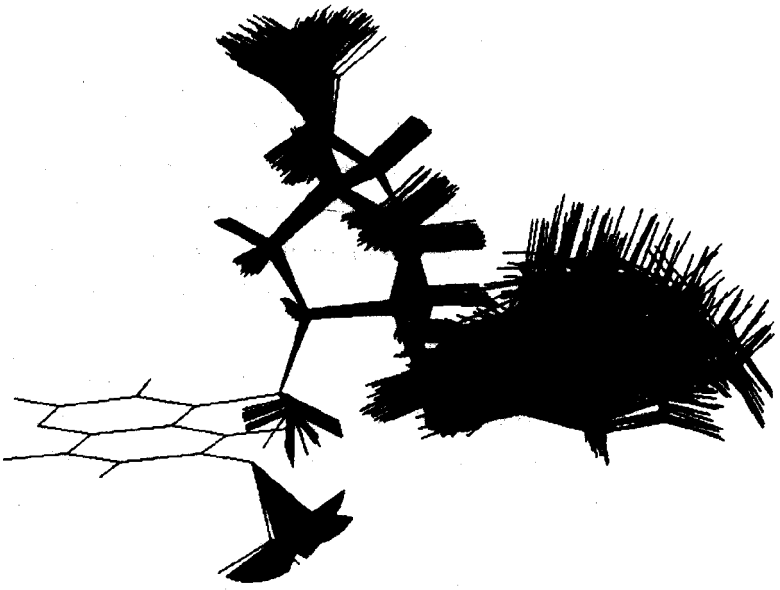

Figure 4.15 All the 300 calculated orientations between 4-methylbenzenethiol and quinine.

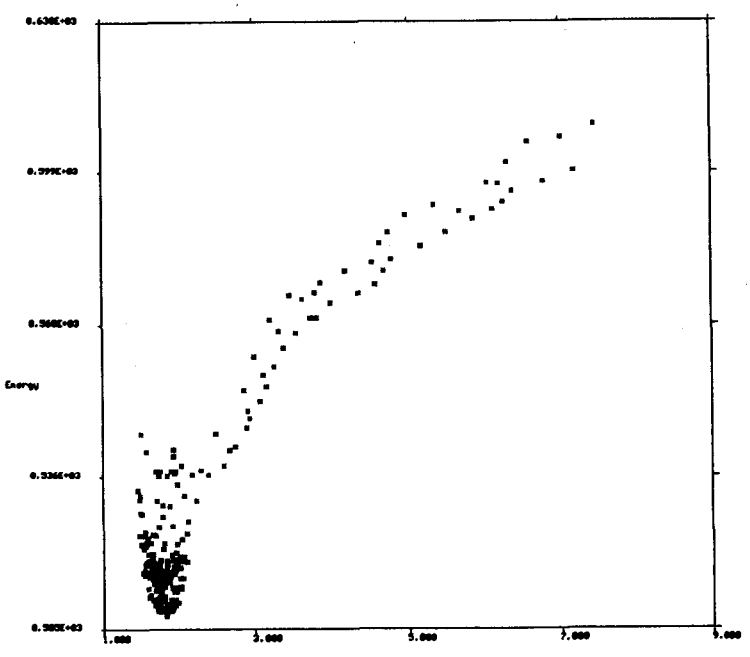

Figure 4.16 300 calculated orientations of 4-methylbenzenethiol and quinine plotted as a function of the MME and distance between the sulfur of the thiol and the proton on the tertiary nitrogen of quinine.

4.4.4 NMR Study of Alkaloid-Thiol Interactions

A conformational transition of the catalyst from the open conformation 3 to the closed conformation 2 is crucial in the description of the mechanism of the asymmetric Michael addition by Hiemstra. In a preceding section (4.3) we have described in some detail the conformational effects of cinchona alkaloids upon protonation by trifluoroacetic acid and DCl and concluded that, in general, the preference of cinchona alkaloids for the open conformation 3 increases upon protonation. These observations are hard to explain with the proposed

conformational transition, induced by protonation, in the mechanism of the Michael addition. Nevertheless, we attempted to obtain evidence for this conformational transition by NMR spectroscopy. The ^{1}H NMR and NOESY spectra of quinine and quinidine in the presence of 4-methylbenzenethiol, as well as *p*-tertiarybutylbenzenethiol (at various thiol/alkaloid ratios) were recorded in $CDCl_3$ and C_6D_6 at room temperature. Interpretation of the spectra, along the lines described before, did not reveal any indication for a conformational transition to the closed conformation 2 on formation of the ion pair. Moreover, observation of intermolecular NOE's between the phenyl protons of 4-methylbenzenethiol with the protons of the alkaloid skeleton (marked by arrows in Figure 4.17) allows placement of the thiol relative to the alkaloid skeleton as depicted in Figure 4.17. This orientation is the same as found with the docking study (4.4.3).

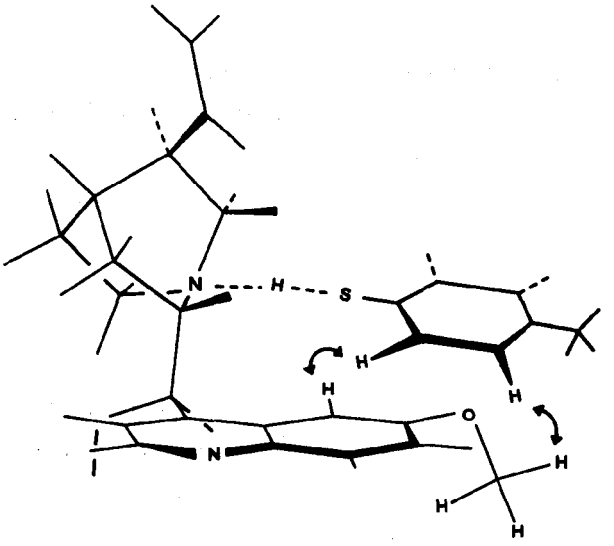

Figure 4.17 Quinine-thiol ion pair. The observed NOE interactions are indicated with arrows.

4.4.5 Discussion

Inspired by the recent conformational information, obtained by the combined MD, molecular docking, and NMR study, we propose two alternative diastereomeric transition states for the asymmetric Michael addition between aromatic thiols and conjugated enones[19] (Figure 4.7). These are depicted in Figures 4.18 and 4.19. We realize the possibility that the catalytic activity is derived solely from a minor species[20] . However, the geometries of both diastereomeric transition states depicted in Figures 4.18 and 4.19 are in good agreement with the NMR and the calculational results. As we will demonstrate, they are also in good agreement with the experimental findings of Hiemstra[9]. Moreover, the effect on the e.e. of the presence or absense of a methoxy group on the quinoline ring of the alkaloids can be explained. In the Hiemstra model[9], advanced some years ago on the basis of kinetic data and product studies, a transition from an open to a closed alkaloid conformation upon formation of an ion pair between the aromatic thiol and quinuclidine nitrogen was postulated. Evidence from the NMR analysis revealed that the open conformation 3 does not close upon protonation on the quinuclidine nitrogen, and the transition states, depicted in Figures 4.18 and 4.19, consistent with the newly available conformational information have been advanced.

Figure 4.18 shows the proposed transition state of the Michael addition between 4-methylbenzenethiol and 2-cyclohexenone, leading to product with S configuration. In this transition state steric repulsion exists between the ring moiety of cyclohexenone opposite to the double bond and the quinoline ring of the alkaloid (quinine). This steric hindrance is absent in the other transition state, depicted in Figure 4.19. This transition state leads to product with R configuration. The steric repulsion between cyclohexenone and quinine is not present now, because in this case the ring moiety of cyclohexenone, opposite to the double bond, is moved away from the quinoline ring of quinine.

These proposed geometries for both transition states are consistent with the observations of Hiemstra[9] that a larger fragment on the opposite side of the double bond in cyclohexenone increases the enantiomeric excess of the reaction. Hiemstra

found better results (higher e.e.'s) for the conjugated cycloheptenone, for 5,5-dimethyl-2-cyclohexenone, and for spiro[5.5]-undec-3-en-2-one (see Table 4.3). For all these molecules it can be expected that the steric repulsion between the catalyst and the ring moiety opposite the double bond of the enones increases with respect to cyclohexenone in the case of a reaction leading to product with S configuration. Because this steric repulsion is not present in the transition state leading to product with R configuration, these observations are in good agreement with the observed increase of the e.e.

The transition states depicted in Figures 4.18 and 4.19 also explain the influence of the methoxy group on the e.e. In the tight ion pair between the protonated catalyst and deprotonated thiol the sulfur atom of the aromatic thiol is negatively charged. This causes repulsive interactions with the nearby oxygen of the methoxy group. As a consequence the sulfur is pushed away from the quinoline ring which results in decreased discrimination between the two diastereomeric transition states.

We already mentioned that attempts to optimize the e.e. revolved around the previous model (Figure 4.9) of the transition state and failed[10]. Based on our new model, we will discuss novel possibilities to improve the success of this asymmetric Michael addition in chapter 6.

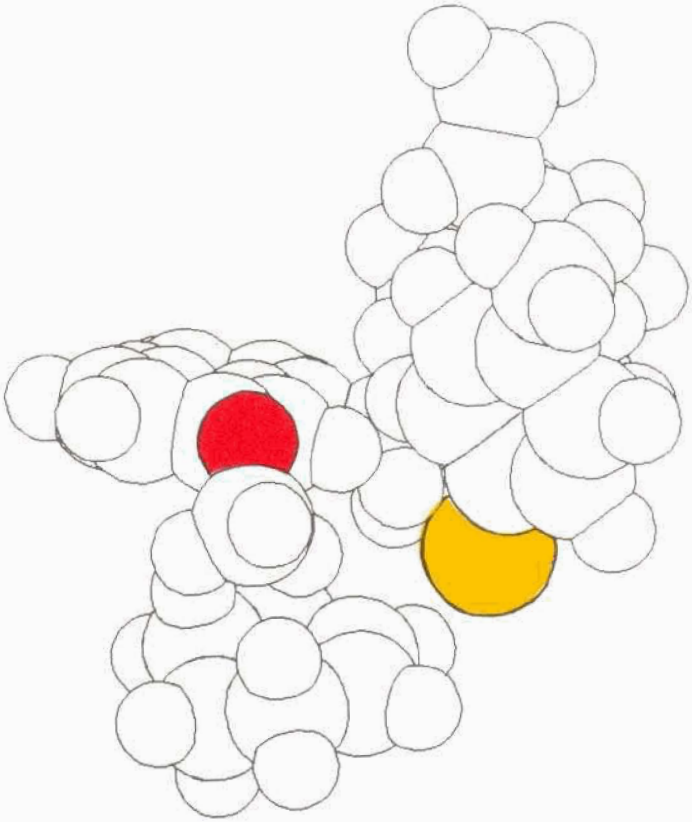

Figure 4.18 Proposed transition state of the Michael addition between 4-methylbenzenethiol (in front) and 2-cyclohexenone (under), catalyzed by quinine (partly hidden behind the thiol) leading to product with S configuration.

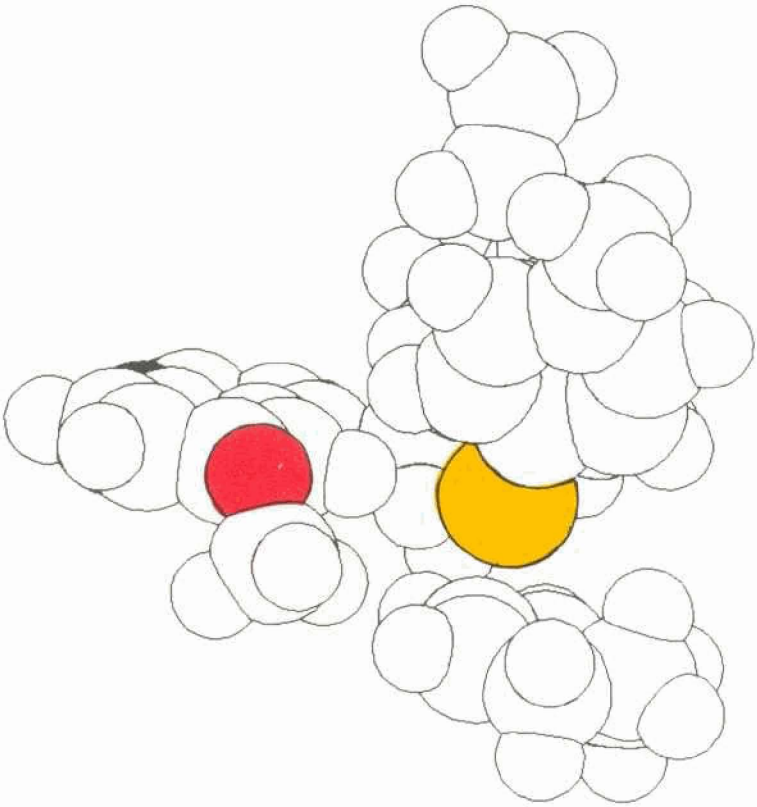

Figure 4.19 Proposed transition state of the Michael addition between 4-methylbenzenethiol (in front) and 2-cyclohexenone (under), catalyzed by quinine (partly hidden behind the thiol) leading to product with R configuration.

Table 4.3. Influence of the structure of the conjugated enone on the e.e of the asymmetric Michael addition[21] .

conjugated cyclealkenone	product R= 	e.e. (%)
	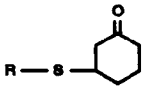	62
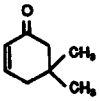	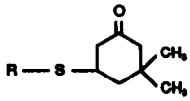	75
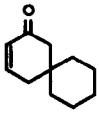	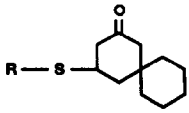	71
	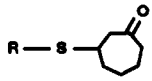	65

Table 4.3 Influence of the structure of the conjugated enone on the course of the asymmetric thiol addition.

4.5 EXPERIMENTAL PART

The NOESY and COSY spectra were measured as 0.05-0.1 M solutions in a 5 mm NMR tube. In case of the NOESY spectra the oxygen was removed by freeze-pump-thaw cycles and the NMR tubes were sealed under reduced pressure. All

spectra (^{1}H NMR, COSY, NOE-diff., and NOESY) were recorded using a Varian VXR-300 and VXR-500 spectrometer at 20°C. For each NOESY spectrum between 512 and 1024 FID's of between 1024 and 2048 data points each were collected. The spectral width was chosen as narrow as possible (about 3000 Hz). Corrections with weighting functions (mostly shifted sine bells[22]) were used before Fourier transformations in the t_2 and t_1 dimensions. All NOESY spectra were recorded in phase sensitive mode[23] . Energy calculations were performed on a MicroVAX 2000, a Convex C120[24] , or on a VAX 8650 computer[25] . The calculational results were evaluated with either CHEMX or SYBYL. All optimizations were performed either over all internal coordinates or the cartesian coordinate system was used, until the root-mean-square of the gradient of the energy was less than 0.5 kcal/A.

4.6 REFERENCES

1. Hentges, S. G.; Sharpless, K. B. *J. Am. Chem. Soc.* 1980, *102*, 4264.
   Jacobsen, E. J.; Marko, I; Mungall, W. S.; Schroder, G.; Sharpless, K. B. *J. Am. Chem. Soc.* 1988, *110*, 1968.
   Wai, J. S. M.; Marko, I.; Svendsen, J. S.; Finn, M. G.; Jacobsen, E. J.; Sharpless, K. B. *J. Am. Chem. Soc.* 1989, *111*, 1123.
   Lohray, B. B.; Kalanter, T. H.; Kim, B. M.; Park, C. Y.; Shibata, T.; Wai, J. S.; Sharpless, K. B. *Tetrahedron Lett.* 1989, *30*, 2041.
   For cinchona alkaloids as chiral ligands see also e.g.:
   Cabaret, D; Welvart, J. *J. Organomet. Chem.* 1974, *78*, 295.
   Boireau, G; Abenhaim, D; Henry-Basch, E. *Tetrahedron* 1979, *35*, 1457.
   Bergstein, W; Kleeman, A; Martens,J. *Synthesis* 1981, *76*, and references therein.
   Ohgo, Y; Natori, Y.; Takeuchi, S; Yoshimura, J. *Chem. Lett.* 1974, *78*, 1327.
2. Criegee, R. *Justus Liebigs Ann. Chem.* 1933, *522*, 75.
   Criegee, R.; Marchand, B.; Wannowius, H. *Justus Liebigs Ann. Chem.* 1942, *550*, 99.

Footnote Cont. Next Page

Footnote 3 Cont.

3. Cleare, M. J.; Hydes, P. C.; Griffith, W. P.; Wright, M. J. *J. Chem. Soc, Dalton Trans* 1977, 941.
4. Svendsen, J. S.; Marko, I.; Jacobsen E. N.; Rao, Ch. P.; Bott, S.; Sharpless, K. B. *J. Org. Chem.* 1989, *54*, 2264.
5. Jacobsen, E. N.; Marko, I.; Svendsen, J. S.; Sharpless, K. B. *J. Am. Chem. Soc.* 1989, *111*, 737.
6. Corey, E. J.; Lotto, G. I. *Tetrahedron Lett.* 1990, *19*, 2665.
7. Corey, E. J.; Jardine, P.; Yuen, P.; Virgil, S.; Connell R. D. *J. Am. Chem. Soc.* 1989, *111*, 9243.
8. Kolthoff, J. *Biochem. Z.* 1925, *162*, 289.
9. Hiemstra, H.; Wijnberg, H. *J. Am. Chem. Soc.* 1981, *103*, 417.
   Hiemstra, H. Ph. D. Thesis, Groningen, 1980.
10. Pluim, H. Ph. D. Thesis, Groningen, 1982.
11. Karplus, M.;McCammon, J. A. *Ann. Rev. Biochem.* 1983, *52*, 263.
    McCammon, J. A.; Harvey, S. C. *Dynamics of Proteins and Nucleic acids* Cambridge Univerity Press, Cambridge, 1987.
12. Singh, U. C.; Weiner, S. C.; Kollman, P. *Proc. Natl. Acad. Sci. USA* 1985, *82*, 755.
    Harvey, S. C.; Prabhakaran, M.; Mao, B.; McCammon, J. A. *Science* 1984, *223*, 1189
13. Hermans, J. *Molecular Dynamics and Protein Structure* Polycrystal Bookservice P. O. Box 27, Western Springs, USA, 1985
    Elber, R; Karplus, M. *Science* 1987, *235*, 318.
14. SYBYL, Molecular Modelling Software version 5.3, Tripos Associates, Inc. St.Louis, Missouri.
15. Clark, M.; Cramer, R. D.; Opdenbosch N. *J. Comp. Chem.* 1989, *10*, 982.
16. Verlet, L. *Phys. Rev.* 1967, *159*, 98.
17. Maximin, the energy minimization algorith of SYBYL, is used for the geometry optimizations with the TRIPOS force field
18. CHEMX, developed and distributed by Chemical Design Ltd., Oxford, England.
19. Dijkstra, G. D. H.; Kellogg, R. M.; Wijnberg, H. *Recl. Trav. Chim. Pays-Bas* 1989, *108*, 195.
20. e.g. Halpern demonstrated in his study of the rhodium-bisphosphine catalyzed

Footnote Cont. Next Page

Footnote 20 Cont.

asymmetric hydrogenation of α-aminoacrylic acid derivatives that the major product was derived from the minor rhodium hydride intermediate, Halpern, J. *Science* 1982, *217*, 401.

21. Hiemstra, H. Ph. D. Thesis, Groningen, 1980, p.27.
22. Levitt, M. H.; Radloff, C.; Ernst, R. R. *Chem. Phys. Lett.* 1985, *114*, 435.
23. States, D. J.; Haberkorn, R. A.; Ruben, D. J. *J. Magn. Reson.* 1982, *48*, 286.
24. Computer and software are provided by the Dutch CAOS-CAMM center, University of Nijmegen, the Netherlands.
25. These calculations were performed on a VAX 8650 computer of the computer centre of Duphar B.V., Weesp, the Netherlands.

5

MO ANALYSIS ON CINCHONA AND EPHEDRA ALKALOIDS

5.1 INTRODUCTION

The results of the conformational study on cinchona and ephedra alkaloids presented in the preceding chapters have revealed valuable and unexpected information. We have seen that, although the quinidines and quinines display very similar conformational behavior, their conformations can be influenced by varying the substituent at the benzylic position, by changing its configuration, by protonating

the quinuclidine nitrogen, by the nature of the solvent, or by complexation with osmium tetraoxide. The NMR analysis has revealed that chloro cinchona alkaloid derivatives (R=Cl, see Figure 5.1) attain the closed conformation 2 almost exclusively in solution. For the ester derivatives (R=OAc, *p*-ClBz) a definite preference was found for the closed conformation 2. But in this case the open conformation 3 was found as well. The equilibrium between both conformers 2 and 3 is solvent dependent. For the methoxy derivatives (R=OMe) the distinct preference for the closed conformation 2 has vanished. Either conformation 2 or 3 is now found in excess, depending on the solvent. The cinchona alkaloids themselves (R=OH) prefer the open conformation 3 in all solvents. The fact that epicinchona alkaloids are found in open conformation 4 suggests that the configuration of the benzylic C_9 position is important in determining the overall conformation. Finally, we have seen that complexation at, or protonation of the quinuclidine nitrogen induces conformational transitions from closed conformation 2 to open conformation 3.

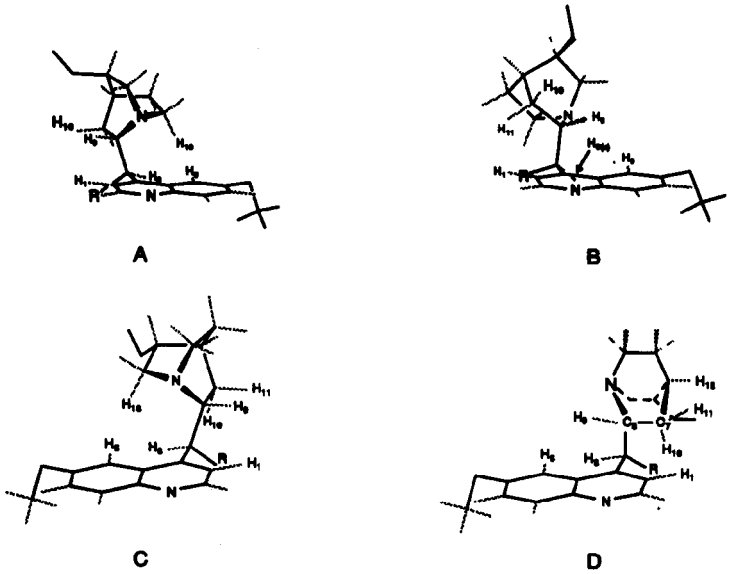

Figure 5.1 Schematic drawings showing (A) the closed conformation 2 and (B) the open conformation 3 of a quinine derivative, and (C) the closed conformation 2 and (D) the open conformation 3 of a quinidine derivative(R=OH, OMe, p-ClBz, OAc, Cl).

In addition, we have presented a molecular mechanics analysis on ephedrine and N-methylephedrine (chapter 2) and demonstrated the similarity between their minimum energy conformations with those of the cinchona alkaloids.

In this chapter we will discuss the results of a molecular orbital (MO) study of some cinchona alkaloids as well as of model compounds of these (5.2), and of ephedrine and N-methylephedrine (5.3). With this calculational approach we will try to explain in some detail the experimentally obtained conformational data[1].

5.2 MO ANALYSIS ON CINCHONA ALKALOIDS AND MODEL COMPOUNDS

5.2.1 MO Calculations

Quantum chemical calculations can provide detailed insight into the electronic nature of a molecular structure and allow one to analyze phenomena not yet parameterized for molecular mechanics. The Schrödinger equation of a given molecular system can be solved either with no approximations (ab initio) or with the introduction of some approximations (semiempirical). Semiempirical treatments such as PM3[2], AM1[3], MNDO[4], CNDO[5], INDO[6], EHT, MINDO[7], and PCILO[8] are some of the most popular semiempirical programs, whereas GAUSSIAN[9] and HONDO[10] are typical ab initio programs. AMPAC and MOPAC are QCPE packages that include the PM3, AM1, MNDO, and MINDO programs. We have used the MOPAC and VAMP[11] packages for the calculations described in this chapter. We have already mentioned in the introduction that the main objective of our calculations is to find explanations of the experimentally obtained conformational data. Note that such a calculational approach is characterized by enormous amounts of numbers generated by the programs which must be interpreted with care. Therefore, we have payed more attention to the variations and the trends of the various calculated molecular properties than to their absolute values.

5.2.2 MO Calculations on Cinchona Alkaloids

We have optimized the complete structures of some cinchona alkaloids using the VAMP package. Starting conformations obtained from the molecular mechanics calculations (chapter 2) were used for these optimizations over all internal coordinates. The VAMP package provides three Hamiltonians; MNDO, AM1, and PM3. First, we have performed some initial calculations to decide which Hamiltonian is able to give the best correlation with our experimental findings. Therefore, the energy differences between the open conformation 3 and the closed conformation 2 have been calculated for quinidine derivatives with 4 different benzylic substituents; chloro (ClQD), acetyl (OAcQD), methoxy (OMeQD), and hydroxy (QD). The results are summarized in Table 5.1.

Table 5.1 Heat of formation and heat of formation differences (kcal/mol) between the open conformation 3 and closed conformation 2 of some quinidine derivatives. (_2 refers to closed conformation 2, _3 refers to open conformation 3).

	MNDO	AM1	PM3	ΔE MNDO	ΔE AM1	ΔE PM3
ClQD_2	35.15	27.50	13.06	1.8	1.8	2.6
ClQD_3	37.70	29.31	14.85			
OAcQD_2	-30.34	-45.8	-58.13	0.9	-0.3	-0.7
OAcQD_3	-31.04	-46.1	-57.28			
OMeQD_2	0.07	-3.8	-15.46	2.5	-0.9	1.1
OMeQD_3	0.99	-4.7	-12.92			
QD_2	0.07	-9.46	-20.83	2.3	-1.9	0.9
QD_3	0.99	-11.40	-18.58			

We know from our experimental findings (chapter 3) that the preference for the closed conformation 2 depends on the nature of the benzylic substituent and increases in the following order: hydroxy < methoxy < acetyl < chloro. It follows from the energy differences between conformations 3 and 2, given in Table 5.1, that this trend is perfectly reflected by the AM1 calculations. Based on this knowledge we decided to perform all subsequent calculations with the AM1 Hamiltonian.

At first sight it is difficult to imagine why the nature of the benzylic substituent and its configuration are so important in determining the conformation. Examination of molecular models results in more confusion, for the benzylic substituent is situated in the 'free space' under the quinoline and quinuclidine ring. However, from Table 5.2, in which some calculated bond lengths and angles are summarized, we see that small but significant differences exist with regard to the geometry around C_9.

Table 5.2 Result of VAMP AM1 optimizations of QD, OMeQD, OAcQD, and ClQD in the closed conformation 2 and open conformation 3.

benzylic substituent	C_4-C_9[a]	C_9-R[a]	C_9-H[a]	$C_3C_4C_9$	C_4C_9R	$C_4C_9C_8$
QD_2	1.504	1.428	1.125	118.6	110.5	111.9
QD_3	1.506	1.423	1.130	120.3	111.1	110.3
OMe_2	1.504	1.436	1.124	118.8	110.4	111.5
OMe_3	1.506	1.431	1.129	120.7	110.9	110.1
OAcQD_2	1.502	1.447	1.124	118.9	106.4	112.3
OAcQD_3	1.504	1.439	1.130	121.1	109.4	110.0
ClQD_2	1.492	1.779	1.120	119.7	109.1	112.8
ClQD_3	1.498	1.775	1.124	121.2	109.9	110.2

[a] bond length in Angstrom.

In the next section we will describe a detailed analysis of the influence of the benzylic substituents on the geometry of this position and the consequences of it.

5.2.3 MO Calculations on Model Compounds

We have constructed model compounds in a calculational approach to elucidate the role of the benzylic position C_9. The structures of the model compounds, which are characterized by five different substituents R at C_9, are given in Figure 5.2. The substituents were chosen such that each model compound resembles one of the cinchona alkaloid derivatives that we have studied. The geometries of the five model compounds were constructed in CHEMX[12] and optimized with MMP2[13]. Then the geometries were refined with the VAMP molecular orbital package using the AM1 Hamiltonian by optimization over all internal coordinates. All subsequent calculations were also performed with VAMP (using the AM1 Hamiltonian).

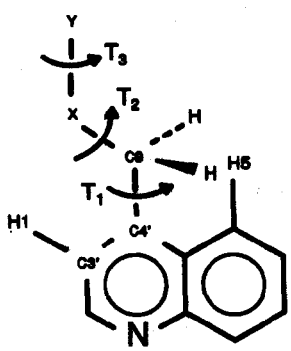

Compound	X	Y
A	H	-
B	O	H
C	O	Me
D	O	C(=O)–Me
E	Cl	-

Figure 5.2 Structures of the model compounds that have been considered. T_1=C3'C4'C9X, T_2=C4'C9XY, and in case of compound D: T_3=C9OC(O)C(H_3).

Compound A. The energy dependence on the torsion angle T_1 has been computed by varying T_1 in steps of 10° (see Figure 5.2 for the definition of T_1). In the optimized starting geometry $T_1=0^o$. The energy has been calculated at each point. The resulting plot, depicted in Figure 5.3, of the energy against T_1 reveals three minimum energy conformations at $T_1=0$, $T_1=120$, and $T_1=240^o$, all three of which are identical because of symmetry. The minima place one of the benzylic protons in the same plane as the quinoline proton H_1. The energy barriers of 2.3 kcal/mol at $T_1=60$, 180, and 300° are caused by steric repulsion between one of the benzylic protons and the quinoline proton H_5.

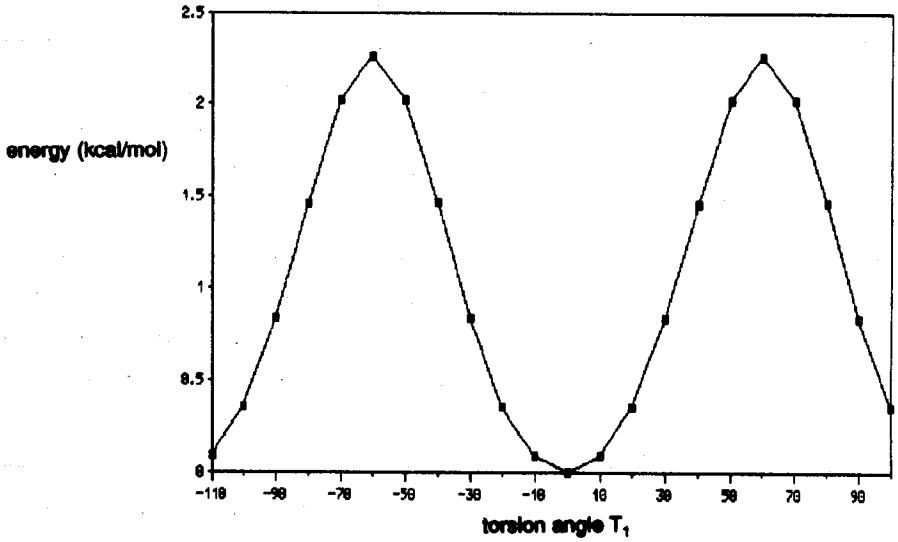

Figure 5.3 Energy (kcal/mol) as a function of T_1 for model compound A.

Compound B. Two conformations have been optimized, one called OH-0-180, starting with $T_1=0^o$ and $T_2=180^o$, and one called OH-120-180, starting with $T_1=120^o$ and $T_2=180^o$. In Table 5.3 some results of these optimizations are summarized. The AM1 calculations predict conformation OH-0-180, with the hydroxy oxygen oriented in the plane of the quinoline ring and directed towards

H_1 (Figure 5.2) to be 1.3 kcal/mol more stable than conformer OH-120-180, in which one of the benzylic protons occupies this position.

Next the preferred orientation of the hydroxyl proton has been investigated. For both OH-0-180 and OH-120-180 T_2 was varied in steps of 20° and the AM1 energy has been calculated at each point. The results of these calculations are summarized in plots of energy against T_2 (Figure 5.4). From these plots it follows that the orientation of the hydroxyl proton is able to affect the energy considerably. For OH-0-180 two absolute minimum energy conformations exist at approximately $T_2=60^o$ and $T_2=300^o$. One relative minimum is found at approximately $T_2=180^o$. This staggered conformation has both oxygen lone pairs oriented between a C-C and a C-H bond, whereas in the two absolute minima one of the two oxygen lone pairs is situated between two C-H bonds, which leads to less electronic repulsion. In the case of OH-120-180 the staggered conformer with $T_2=60^o$ is an energy maximum, because of steric repulsion between the hydroxyl proton and H_5 of the quinoline ring.

The geometries of both OH-0-180 and OH-120-180 have been optimized again, but now starting with $T_2=300^o$. The resulting conformations are called OH-0-300 and OH-120-300, respectively. In Table 5.3 the most important results of these optimizations are summarized. It follows that the initial energy difference between conformers with $T_1=0^o$ and $T_1=120^o$ decreases from 1.3 to 0.5 kcal/mol upon changing T_2 from 180° to 300°. Next all four optimized geometries have been used as starting conformers to study the energy dependence on T_1. Of special interest is plot B of Figure 5.5. This plot shows the energy dependence on T_1 for OH-0-300. Conformer OH-0-300 resembles the open conformation 3 of quinidine. In the closed conformation 2 of quinidine T_1 changes from about 0 to 60°. Thus the height of the energy barrier of plot B of Figure 5.5 at $T_1=60^o$ relative to $T_1=0^o$ is important, because it reflects the amount of destabilization on going from the open conformation 3 to the closed conformation 2. These calculations predict an energy difference of 3.5 kcal/mol.

Table 5.3 Results of VAMP AM1 optimizations for model compound B.

	OH-0-180	OH-120-180	OH-0-300	OH-120-300
energy[a]	2.6	3.9	0.3	0.9
T_1	0.1	121.5	7.0	125.8
T_2	180.0	170.5	-62.2	-53.1
C_9O[b]	1.421	1.421	1.413	1.415
C_9H[b]	1.126	1.126	1.126	1.126
$C_4'C_9$	1.494	1.497	1.495	1.497
$C_4'C_9O$	109.3	109.2	113.6	113.8
$C_4'C_9H$	109.7	109.9	109.9	110.1
$C_3'C_4'C_9$	121.9	119.8	121.6	120.0

[a] energy in kcal/mol.
[b] bond length in Angstrom.

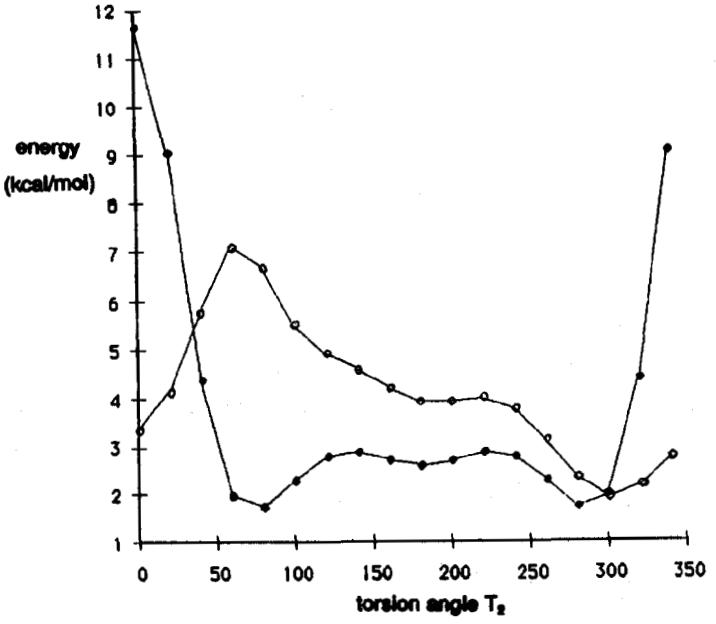

Figure 5.4 Energy (kcal/mol) as a function of T_2 for model compounds OH-0-180 (•) and OH-120-180 (o).

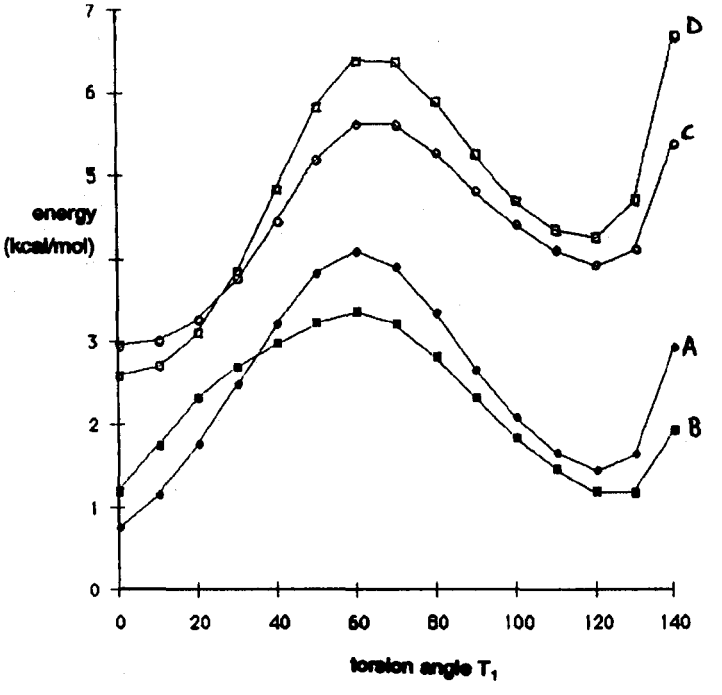

Figure 5.5 Energy (kcal/mol) as a function of T_1. (A), OH-0-180; (B), OH-120-180; (C), OH-0-300; (D), OH-120-300

Compound C. Two conformations have been optimized, one called OMe-0-180, starting with $T_1=0^o$ and $T_2=180^o$, and one called OMe-120-180, starting with $T_1=120^o$ and $T_2=180^o$. Some results of these optimizations are summarized in Table 5.4. Conformer OMe-0-180 with the oxygen oriented in the plane of the quinoline ring and directed towards H_1 is predicted to be 1.2 kcal/mol more stable than conformer OMe-120-180.

The energy dependence for OMe-0-180 as a function of T_2 has been calculated by stepwise variation of T_2 in steps of 10°. The results of these calculations suggest that one absolute minimum exists at approximately $T_2=180^o$. The other two

staggered conformations at approximately T_2=80° and T_2=270° are relative minima.

Conformation OMe-0-180 was optimized again, this time starting with T_2=80°. The optimized geometry is called OMe-0-80 and some results are summarized in Table 5.4. Thus after optimization over all internal coordinates OMe-0-80 turns out to be 0.9 kcal/mol more stable than OMe-0-180. Because conformer OMe-0-80 resembles the open conformation 3 of the methoxy derivative of quinidine the energy dependence on T_1 was further investigated. Both in OMe-0-80 and OMe-0-180 T_1 has been varied in steps of 10° and the AM1 energy has been computed at each point. The plots of Figure 5.6 summarize the results of these calculations. In case of OMe-0-80 the energy barrier on going from T_1=10° to T_1=60° is estimated to be 3.1 kcal/mol.

Table 5.4 Results of VAMP AM1 optimizations for model compound C.

	OMe-0-180	OMe-120-180	OMe-0-80
energy[a]	6.6	7.8	5.7
T_1	2.4	120.3	6.7
T_2	174.0	180.1	81.9
C_9O[b]	1.429	1.429	1.421
C_9H[b]	1.125	1.125	1.125
$C_4'C_9$	1.493	1.495	1.495
$C_4'C_9O$	109.1	108.8	113.5
$C_4'C_9H$	110.1	110.4	109.8
$C_3'C_4'C_9$	122.1	119.8	121.8

[a] energy in kcal/mol.

[b] bond length in Angstrom.

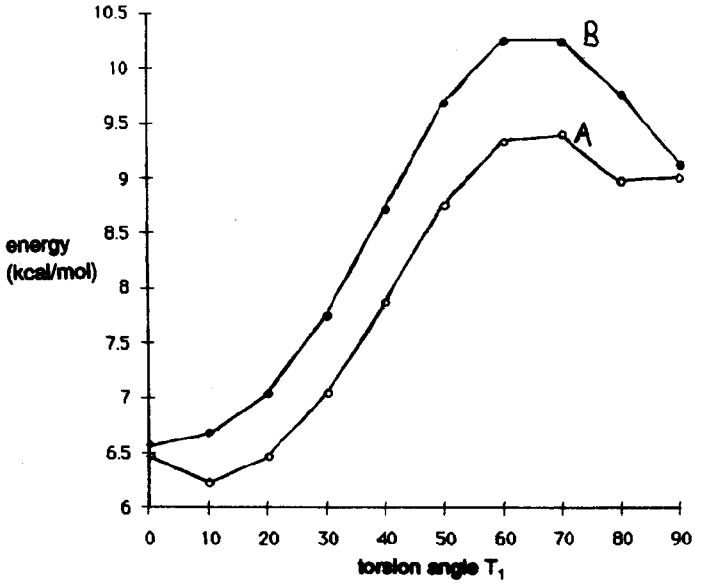

Figure 5.6 Energy (kcal/mol) as a function of T_1. (A), for OMe-0-80; (B), for OMe-0-180

Compound D. The three important dihedrals of D are defined in Figure 5.2. An analysis similar to that described for the other model compounds has been followed. Firstly, five conformations have been optimized; OAc-0-180-0 (T_1=0°, T_2=180°, T_3=0°); OAc-120-180-0 (T_1=120°, T_2=180°, T_3=0°); OAc-0-180-180 (T_1=0°, T_2=180°, T_3=180°); OAc-120-180-180 (T_1=120°, T_2=180°,T_3=180°), and OAc-0-60-180 (T_1=0°, T_2=60°, T_3=180°). The most important results of these optimizations are summarized in Table 5.5.

An energy analysis of T_3 showed a two-fold potential with minima at T_3=0° and T_3=180°. From Table 5.5 it is clear that a distinct preference exists for T_3=180° (ranging from 5.6 to 6.1 kcal/mol). Both optimized geometries OAc-0-60-180 and OAc-0-180-180 have been used to study the energy dependence on T_1. Different conformations were generated by varying T_1 in steps of 10°. From the resulting plots of Figure 5.7 it follows that the energy barrier of conformer OAc-0-60-180 (resembling acetylquinidine) in going from T_1=0° to T_1=60° is 2.6 kcal/mol.

Table 5.5 Results of VAMP AM1 optimizations for model compound D.

	OAc 0-180-0	OAc 120-180-0	OAc 0-180-180	OAc 0-60-180	OAc 120-180-180
energy[a]	-30.8	-29.1	-36.4	-36.2	-35.4
T_1	0.0	119.6	0.1	2.0	116.4
T_2	179.9	182.8	180.5	104.7	198.1
T_3	-0.1	1.7	179.8	181.2	179.0
C_9O[b]	1.432	1.432	1.439	1.431	1.439
C_9H[b]	1.125	1.125	1.124	1.125	1.124
$C_4'C_9$	1.493	1.495	1.491	1.494	1.494
$C_4'C_9O$	108.5	108.6	108.7	111.5	107.9
$C_4'C_9H$	110.1	110.2	111.0	110.2	111.2
$C_3'C_4'C_9$	122.2	119.6	122.7	122.3	119.7

[a] energy in kcal/mol.
[b] bond length in Angstrom.

Table 5.6 Results of VAMP AM1 optimizations for model compound E.

	Cl-0	Cl-120
energy[a]	39.5	39.0
T_1	1.8	102.6
C_9Cl[b]	1.754	1.758
C_9H[b]	1.120	1.118
$C_4'C_9$	1.486	1.484
$C_4'C_9Cl$	115.3	112.0
$C_4'C_9H$	110.0	111.2
$C_3'C_4'C_9$	123.6	119.8

[a] energy in kcal/mol.
[b] bond length in Angstrom.

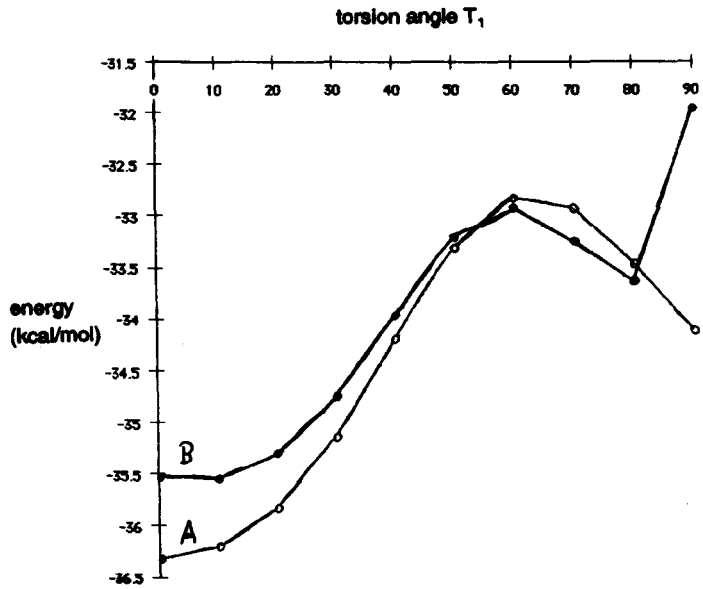

Figure 5.7 Energy (kcal/mol) as a function of T_1. (A), for OAc-60-180; (B), for OAc-0-180-180.

Compound E. Two conformations have been optimized, one starting with T_1=0° called Cl-0 and one starting with T_1=120° called Cl-120. Table 5.6 summarizes the most important results of these optimizations. This time the conformer with T_1=0° is not found as the absolute minimum. Compound Cl-120 with T_1=120° is calculated 0.5 kcal/mol more stable than Cl-0. The energy dependence on T_1 has been computed by stepwise rotation around T_1 in steps of 10°. The optimized geometry of compound Cl-0 was used as starting point. The calculated energies are plotted against T_1 (Figure 5.8). The energy barrier in going from T_1=0° to T_1=60° can be estimated to be 3.0 kcal/mol.

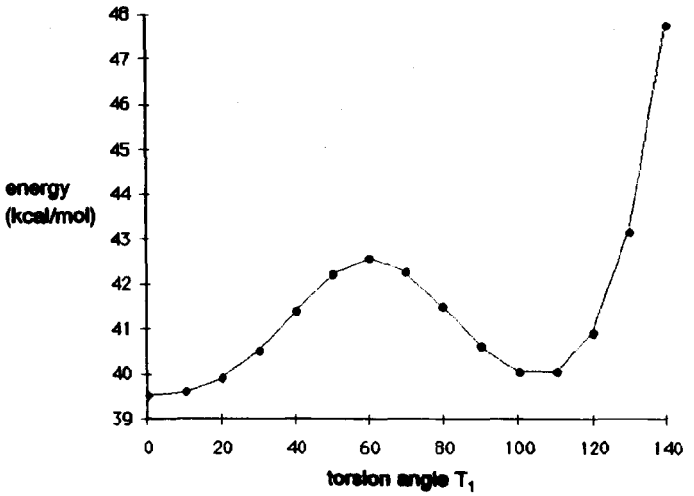

Figure 5.8 Energy (kcal/mol) as a function of T_1 for compound Cl-0.

Effect of C_9-H Bond Length and C_4'C_9H Bond Angle. The results of the calculations described above show that the C_9-H bond length is affected by the nature of the benzylic substituent R. In going from R=OH, OMe, OAc, Cl, H the C_9-H bond length decreases from 1.126 A to 1.118 A. In an attempt to investigate the influence of this bond length on the height of the energy barrier, caused by benzylic H-H_5 repulsion, the C_9-H bond length was systematically varied from 1.110 A to 1.130 A in steps of 0.002 A. In these calculations the geometry of OH-0-180 has been used as basic geometry. At each bond length the height of the energy barrier has been computed by stepwise variation of T_1. No significant effect on the benzylic H-H_5 repulsion could be detected.

The $C_4'C_9H$ bond angle is also affected by the nature of the benzylic substituent. In order to investigate the influence of this bond angle on the benzylic $H\text{-}H_5$ repulsion, the height of the energy barrier has been calculated for $C_4'C_9H$ bond angles of 109° and 112°, together with C_9H bond lengths of 1.110, 1.120, and 1.130 A, respectively. Again the geometry of OH-0-180 has been used as basic geometry for these calculations. In Figure 5.9 only the results of the calculations with a C_9H bond length of 1.120 A are given; results for the other two bond length were very similar. It follows that a decrease of the bond angle from 112° to 109° causes an increase of the benzylic $H\text{-}H_5$ repulsion of about 0.4 kcal/mol.

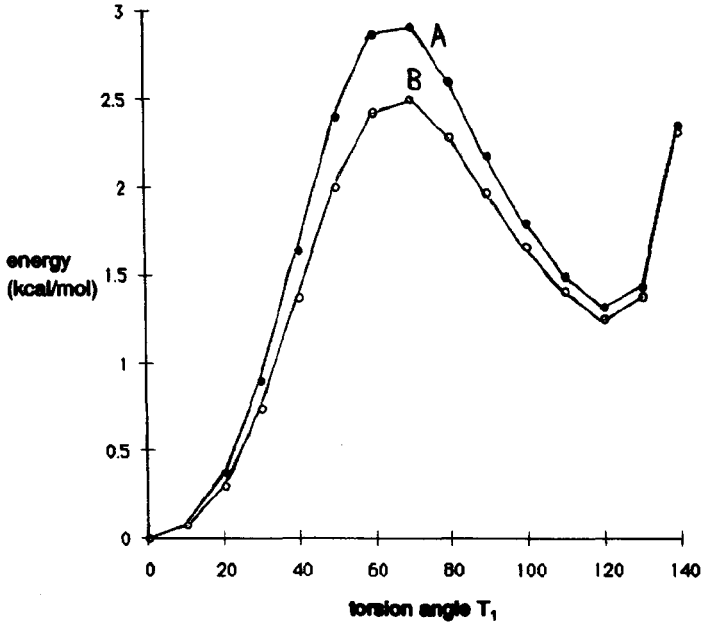

Figure 5.9 Energy (kcal/mol) as a function of T_1 for a model compound with a C_9H bond length of 1.120 A and (A) a $C_4'C_9H$ of 109°, (B) a $C_4'C_9H$ of 112°.

Effect of C_9O Bond Length and $C_4'C_9O$ Bond Angle. In going from R=OH, R=OMe, R=OAc the C_9O bond length increases from about 1.140 to 1.145 A, whereas the $C_4'C_9O$ bond angle tends to decrease (see Tables 5.3, 5.4, 5.5). To study the effect of this bond length and angle on the interaction between oxygen and the quinoline proton H_1 four energy plots have been calculated. The geometry of OH-0-180 has been used as starting conformation in all calculations. The results of the calculations are summarized in Figure 5.10 Plot A gives the energy curve for $C_4'C_9O=108^o$ and C_9O=1.140 A; plot B for $C_4'C_9O=108^o$ and C_9O=1.145 A; plot C for $C_4'C_9O=112^o$ and C_9O=1.140 A; plot D for $C_4'C_9O=112^o$ and C_9O=1.145 A. From these plots it follows that the energy decreases only about 0.03 kcal/mol when the C_9O bond length increase from 1.140 to 1.145 A, whereas increasing the $C_4'C_9O$ bond angle from 108 to 112° causes a stabilization of the minimum energy conformation at $T_1=0^o$ of about 0.3 kcal/mol.

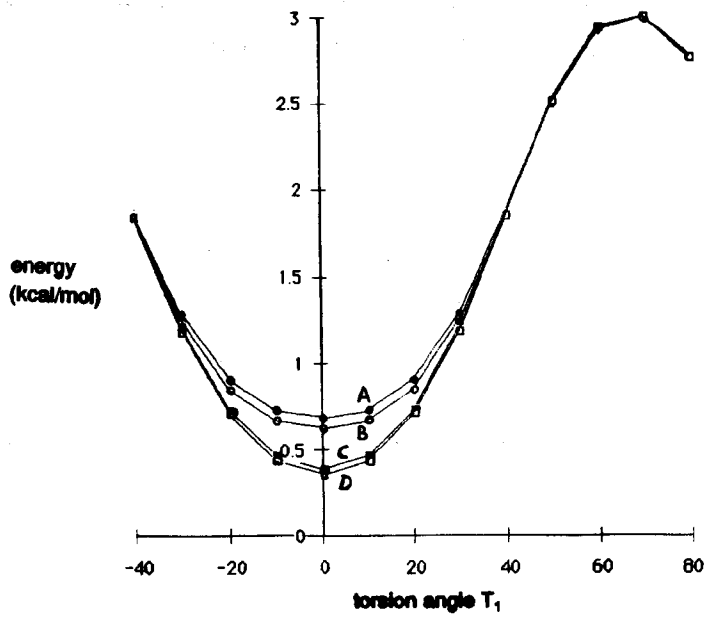

Figure 5.10 Energy (kcal/mol) as a function of T_1. (A), for $C_4'C_9O=108^o$ and C_9O=1.140 A; (B), for $C_4'C_9O=108^o$ and C_9O=1.145 A; (C), for $C_4'C_9O=112^o$ and $C_9O=140^o$; (D), for $C_4'C_9O=112^o$ and C_9O=1.145 A.

Effect of the $C_3'C_4'C_9$ Bond Angle. The VAMP calculations on the model compounds as well as on the complete cinchona alkaloids have shown that the $C_3'C_4'C_9$ bond angle is strongly affected by the benzylic substituent R (variation from 118.8 to 123.5°). Probably this is to reduce steric repulsion between the quinoline proton H_1 and the benzylic substituent R. The $C_3'C_4'C_9$ bond angle increases when the C_9O bond length increases or when the $C_4'C_9O$ bond angle decreases.

Using the OH-0-180 basic geometry, T_1 has been varied from 0 to 130° in steps of 10°. This has been done for six different $C_3'C_4'C_9$ bond angles, ranging from 118.5 to 123.5°. Figure 5.11 shows the resulting six plots of energy against T_1. It follows that there exist two different effects on the energy. Firstly, decrease of the $C_3'C_4'C_9$ bond angle causes a destabilization of the absolute minimum at T_1=0° (increased steric interactions between O and H_1). This is a relatively small energy effect (0.7 kcal/mol). Secondly, decrease of the $C_3'C_4'C_9$ bond angle causes a relatively large energy effect on the benzylic H-H_5 repulsion; it decreases by about 2 kcal/mol.

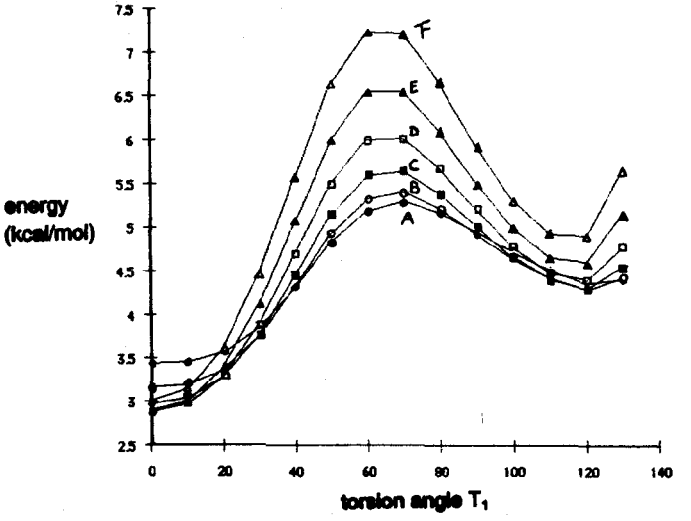

Figure 5.11 Energy (kcal/mol) as a function of T_1 for $C_3'C_4'C_9$ is respectively, (A) 118.5; (B) 119.5; (C) 120.5; (D) 121.5; (E) 122.5; (F) 123.5°.

5.2.4 Alkaloid-Solute Interactions

We know that the conformational behavior of cinchona alkaloids is influenced by the nature of the solvent. In case of complexation with osmium tetraoxide or protonation by an acid there is an obvious interaction between the solute and alkaloid. However, we have also discussed less obvious examples, e.g. methoxyquinidine, which adopts predominantly the open conformation 3 in $CDCl_3$ and the closed conformation 2 in CD_2Cl_2. Apparently the interactions between alkaloid and solvent differ for the closed conformation 2 and open conformation 3.

In chapter 4 we have demonstrated that methoxy and ester derivatives of cinchona alkaloids exist as an equilibrium of conformers 2 and 3 in various solvents. This equilibrium shifts completely towards conformer 2 in methanol. This conformational shift was not observed for chloroquinidine. We have tried to calculate the energy gain caused by interactions between chloroquinidine and one molecule of methanol. In the starting geometries methanol was positioned relative towards chloroquinidine in such a manner that a hydrogen bond between the hydroxyl proton of methanol and quinuclidine nitrogen of the alkaloid exists. As a consequence the methanol molecule resides above the quinoline ring in case of the closed conformation 2 (ClQD_2_Met) and in free space in case of the open conformation 3 (ClQD_3_Met). AM1 optimizations of the complexes were unsuccessful, in both cases the hydrogen bond disappeared. After optimization the distances between the hydroxyl proton of methanol and the quinuclidine nitrogen hydrogen bond were increased to 2.65 and 2.71 A for ClQD_2_Met and ClQD_3_Met, respectively. The PM3 method is known to give better results for systems containing hydrogen bonds. Thus both optimizations were repeated using PM3. It turned out that after a PM3 optimization in both complexes methanol is hydrogen-bonded to the alkaloid as revealed by proton-nitrogen distances of 1.91 and 1.85 A and O-H-N bond angles of 162.0 and 178.0 for ClQD_2_Met and ClQD_3_Met, respectively. Figure 5.12 gives the PM3 optimized complex between quinidine in the open conformation 3 and methanol (ClQD_3_Met). PM3 optimizations were also performed on isolated methanol, chloroquinidine in conformation 2

(ClQD_2), and chloroquinidine in conformation 3 (ClQD_3). The results are summarized in Table 5.7.

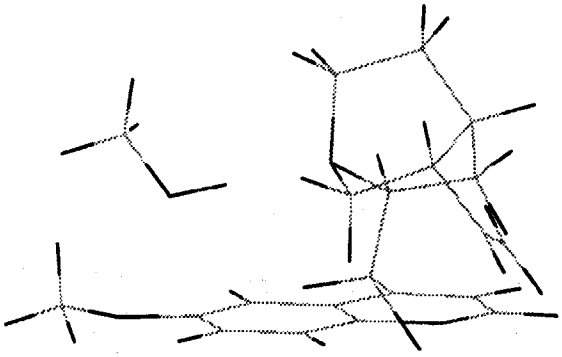

Figure 5.12 PM3 optimized complex between quinidine in the open conformation 3 and methanol.

Table 5.7 Results of PM3 optimizations of chloroquinidine-methanol interactions.

	Energy (kcal/mol)
ClQD_2	13.06
ClQD_3	14.85
ClQD_2_Met	-39.92
ClQD_3_Met	-38.92
Methanol	-51.88

Based on the calculated energies of the isolated molecules one expects an energy of -38.82 kcal/mol (-51.88-13.06) for ClQD_2_Met and -37.03 kcal/mol (-51.88-14.85) for ClQD_3_Met. We found, however, -39.92 and -38.92 kcal/mol for ClQD_2_Met and ClQD_3_Met, respectively. Thus the methanol-alkaloid interactions cause an energy gain of 1.10 kcal/mol for chloroquinidine in the closed conformation 2 and 1.89 kcal/mol for chloroquinidine in the open conformation 3, the initial energy difference between conformers 2 and 3 of 1.79 kcal/mol decreases to 1.00 kcal/mol.

5.2.5 DISCUSSION

When we examine the data of the T_1 dependence on the energy of the model compounds that have been studied, it is easily concluded that all plots of energy against T_1 are very similar. Three minima are located at approximately $T_1=0^o$, $T_1=120^o$, and $T_1=240^o$. In all cases, except for the chloro model compound, the absolute minimum is found at about $T_1=0^o$, whereas at about $T_1=120$ and $T_1=240^o$ relative minima are found. In all cases these three minima are separated by one large (>10 kcal/mol) and two relatively small (<4 kcal/mol) energy barriers. The two small energy barriers at approximately $T_1=60$ and $T_1=300^o$ are caused by repulsion between the benzylic proton and H_5. The huge energy barrier is caused by repulsion between the benzylic R substituent and H_5.

In the open conformation 3 of the cinchona alkaloids the benzylic substituent is situated in the same plane as the quinoline ring and directed towards H_1 (thus resembling the absolute minima of the model compounds) (see Figure 5.13). In the closed conformation 2 of the cinchona alkaloids the situation with respect to the benzylic substituents is different. The benzylic hydrogen is now oriented in the same plane as the quinoline ring, pointing towards H_5, whereas the benzylic R substituent has turned about 60° out of the quinoline plane (thus resembling the relative maxima of the model compounds). In cases analogous to the open conformation 4 the benzylic substituent R is also oriented in the quinoline plane, but now

it points towards H_5 instead of towards H_1. From the calculational results we have seen that this is very unfavourable (huge energy barrier) because of the relatively large repulsion between the benzylic R and H_5. The configuration at C_9 of the epicinchona alkaloids is opposite to that of the cinchona series, thus now closed conformation 2 and to a lesser extend open conformation 3 are unlikely for the same reason. Deoxycinchona alkaloids do not have a benzylic substituent and thus miss the discrimination caused by the configuration at C_9. Indeed, deoxycinchona alkaloids are found both in conformation 1 and 3.

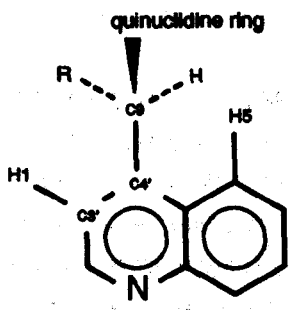

Figure 5.13 Schematic drawing of the substitution of the benzylic carbon C_9 of cinchona alkaloids.

We have also optimized some complete cinchona derivatives. The results of these calculations for quinidine predict the *open* conformation 3 to be 2.0 kcal/mol more stable than the closed conformation 2. For the methoxy derivative this energy difference decreases to 0.9 kcal/mol, and for acetylquinidine the energy difference decreases further to 0.3 kcal/mol. AM1 predicts the chloro derivative in the *closed* conformation 2 to be 1.8 kcal/mol more stable than in the open conformation 3. Ignoring the precise absolute magnitudes of the energy differences, we conclude that there exists excellent agreement between these calculational results and the experimental observations in solution and in the solid state. This suggests that the AM1 calculations are well suited to predict experimentally observed trends in

energy differences between possible conformations of a certain cinchona derivative and between the different derivatives of cinchona alkaloids.

However, the main object of our calculations is not to find good correlations between experimental observations and theoretical predictions, but to find explanations for the conformational behavior of the cinchona alkaloids. Let us return to the model compounds and concentrate on the benzylic H-H_5 and benzylic R-H_1 repulsions. The calculations on the model compounds suggest the existence of a delicate balance between benzylic R-H_1 and benzylic H-H_5 interactions. Increase of the C_9R bond length or decrease of the C_4'C_9R bond angle causes a decrease of the benzylic R-H_1 interatomic distance and thus an increased steric repulsion. This can be released by increasing the C_3'C_4'C_9 bond angle, but at the same time this has considerable consequences for the benzylic H-H_5 repulsion (Figure 5.13). In going from R=OH, OMe, OAc the electron withdrawing capacity of the R-group increases, as a result the C_9O bond length increases. In the same order the C_4'C_9O bond angle decreases. This explains why the situation resembling the open conformation 3 (T_1 is approximately 0°) will be destabilized in going from R=OH, OMe, OAc. In the same time, for closed conformation 2 (T_1 is approximately 60°), the benzylic H-H_5 repulsion can be relieved significantly by decreasing the C_3'C_4'C_9 bond angle and to a lesser amount by increasing the C_4'C_9H bond angle. Both trends are indeed present in going from R=OH, OMe, OAc, Cl. Thus the geometry resembling the closed conformation 2 will be stabilized in the same order.

Another aspect are the solvent-alkaloid interactions. These too are able to influence the conformational behavior. In this thesis several examples have been mentioned, e.g.; methoxyquinidine, which adopts predominantly the open conformation 3 in $CDCl_3$ and closed conformation 2 in CD_2Cl_2; benzoylquinidine, which predominantly adopts the closed conformation 2 in all solvents except CD_3OD, in which it is found chiefly in the open conformation 3. But also complexation with osmium tetraoxide[7] or protonation of the alkaloid are able to induce conformational transitions from the closed conformation 2 to the open conformation 3, except for chloroquinine, where this conformational transition could

not be induced upon protonation. These examples clearly indicate that solute-alkaloid interaction are able to dictate the conformation only in certain circumstances. From NMR and X-ray data we know that especially the quinuclidine nitrogen is involved in the interactions with solvents (e.g. methanol, acetic acid) or electrophiles (e.g. aromatic thiols, osmium tetraoxide). We do not have much quantitative information about the energy gain caused by these interactions, but PM3 calculations suggest the magnitude of these to be in the order of 1-3 kcal/mol (and of course for these data entropy effects are not taken into account). In the closed conformation 2 of the cinchona alkaloids it is practical impossible, because of geometrical reasons, for the quinuclidine nitrogen lone pair to participate in alkaloid-solute interactions, whereas in case of the open conformation 3 the nitrogen lone pair is freely accessible to ligand or solute (this explains why we have called the conformations 'closed' or 'open').

With all this information in hand we think that the picture is complete enough to propose an integral rationalization for the conformational behavior of the cinchona alkaloids. Because of reasons discussed above chloro cinchona alkaloids adopt closed conformation 2 almost exclusively. The energy difference between closed conformation 2 and open conformation 3 is too large to be compensated by energy gain as a result of interactions between open conformation 3 of the chloro derivative with solute or ligand. In case of ester derivatives the energy difference between closed and open conformation is less and is probably of the same order of magnitude as the amount of stabilization caused by interactions with solutes, such as methanol or weak acids, or with strong electrophiles, such as osmium tetraoxide. In case of the methoxy derivatives the energy difference between closed conformation 2 and open conformation 3 has vanished. In non-coordinating solvents like CD_2Cl_2, the methoxy derivatives are still predominantly found in the closed conformation 2, but in the presence of any electrophile the equilibrium shifts in favor of the open conformation 3. Quinine and quinidine (and other hydroxy derivatives) by themselves already possess a distinct preference for the open conformation 3 and thus do not depend on extra stabilization caused by interactions with solute.

5.3 MO ANALYSIS ON EPHEDRINE

In chapter 2 we have presented a molecular mechanics (mm) analysis of ephedrine and N-methylephedrine. The minimum energy conformations were found by systematical variation of the four torsion angles T_1, T_2, T_3, and Ψ that determine the gross conformation (see Figure 5.14 for definitions of the torsion angle).

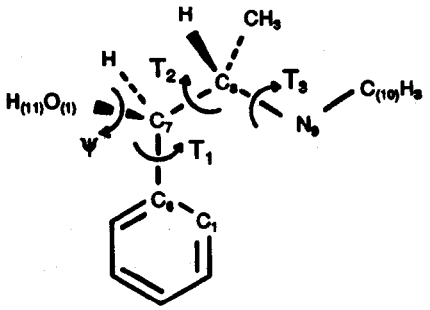

Figure 5.14 The structure and absolute configuration of (-)-ephedrine . T_1=$C_1C_6C_7C_8$, T_2=$C_6C_7C_8N_9$, T_3=$C_7C_8N_9C_{10}$, Ψ=$C_6C_7O_1H_{11}$.

It turned out that nine minima were found for ephedrine. With respect to T_1 (the position of the β-hydroxyamine side chain relative to the phenyl ring) a more or less perpendicular orientation was found. The orientation around T_2 determines whether the gross conformation is gauche (the side chain folds back) or trans (extended conformation). We have divided the predicted minima into three 'gauche -60' (T_2=-60°), three 'gauche 60' (T_2=60°), and three trans conformers (T_2=180°). Depending on the orientation of the hydroxy group (Ψ) each of the nine conformers could be split up further into three other ones. Based on the relative energy differences we have concluded that a slight preference exits for the 'gauche -60' conformers. In case of N-methylephedrine seven minima were identified. The introduction of a methyl group on the nitrogen caused a change in

the conformational behavior, now a preference for the 'gauche 60' conformers was observed. Note that these 'gauche 60' conformers resemble the closed conformation 2 of quinine.

We have optimized all conformations predicted by the molecular mechanics analysis of ephedrine and N-methylephedrine using the AM1 and PM3 Hamiltonians. The results are summarized in Tables 5.8 and 5.9 for ephedrine and in Tables 5.10 and 5.11 for N-methylephedrine. First, we will discuss the outcomes obtained for ephedrine.

Ephedrine. The AM1 and PM3 calculational results are very similar; both predict the trans conformer ephedrine_9c as the absolute minimum, trends in relative energy differences are similar, as well as the optimized geometries. These results are consistent with a PCILO3[14] mo analysis of Pullman[15] who also found a preference for the trans conformers. Our MO optimizations predict the same nine minimum energy conformations as found by the molecular mechanics analysis, three 'gauche 60', three 'gauche -60', and three trans conformers. Another similarity between the MO and molecular mechanics calculations is the influence on the energy of the orientation of the hydroxy group. The energy differences between the three staggered orientations are up to 4.5 kcal/mol. However, the molecular mechanics analysis predicted the staggered conformers characterized by $\Psi=180^{o}$ as absolute minima, whereas the MO calculations predict conformers with $\Psi=-60^{o}$ to be more stable. Another difference between the MO and molecular mechanics calculations is the slight preference for the 'gauche -60' conformers, predicted by the molecular mechanics calculations.

With respect to T_3 for both 'gauche -60' and trans conformers a preference for $T_3=-60^{o}$ exist. This places the methyl groups on C_8 and N_9 in an anti orientation. In case of the 'gauche 60' conformers another preference for T_3 is found of approximately 160°. An anti ($T_3=-60^{o}$) orientation of both methyl groups in a 'gauche 60' conformer places the N_9-methyl directly above the phenyl ring, causing steric hindrance.

Table 5.8 Results of AM1 calculations on (-)-ephedrine. Energy in kcal/mol.

conformation	T_1	T_2	T_3	Ψ	energy	relative energy
ephedrine _1a	-88.7	-56.8	-148.2	66.4	-29.4	3.5
_1b	-90.6	-56.9	-156.7	-173.3	-30.9	2.0
_1c	-92.2	-60.0	-176.8	-80.6	-30.1	2.7
ephedrine _2a	-90.9	-56.1	-78.0	59.0	-30.9	1.9
_2b	-93.7	-53.3	-82.4	-170.8	-32.6	0.3
_2c	-97.5	-50.2	-80.5	-73.0	-32.2	0.7
ephedrine _3b	-92.9	-53.7	95.0	-157.5	-28.1	4.8
_3c	-89.1	-61.0	90.9	-59.7	-31.3	1.6
ephedrine _4a	-110.2	46.5	66.2	74.6	-28.1	4.8
_4b	-105.6	51.0	69.3	-161.4	-29.7	3.2
_4c	-118.7	47.3	61.7	-68.5	-30.8	2.1
ephedrine _5a	-101.2	53.0	-91.8	74.0	-29.3	3.6
_5b	-100.9	55.5	-91.4	-175.9	-30.4	2.5
_5c	-114.5	62.5	-86.1	-66.0	-30.9	1.9
ephedrine _6a	-98.8	55.1	-157.6	76.3	-29.8	3.1
_6b	-98.2	55.3	-168.8	-174.9	-30.8	2.1
_6c	-113.2	56.9	-161.6	-65.8	-31.5	1.4
ephedrine _7b	-86.1	164.4	-139.6	-175.2	-28.3	4.5
_7c	-75.0	-179.8	-144.4	-46.0	-30.7	2.2
ephedrine _8a	-82.4	149.0	71.9	56.7	-29.4	3.4
_8b	-82.7	154.6	66.3	-177.3	-30.8	2.1
_8c	-81.8	154.7	64.1	-59.6	-31.6	1.2
ephedrine _9a	-79.9	176.3	-57.1	78.1	-29.8	3.1
_9b	-85.8	177.8	-64.1	-175.7	-32.0	0.9
_9c	-83.8	169.7	-71.7	-62.2	-32.9	0.0

Table 5.9 Results of PM3 calculations on (-)-ephedrine. Energy in kcal/mol.

conformation	T_1	T_2	T_3	Ψ	energy	relative energy
ephedrine _1a	-88.8	-54.5	-147.5	61.7	-27.1	4.8
_1b	-90.4	-55.1	-155.5	-169.7	-28.4	3.5
_1c	-86.6	-59.1	-175.6	-88.0	-28.7	3.2
ephedrine _2a	-94.8	-54.1	-79.7	54.6	-28.5	3.4
_2b	-93.7	-53.3	-82.4	-170.8	-29.6	2.3
_2c	-91.8	-52.2	-74.8	-67.0	-31.3	0.6
ephedrine _3b	-89.5	-58.0	90.0	-165.6	-25.9	6.0
_3c	-89.6	-61.6	90.7	-72.6	-29.2	2.7
ephedrine _4a	-114.1	48.9	66.1	45.8	-27.7	4.2
_4b	-110.3	50.9	69.2	-154.2	-28.1	3.8
_4c	-116.7	45.2	65.6	-72.5	-29.6	2.3
ephedrine _5a	-109.3	57.4	-98.0	42.3	-29.1	2.8
_5b	-108.0	58.7	-94.3	-169.6	-28.5	3.4
_5c	-116.0	63.5	-86.2	-66.7	-30.0	1.9
ephedrine _6a	-114.0	59.4	-159.4	44.0	-29.2	2.7
_6b	-110.9	57.6	-167.4	-170.5	-28.5	3.4
_6c	-115.4	57.9	-160.4	-63.5	-30.3	1.6
ephedrine _7b	-88.3	165.1	-140.9	-170.8	-26.9	5.0
_7c	-84.9	165.6	-150.0	-41.1	-29.9	2.0
ephedrine _8a	-89.3	150.7	72.0	57.0	-28.8	3.1
_8b	-85.8	153.8	68.3	-173.8	-28.1	3.8
_8c	-82.4	154.4	65.7	-75.1	-30.0	1.9
ephedrine _9a	-80.8	176.9	-56.6	73.2	-27.4	4.5
_9b	-87.4	178.2	-61.3	-169.2	-29.2	2.7
_9c	-84.6	169.3	-67.6	-77.6	-31.9	0.0

Table 5.10 Results of AM1 calculations on (-)-N-methylephedrine. Energy in kcal/mol.

conformation	T_1	T_2	T_3	Ψ	energy	relative energy
N-methyleph _1b	-92.6	-45.1	-20.0	-164.4	-23.4	3.4
_1c	-87.5	-61.6	-23.4	-60.1	-26.3	0.5
N-methyleph _3a	-83.7	-61.6	-168.5	48.4	-23.1	3.7
_3b	-84.6	-59.8	-169.1	179.5	-24.6	2.3
_3c	-84.6	-50.7	-171.5	-67.1	-24.5	2.3
N-methyleph _4a	-88.3	63.5	-35.8	75.0	-23.8	3.0
_4b	-91.8	58.7	-36.0	-169.7	-25.0	1.8
_4c	-113.0	55.6	-39.9	-69.0	-25.7	1.1
N-methyleph _6a	-106.8	66.7	163.6	74.7	-23.3	3.5
_6b	-107.1	64.9	163.9	-171.1	-24.4	2.4
_6c	-116.7	62.6	160.3	-66.4	-25.2	1.6
N-methyleph _7a	-74.9	168.1	-20.8	77.1	-24.7	2.1
_7b	-82.8	153.3	-42.4	-178.6	-25.9	0.9
_7c	-70.4	152.8	-46.9	-59.2	-26.8	0.0
N-methyleph _8a	-74.2	164.4	28.5	54.6	-24.3	2.5
_8c	-67.9	173.8	90.9	-47.2	-24.3	2.5
N-methyleph _9b	-82.4	162.5	-174.6	-175.1	-25.6	1.3
_9c	-66.3	163.2	170.4	-57.1	-26.4	0.5

Table 5.11 Results of PM3 calculations on (-)-N-methylephedrine. Energy in kcal/mol.

conformation	T_1	T_2	T_3	Ψ	energy	relative energy
N-methyleph _1c	-86.7	-63.5	-26.0	-73.2	-31.3	1.7
N-methyleph _3a	-75.2	-49.2	-174.1	34.2	-27.3	5.7
_3b	-75.9	-48.3	-176.3	179.6	-28.3	4.7
_3c	-74.4	-50.3	-175.7	-74.0	-30.3	2.7
N-methyleph _4a	-111.6	62.9	-49.5	41.9	-30.1	2.9
_4b	-109.1	65.6	-47.5	-161.7	-30.3	2.7
_4c	-114.1	67.0	-48.3	-67.0	-32.0	1.0
N-methyleph _6a	-113.2	62.2	166.7	44.8	-29.9	3.1
_6b	-114.1	60.8	161.7	-170.5	-29.2	3.8
_6c	-116.1	66.4	161.8	-63.0	-31.0	2.0
N-methyleph _7a	-89.0	153.0	-33.9	54.5	-30.9	2.1
_7b	-90.1	146.6	-40.0	-173.4	-30.0	3.0
_7c	-86.4	146.3	-41.2	-73.5	-32.0	1.0
N-methyleph _8a	-82.7	164.7	47.0	42.3	-29.8	3.2
_8b	-109.2	150.0	48.7	-176.3	-28.4	4.6
_8c	-82.0	165.3	61.6	-39.4	-31.1	1.9
N-methyleph _9a	-84.5	171.9	-137.5	65.1	-25.9	7.1
_9b	-86.5	154.6	-175.3	-169.0	-30.4	2.6
_9c	-114.1	149.1	-176.1	-66.7	-33.0	0.0

5.4 EXPERIMENTAL PART

Energy calculations were either performed on a Convex C120 computer with VAMP version 4.10, a vectorized molecular orbital package based on AMPAC 1.0 and MOPAC 4.10[16], or with a VAX 8650 computer with MOPAC 5.0[17]. The calculational results were evaluated with either CHEMX or SYBYL[18]. All optimizations were performed either over all internal coordinates or the cartesian coordinate system was used, until the root-mean-square of the gradient of the energy was less than 0.5 kcal/A.

5.5 REFERENCES

1. Parts of the work presented in chapter 5 have been published; Dijkstra, G. D. H.; Kellogg, R. M.; Wijnberg, H. *J. Org. Chem.* **1990**, *55*, 6121.
2. Stewart, J. J. P. *J. Comp. Chem.* **1989**, *10*, 209
3. AM1, Dewar, M. J. S. *J. Am. Chem. Soc.* **1985**, *107*, 3902.
4. Dewar, M. J. S.; Thiel, W. *J. Am. Chem. Soc.* **1977**, *99*, 4899.
5. Pople, J. A.; Segal, G. A. *J. Chem. Phys.* **1965**, *43*, 136.
   Pople, J. A.; Segal, G. A. *J. Chem. Phys.* **1966**, *44*, 3289.
6. Pople, J. A.; Beveridge, D. L.; Dobosh, P. A. *J. Chem. Phys.* **1967**, *47*, 2026.
7. Bingham, R. C.; Dewar, M. J. S.; Lo, D. H. *J. Am. Chem. Soc.* **1975**, *97*, 1302.
8. Diner, S.; Malrieu, J. P.; Claverie, P. *Theor. Chim. Acta* **1969**, *13*, 1.
   Diner, S.; Malrieu, J. P.; Jordan, F.; Gilbert, M. *Theor. Chim. Acta* **1969**, *15*, 100.
9. Hehre, W. J.; Radom, L.; Schleyer, P. v. R.; Pople, J. A. *Ab Initio Molecular Orbital Theory* John Wiley & Sons: New York, 1986.
10. Dupuis, M.; Rys, J.; King, H. F. *HONDO*, Quantum Chemistry Program Exchange, Indiana University: Bloomington, 1976.
11. VAMP, Erlangen Vectorized Molecular Orbital Package, version 4.10 (based on AMPAC 1.0 and MOPAC 4.0) molecular orbital package.
12. CHEMX, developed and distributed by Chemical Design Ltd., Oxford, England.

Footnote Cont. Next Page

Footnote 13 Cont.

13. QCPE Program 395/400. Allinger Force Field Molecular Mechanics Calculations, Allinger, N. L., Ed., Dept. of Chem., University of Georgia, Athens, GA 30602.
14. PCILO3, QCPE Program 462, Perturbative Configuration Interaction, Ed. Roman Boca, Dept. of Inorg. Chem. Slovak Techn. Univ. Bratislava, Czechoslovakin.
15. Pullman, B.; Coubeils, J. L; Couriere. Ph.; Gervois, J. P. *J. Med. Chem* 1971, *15*, 17.
16. Computer and software are provided by the Dutch CAOS-CAMM center, University of Nijmegen, the Netherlands.
17. These calculations were performed on a VAX 8650 computer of the computer centre of Duphar B.V., Weesp, the Netherlands.
18. SYBYL, developed and distributed by Tripos Associates Inc, St. Louis, Missouri.

6

EXPERIMENTS AND DISCUSSION

6.1 INTRODUCTION

In the preceding chapters we have presented a conformational study of cinchona and ephedra alkaloids. Most attention has been paid to the cinchona alkaloids. The results have been obtained by a combined experimental (NMR) and theoretical approach. Both cinchona and ephedra alkaloids are applied in numerous interesting areas of chemistry and medicine. The next challenge is to match the knowledge of the conformational behavior of these alkaloids with their chemical and biological

function. This is a rational approach to these appealing questions. In chapter 4 we have mentioned two examples of mechanistic research inspired by the recent conformational information; the asymmetric Michael addition between aromatic thiols and cyclic ketones and the asymmetric hydroxylation of olefins. The latter is currently under investigation in the Sharpless group[1] . An alternative geometry for the transition state of the Michael addition has been proposed by us[2] . In the Hiemstra model[3] , advanced some years ago on the basis of kinetic data and product studies, a transition from an open to a closed alkaloid conformation upon the formation of an ion pair between aromatic thiol and quinuclidine nitrogen was postulated. Evidence from a NMR analysis revealed that the open conformation 3 did not close upon protonation on the quinuclidine nitrogen, and a mechanism consistent with the newly available conformational information has been advanced. In this last chapter we will pay further attention on this reaction. The transition states proposed for the addition of diethylzinc to aldehydes[4] , and for the [2+2] cycloadditions between chloral and ketene[5] need now to be reexamined on the basis of this newly available conformational information.

At this time we will not address all these issues. In this last chapter we will direct attention again to the Michael addition and describe also initial experiments in which ephedra alkaloids are used as chiral catalyst. Based on these and other results we conclude with a discussion on possible future improvements.

6.2 EPHEDRA DERIVATIVES AS CHIRAL CATALYSTS IN THE MICHAEL ADDITION

In this thesis the cinchona alkaloids have received most attention. Conformational aspects of ephedra alkaloids are described only in chapters 2 and 5. The consequences deserve more attention. From the rigid fitting plots between calculated minimum energy conformations of cinchona and ephedra alkaloids (Figure 2.19) we have seen that, despite the profound structural differences between the two classes of alkaloids, great similarities exist in the minimum energy con-

formations they can adopt. Especially the interesting β-hydroxyamino segments of both classes of alkaloids have virtually identical preferred conformations. It is known that ephedra alkaloids, like cinchona alkaloids, catalyze the Michael addition between aromatic thiols and conjugated cyclic alkenones[6], but the e.e.'s are disappointing. The best result obtained by Hiemstra was an e.e of 29% with N-methylephedrine in a standard reaction between *p*-t-butylthiophenol to 2-cyclohexen-1-one in benzene (Figure 6.1). Because Hiemstra had obtained an e.e. of 62% with cinchonidine under the same conditions, no further attention was paid to ephedra alkaloids as catalysts for this reaction.

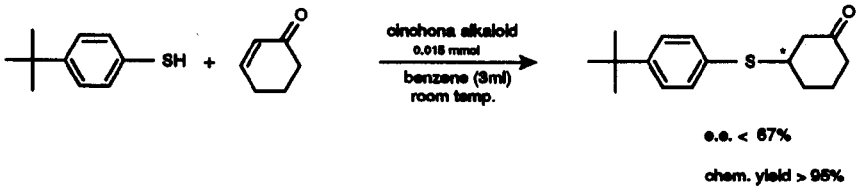

Figure 6.1 Asymmetric Michael addition between aromatic thiols and cyclohexenone. The standard reaction

Because synthetic manipulations on the structures of ephedra alkaloids are relatively simple, they are well suited for a study of the influence of their structures on the e.e. In this respect some ephedra derivatives have been synthesized and tested as chiral catalyst in the Michael addition. The reaction, developed by Hiemstra (Figure 6.1), has been used as a standard reaction. This makes it easier to compare our results obtained with ephedra catalysts with those obtained with cinchona alkaloids.

The formation of a tight ion pair between catalyst and aromatic thiol in the transition state plays a crucial role in our mechanism of the asymmetric Michael addition. From a kinetic study of Hiemstra[3] it follows that this ion pair is most

probably the reactive intermediate in the thiol addition reaction, when carried out in apolar solvents. The ion pair then reacts with the conjugated enone in the rate determining step. This implies that the basicity of the catalyst must be important. In chapter 4 we have demonstrated that the quinuclidine nitrogen of the cinchona alkaloids acts as the basic site of the catalyst. It is easily seen from the structure of the cinchona alkaloids that it is difficult to modify the basicity of the quinuclidine nitrogen. By replacing the hydrogen atom on the nitrogen of ephedrine with different substituents the structure and basicity are affected in a direct way. The structures of (-)-ephedrine and some derivatives which have been synthesized and tested in the standard reaction are depicted in Figure 6.2. In Table 6.1 the resulting e.e's of these ephedra alkaloid derivatives in the standard reaction are given.

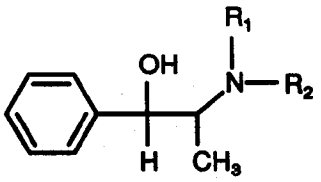

	R_1	R_2
ephedrine	H	CH_3
N-methylephedrine	CH_3	CH_3
N-ethylephedrine	C_2H_5	CH_3
N-propylephedrine	C_3H_7	CH_3
N-butylephedrine	C_4H_9	CH_3
N-pentylephedrine	C_5H_{11}	CH_3
N-hexylephedrine	C_6H_{13}	CH_3
N,N-diethylnorephedrine	C_2H_5	C_2H_5
N-trimethylsilylmethylephedrine	$(CH_3)_3SiCH_2$	CH_3

Figure 6.2 The structures of ephedra alkaloid derivatives that have been synthesized and tested as chiral catalyst.

Initially it was difficult to reproduce the e.e's in the standard reaction. This problem was solved by carrying out the reactions in a dry box with freshly distilled 2-cyclohexen-1-one, *p*-t-butylbenzenethiol, and toluene in a nitrogen atmosphere. The catalysts had to be purified and dried carefully in order to obtain highest e.e's. Under these conditions the results improved immediately, and the e.e. obtained with N-methylephedrine increased from 29 to 36%. The chemical yields varied between 70-100%, and were far less sensitive to the purity of the reagents. This suggests that small amounts of moisture mainly effect the e.e.'s.

Table 6.1 E.e.'s obtained with some ephedra derivatives in the standard reaction.

	e.e. (%)
N-methylephedrine	36
N-ethylephedrine	44
N-propylephedrine	36
N-butylephedrine	53
N-pentylephedrine	36
N-hexylephedrine	47
N-trimethylsilylmethylephedrine	53

First we have investigated if a change in the conformational behavior is responsible for the observed effects on the e.e. of the different ephedrine derivatives. Based on the conformational analysis of ephedrine and N-methylephedrine, described in chapters 2 and 5, we expect that three 'gauche 60', three 'gauche -60', and three trans conformers are potential energy minima. We have constructed nine starting conformers of N-ethylephedrine and protonated N-methylephedrine with T_1=-90°, T_2=-60, 60, or 180°, T_3=-60, 60, or 180°, T_4=180°, and Ψ= -60, 60, or 180° (in case of N-ethylephedrine only conformers with Ψ=-60° were considered). These torsional angles are defined in Figure 6.3. All conformers have been optimized

using MOPAC[7] and the PM3 Hamiltonian[8] . Some results of these geometry optimizations are summarized in Tables 6.2 and 6.3. It follows from the results presented in Table 6.2 that the replacement of one of the N-methyl substituents with an ethyl group does not change the conformational behavior significantly. Again nine minimum energy conformations exist, which resemble the ones found for N-methylephedrine. The energy differences between the various conformers are somewhat less pronounced than in the parent ephedrines. This implies an enhanced conformational freedom of N-ethylephedrine, which is difficult to explain with the observed increase of the e.e. Examination of the structures of the minimum energy conformations of N-ethylephedrine shows that the ethyl substituent on nitrogen is pointing into the 'free space'. Therefore, it can be expected that also the introduction of larger alkyl groups than an ethyl group on nitrogen will not cause significant conformational changes. We conclude that it is unlikely that a conformational effect is responsible for the observed effects on the e.e. (Table 6.1).

In Table 6.3 the effect of protonation on the conformational behavior of N-methylephedrine is summarized. It follows that also protonation does not influence the conformational behavior significantly. Only a minor effect on the conformational freedom with respect to Ψ is observed. In case of the two 'gauche -60' conformers only Ψ values of about 180° are found. In case of the two 'gauche 60' conformers a preference for Ψ of about -90° exists. In case of the trans conformers a strong preference is predicted for $\Psi=-100^{o}$.

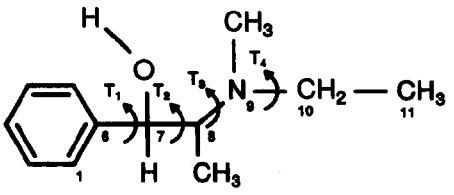

Figure 6.3 Definition of the torsion angles that define the gross conformation of N-ethylephedrine. $T_1=C_1C_6C_7C_8$, $T_2=C_6C_7C_8N_9$, $T_3=C_7C_8N_9N_{lone\ pair}$, $T_4=C_8N_9C_{10}C_{11}$, $\Psi=C_8C_7OH$.

Table 6.2 Results of PM3 optimizations on N-ethylephedrine. Energy in kcal/mol.

	T_1	T_2	T_3	T_4	Ψ	energy	N_{charge}
ethyl_1	-87.8	-65.1	-26.7	-162.3	-72.0	-36.5	-0.08
ethyl_2	-81.4	-57.7	-176.0	-163.8	-74.6	-34.8	-0.08
ethyl_3	-90.7	-49.0	53.3	-163.6	-77.6	-35.1	-0.07
ethyl_4	-94.7	59.7	-58.8	-169.0	-74.5	-36.5	-0.07
ethyl_5	-115.8	66.0	163.3	-159.1	-62.9	-35.9	-0.07
ethyl_6	-139.8	83.1	70.7	-162.7	-65.6	-33.9	-0.07
ethyl_7	-93.3	147.5	-50.4	-168.3	-45.8	-36.4	-0.07
ethyl_8	-82.3	164.4	61.7	-163.8	-39.1	-36.0	-0.07
ethyl_9	-88.4	153.0	-173.6	-170.7	-45.3	-36.6	-0.07

Table 6.3 Results of PM3 optimizations of protonated N-methylephedrine. Energy in kcal/mol.

	T_1	T_2	T_3	Ψ	energy	N_{charge}
methylh_1b	-89.0	-61.3	-27.7	179.7	121.9	0.66
methylh_3b	-75.1	-49.4	-174.1	170.1	124.8	0.68
methylh_4b	-112.7	60.7	-51.9	-145.8	123.6	0.64
methylh_4c	-115.7	63.0	-52.4	-92.4	123.3	0.65
methylh_6a	-116.0	63.8	162.5	106.7	128.2	0.67
methylh_6b	-116.4	62.0	167.4	-157.6	126.3	0.66
methylh_6c	-120.8	61.0	159.0	-90.8	125.4	0.67
methylh_7a	-92.1	152.3	-49.9	90.0	130.4	0.65
methylh_7c	-90.0	160.5	-34.1	-98.2	123.2	0.66
methylh_8c	-82.4	174.6	60.4	-105.6	121.1	0.66
methylh_9b	-92.0	159.4	-177.9	-150.4	123.4	0.65
methylh_9c	-84.5	155.3	-178.3	-97.4	122.7	0.66

Next we have investigated if the basicities of the ephedra derivatives are affected by the different substituents on the nitrogen atom or by the conformation of the catalyst. Basicity is a bulk thermodynamic property and thus not strictly correlated with the electron density on the nitrogen. However, because of the similarity between the different catalysts and the fact that they all have been tested under the same conditions, it can be expected that the electron densities on nitrogen before and after protonation will give a reasonable indication of the basicity. The partial charges, derived from the electron density, on nitrogen (Tables 6.2 and 6.3) have been computed with PM3 calculations. From the partial charges given in Table 6.2 it follows that differences in conformations of N-ethylephedrine do not influence the partial charge on nitrogen significantly. Also in the case of protonated N-methylephedrine (Table 6.3) there exits only a minor conformational effect on the partial charges of nitrogen. Therefore, we conclude that the partial charges, and thus the basicities of both protonated and unprotonated ephedrine derivatives are not influenced by the conformation. Finally, we have investigated if the different substituents on nitrogen are able to affect the partial charge. In this study we have considered the six derivatives given in Table 6.4. Because of the possibility that the lone pairs of the nearby oxygen of the hydroxy group affect the electron density on nitrogen we have optimized for each derivative three different geometries (basic geometry is that of conformer_7 with T_1=-90, T_2=160, T_3=-50°, and starting with three different staggered hydroxy orientations; Ψ=60, -60, 180°). From the calculated partial charges on nitrogen, given in Table 6.4, it follows that the different substituents on nitrogen do not affect the partial charge, and that only a minor effect exists of the orientation of the hydroxy group.

We have also optimized the protonated forms of the derivatives listed in Table 6.4. After PM3 optimizations it turned out that only one low energy orientation of the hydroxy substituent occurs with a Ψ of about -95°. Orientations with a Ψ of about 85° are more than 6 kcal/mol higher in energy. The calculated (PM3) partial charges on nitrogen are given in Table 6.5.

Table 6.4 Partial charge on nitrogen of some ephedra derivatives calculated with PM3. For each derivative 3 geometries have been optimized (Ψ= -60, 60, 180°).

	Ψ=60°	Ψ=-60°	Ψ=180°
methyl_7	-0.08	-0.07	-0.08
ethyl_7	-0.08	-0.07	-0.08
propyl_7	-0.08	-0.07	-0.08
butyl_7	-0.08	-0.07	-0.08
pentyl_7	-0.08	-0.07	-0.08
hexyl_7	-0.08	-0.07	-0.08

Table 6.5 Partial (PM3) charges on nitrogen for various protonated ephedra derivatives.

	partial charge
methyl_7	0.66
ethyl_7	0.63
propyl_7	0.64
butyl_7	0.63
pentyl_7	0.64
hexyl_7	0.63

In Figure 6.4 we have plotted these partial charges against the e.e's obtained with the corresponding ephedra derivatives. This plot illustrates that no clear correlation exists between the partial charge and e.e., maybe some trend exists between a lower charge on the protonated nitrogen and a higher e.e.

Therefore, we conclude that the observed effects on the e.e of the different ephedrine derivatives are difficult to explain with conformational or electronic arguments. Maybe the basicity of the catalysts is playing some role, but this is not clearly demonstrated. It is an unsatisfactory situation to admit that despite all our

detailed information we are not able to explain the observed trend of the e.e. with straightforward structural or electronic arguments.

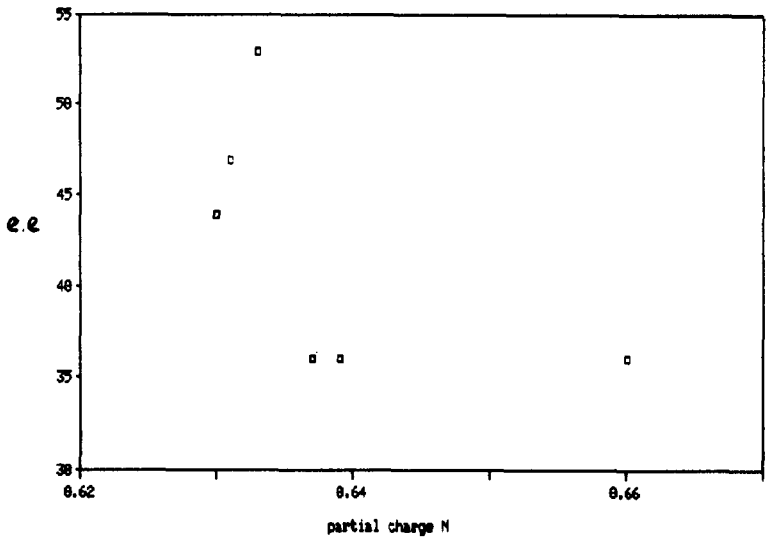

Figure 6.4 Plot of partial charge on x-axis against e.e. on y-axis.

6.3 DISCUSSION

In chapter 4 we have proposed two geometries for the transition states leading to both enantiomeric product molecules in the Michael addition between aromatic thiols and alkenones (Figures 4.18 and 4.19). With these geometries in mind it is difficult to rationalize the e.e. of 53% obtained with N-butylephedrine or 44% with N-ethylephedrine as compared to the 44% e.e. obtained with quinine. In chapter 4 we have argued that the main difference in $\Delta\Delta G$ values between both diastereomeric transition states is caused by interactions between the quinoline ring and the ring moiety opposite of the double bond of 2-cyclohexenone. As shown in Figure 6.5 the part of the quinoline ring responsible for these steric interactions is completely absent in case of the ephedra derivatives.

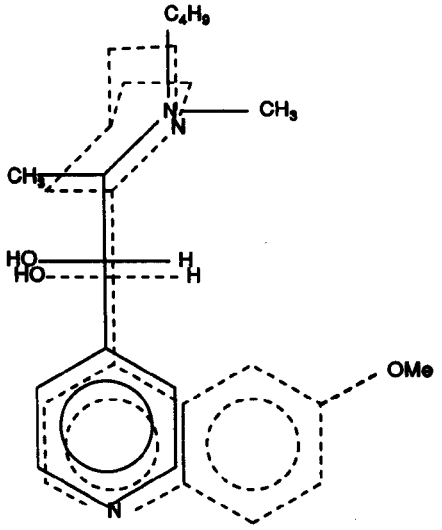

Figure 6.5 Structures of N-butylephedrine (solid lines) and quinine (dashed lines).

In case of cinchonidine Hiemstra obtained an e.e. of 62%. The only difference between quinine and cinchonidine is the presence of the methoxy group of quinine on the quinoline ring. Based on steric arguments the presence of the methoxy group should favor the discrimination between both diastereomeric transition states, because now the unfavorable interactions with the ring of cyclohexenone increase in the case of the transition state leading to product with S configuration. But as already pointed out in chapter 4, the decrease in e.e. from 62 to 44% in going from cinchonidine to quinine can be explained with electronic rather than steric arguments. The presence of the methoxy group on the quinoline ring causes a less tight transition state geometry, because the partially negatively charged (deprotonated) sulfur of the aromatic thiol is pushed away from the catalyst by the electron density on the methoxy oxygen atom. In this light, the relatively high e.e. obtained for N-butylephedrine is more easily understood, when we indeed assume

that steric arguments are less important. The observed trend between e.e. and partial charge on nitrogen of the protonated ephedrine derivatives may be another indication of the importance of electronic effects for the success of the reaction. Also indicative of the minor role of steric effects is the resulting e.e. of the quinine derivative shown in Figure 6.6.

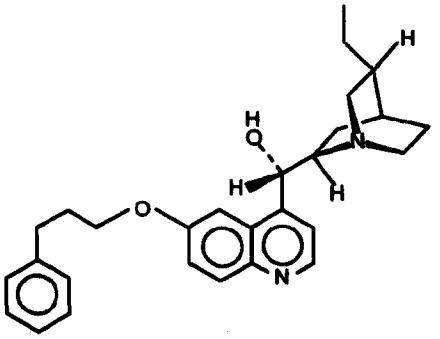

Figure 6.6 Quinine derivative designed to introduce a large group under the quinoline ring.

This catalyst was designed to introduce a large group under the quinoline ring of quinine. Based on steric arguments the discrimination between both diastereomeric transition states is expected to increase significantly. But an e.e. of only 13% was obtained with this catalyst in the standard reaction. The comparison of results obtained with ephedra and cinchona alkaloids in the Michael addition leads to the hypothesis that the electronic character of the catalyst is probably the most important factor that determines success of the reaction. Apparently, the chiral β-hydroxy amino segment is essential for obtaining discrimination between both possible enantiomeric products. The consequences for optimization strategies are readily perceived. Attention has to be focussed on the electronic aspects of the catalysts. These direct the affinity for the substrate molecules, but also for the intermediates of the reaction and the final products. If the affinity of a chiral catalyst for an intermediate or product is high it will have direct consequences for the

e.e. when alternative non selective or less selective reaction path are possible as well (and they often are!). In our case of the chiral Michael addition both the intermediate, as well as the product still contain the carbonyl functionality. Although it can be argued that the hydrogen bond between alkaloid and cyclohexenone is stronger than the hydrogen bond between product and alkaloid, the affinity of the catalyst for the product will decrease the turn-over rate of the catalyst and thus favor competing reaction routes.

All of this is well known. However, when looking at most discussions of stereoselective reactions the attention is focussed on steric aspects. On these grounds other substrate molecules are designed and synthesized, and new derivatives of the chiral catalyst are developed. Catalyst design or optimization of reaction conditions entirely based on the *catalytic power* of the catalyst, thus on turn-over rate is futile. The reason is maybe that the optimization of reaction conditions or catalysts is mostly directed by a proposed geometry of a transition state. These are often visualized by a 3D-picture (like we did in chapter 4). These pictures emphasize steric interactions and electronic effects remain hidden.

For future research we propose two ways to optimize the e.e. in the asymmetric Michael addition.

- *First*, a careful analysis of alternative reaction routes is needed. Based on this, design alternative reaction conditions such that these disfavor unwanted routes or favor the desired route. A fine example that attempts to disfavor non or less selective alternative reaction paths can be very successful has recently been given by Sharpless[9] : "We have discovered that the general procedure in our original communication[10] on the osmium-catalyzed asymmetric dihydroxylation of olefins is probably among the least effective that could be devised for running that process. We now report that with the trivial modification of adding the olefin slowly, virtually all olefins give higher e.e. and react faster than in the earlier method where all reactants, including the olefin, are present from the start". In the Michael addition several interfering reaction routes are possible. The most obvious one, reaction between thiol and alkenone without intervention of the catalyst, is

negligible under the reaction conditions. However, Hiemstra[11] reported that in an eight times more concentrated reaction mixture (without base) the addition product had been formed in about 70% yield after three days. The observation that even the uncatalyzed reaction can take place is important. What happens if only *one* of the substrate molecules is activated by the chiral catalyst? Other alternative less selective routes might involve reaction between activated cyclohexenone (hydrogen bonded to the catalyst) and thiol or activated thiol (deprotonated by catalyst) and cyclohexenone.

- *Second*, optimize the catalytic power of the catalyst. By this we mean: based on a 3D-picture of the transition state, design derivatives by 'forgetting' the steric implications of the model and concentrate on electronic aspects (remember the influence of the methoxy group of cinchona alkaloids on e.e.).

'Design' of a catalyst is clearly a multifacetted process. We restrict the question of 'design' to homogenous reactions and to the particular case of the alkaloid catalyzed reactions discussed in this thesis.

What do we know? First, we understand the conformational behavior of the catalysts quite well and we probably can predict properly the conformation of the transition state. If we predict this correctly then we are in a position to identify those steric, electronic, solvation. etc. factors that determine the enantioselectivity. To use a simpler metaphor, we probably understand the shapes (morphologies) of the components in the transition state. Second, and this is a corollary of the first point, we know that in one reaction, the Michael addition of thiols, an ion pair is involved as a critical step on the way to the transition state. Charge has been introduced into the picture.

What information is missing from the picture? Probably the most important piece of information regards the number of possible reaction paths. It is quite probable that achiral reaction paths may compete with the reaction path through a tight ion pair that leads to enantioselection. The simplest formulation of such an achiral path involves participation of water (the final traces of water are nearly impossible to remove). For example, suppose that at the stage of thiol addition to

cyclohexenone the enolate generated is protonated by water. Hydroxide is formed, which can deprotonate thiol, which then can react with cyclohexenone via an achiral pathway (see Figure 6.7). The result would be difficult to reproduce e.e.'s, which is indeed what is observed. Moreover, should there be competing achiral path-ways we would have to conclude that we do not know the *intrinsic enantio-selectivity* of the catalyst. It is even conceivable that quinine and/or quinidine have the capability, not realized, of absolute enantioselectivity[12].

The question posed above can be formulated differently and alternative reaction possibilities can be devised. The central question remains, irregardless of the specific chemical detail, whether the rate of formation of optically active products is identical to the total rate of the reaction. If not, there must be an achiral component. A kinetic analysis that provides an answer to this question should be possible.

An aspect of 'design' becomes then also the capacity to ensure that the enantioselective reaction designed is, and remains, the only reaction path.

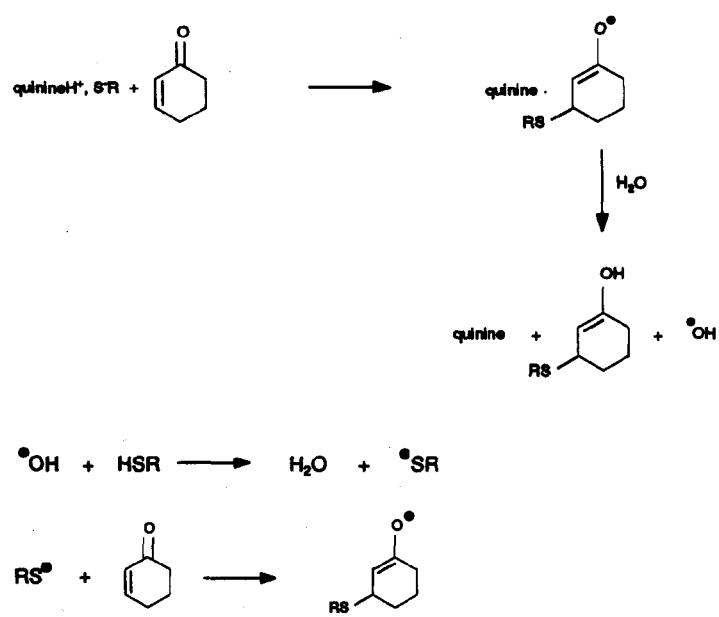

Figure 6.7 Effect of water on the Michael addition between aromatic thiols and cyclohexenone.

6.4 EXPERIMENTAL PART.

1-Phenyl-2-(methylethylamino)propanol-(1) hydrochloride (A). A mixture of ephedrine (3.2 g, 19.4 mmol) and C_2H_5I (3.4 g, 21.8 mmol) was warmed for 1 hr on a water bath. Next the reaction mixture was diluted with 20 ml water and acidified with 10% HCl solution. The reaction mixture was washed 3 times with ether, to remove the unreacted substances and impurities. The aqueous layer was made basic with 15% NaOH and extracted 3 times with CH_2Cl_2. The combined organic layers were dried over $MgSO_4$. The CH_2Cl_2 was evaporated. By passing HCl gas through an etherel solution of the residue, the hydrochloride salt was obtained, which was purified by two precipitations from small amounts of abs. ethanol/ether. Colorless fine needles were obtained in an overall yield of 57%, m.p. 175-177°.

1-Phenyl-2-(methylpropylamino)propanol-(1) hydrochloride (B). Ephedrine (3.1 g, 18.8 mmol) was heated with 1-bromopropane (2.9 g, 23.6 mmol) in an autoclave for 3 hrs at 130° (oil bath). The work-up procedure for A was followed further. The yield of N-propylephedrine was 66%, b.p. 130-135°. Hydrochloride salt : colorless needles, m.p. 141-144°. Alternatively, a yield of 92% was obtained by refluxing the same amounts of ephedrine and 1-bromopropane in 25 ml benzene for 72 hrs.

1-Phenyl-2-(methylbutylamino)propanol-(1) hydrochloride (C). Ephedrine (3.1 g, 18.8 mmol) was heated with 1-bromobutane (3.2 g, 23.4 mmol) in an autoclave for 3 hrs at 130° (oil bath). The work-up procedure for A was followed further. Reaction in the autoclave yielded 63% N-butylephedrine, b.p. 140-148°. Hydrochloride salt : Colorless needles, m.p. 95-97°. Reaction by refluxing 72 hrs in benzene again was more successful and provided N-butylephedrine in 95%.

1-Phenyl-2-(methylhexylamino)propanol-(1) hydrochloride (D). A mixture of ephedrine (1.0 g, 6.1 mmol) , powdered KOH (0.35 g, 2.6 mmol), and hexyl bromide (1.0 g, mmol) was heated for 5 hrs at 140° in an autoclave. Work up procedure of A was followed. Colorless plates of N-hexylephedrine hydrochloride were obtained in 53% yield, m.p. 121-124°.

Trimethylsilylmethylephedrine (E). A mixture of ephedrine (1.5 g, 9.1 mmol) and chloromethyltrimethylsilane (1.5 g, 12.2 mmol) was refluxed for 10 hrs. The reaction mixture was dissolved in 2N KOH and extracted 3 times with benzene. The combined organic layers were evaporated and dried over $MgSO_4$. The 56% of crude reaction product contained unreacted ephedrine. After distillation trimethylsilylmethylephedrine was isolated in 25% yield as a colorless oil.

1-Phenyl-2-(diethylamino)propanol-(1) hydrochloride (F). A mixture of norephedrine (1.5 g, 9.9 mmol), 7.5 ml Et_3N, 10 ml benzene, and 2 ml C_2H_5I was heated for 3 hrs at 60°. The work up procedure described for A was used. In 98% yield compound F was isolated.

6'-Phenylpropylether of quinine (Figure 6.6). Quinine (1.95 g, 6.0 mmol) was dissolved in 100 ml dry methylene chloride. The solution was cooled to -30^oC. Then a threefold excess of BBr_3 (4.8 g, 19.5 mmol) was added dropwise and the temperature was kept for 2 hrs at 0^oC. After another 2 hrs at room temperature, amply sufficient water was added (careful) to destroy the excess of BBr_3 and the boron complex by vigorously shaking. The acidic solution was neutralized with 2N NaOH to pH of about 8 and extracted several times with chloroform. Drying ($MgSO_4$) and evaporation of the solvent gave, after crystallization from methanol-ligroin (1:1), cupreine in 49% yield. Mp 201-203^0C.

Cupreine (0.99 g, 3.2 mmol) was dissolved in 100 ml dry methanol. Cs_2CO_3 (1.05 g, 3.2 mmol) was added to the solution. After 15 minutes (when all Cs_2CO_3) was dissolved) the methanol was evaporated. The cesium salt was dissolved in 50 ml DMF and a solution of 1-bromo-3-phenylpropaan (0.63 g, 3.2 mmol) in 50 ml DMF was added dropwise at 70^oC. After stirring overnight at 70^oC the CsBr was removed by filtration and the DMF by evaporation. 100 ml methylene chloride was added to the residue. The solution was washed 3 times with water and dried over Na_2SO_4. Evaporation of the solvent yielded 0.50 g product. After chromatography (silica gel, CH_2Cl_2/MeOH 4:1) 0.06 g of the 6'-phenylpropylether of quinine was isolated as a red oil.

6.5 REFERENCES

1. Hentges, S. G.; Sharpless, K. B. *J. Am. Chem. Soc.* **1980**, *102*, 4264.
   Jacobsen, E. J.; Marko, I.; Mungall, W. S.; Schroder, G.; Sharpless, K. B. *J. Am. Chem. Soc.* **1988**, *110*, 1968.
   Wai, J. S. M.; Marko, I.; Svendsen, J. S.; Finn, M. G.; Jacobsen, E. N.; Sharpless, K. B. *J. Am. Chem. Soc.* **1989**, *111*, 1123.
2. Dijkstra, G. D. H.; Kellogg, R. M.; Wijnberg, H. *Recl. Trav. Chim. Pays-Bas* **1989**, *108*, 195.
3. Hiemstra, H; Wijnberg, H. *J. Am. Chem. Soc.* **1981**, *103*, 417.
4. Smaardijk, A. A.; Wijnberg, H. *J. Org. Chem.* **1987**, *52*, 135.
   Smaardijk, A. A. Ph. D. Thesis, Groningen, 1986, p.131-132.
5. Wijnberg, H.; Staring, A. G. J. *J. Am. Chem. Soc.* **1982**, *104*, 166.
   Wijnberg, H; Staring, A. G. J. *J. Chem. Soc., Chem. Commun.* **1984**, 1181.
   Staring, A. G. J. Ph. D. Thesis, Groningen, 1985, p.141-147.
6. Hiemstra, H. Ph. D. Thesis, Groningen, 1980, p.22.
7. Stewart, J. J. P. *J. Comp. Aided Molec. Des.* **1990**, *4*, 1.
8. Stewart, J. J. P. *J. Comp. Chem.* **1989**, *10*, 209.
   Stewart, J. J. P. *J. Am. Chem. Soc.* **1989**, *10*, 221.
9. Wai, J. S. M.; Marko, I.; Svendsen, J. S.; Finn, M. G.; Jacobsen, E. N.; Sharpless, K. B. *J. Am. Chem. Soc.* **1989**, *111*, 1123.
10. Jacobsen, E. N.; Marko, I.; Mungall, W. S.; Schroder, G.; Sharpless, K. B. *J. Am. Chem. Soc.* **1988**, *110*, 1968.
11. Hiemstra, H. *Ph. D. Thesis* **1980**, Groningen, page 20.
12. At this moment, we have some indications that the intrinsic enantioselectivity of the cinchona alkaloids has not yet been reached in the Michael addition (Figure 6.1). These indications are based on preliminary results which have been obtained by performing this Michael addition in an ultrasone bath. In all cases cinchonidine is used as catalyst and about 40 experiments have been carried out. The chemical yields are almost quantitative after 20 minutes of reaction time and the e.e.'s vary from about 40% to almost the quantitative formation of one enantiomer. Because we have not been able to reproduce these recent results satisfactorily, we will not discuss these and recommend further investigation.

SUMMARY

The different behavior of enantiomers in living systems is the great stimulus for current interest in stereoselective synthesis. Cinchona and ephedra alkaloids are two classes of naturally occurring bases, which have found wide application as chiral catalysts in stereoselective synthesis. They have been applied successfully in carbon-carbon, carbon-sulfur, carbon-selenium, and carbon-phosphorous bond formation, as chiral phase-transfer catalysts, and as chiral ligands. Their role in medicine is firmly established. Furthermore, examples where cinchona alkaloids are used as chiral resolving agents are countless. In all these examples of the use of the alkaloids their ability for intimate interaction, discrimination and recognition are crucial to their success. In this thesis we have presented the results of a conformational study on cinchona and ephedra alkaloids. The salient features of ground state conformations of cinchona and ephedra alkaloids, the N-protonated forms of cinchona alkaloids, as well as an osmium tetraoxide-alkaloid complex have been described in detail, using a combined molecular modelling, NMR and X-ray analysis.

In Chapter 1 the cinchona and ephedra alkaloids are introduced. Also an introduction to stereoselective synthesis, illustrated with examples from the literature, is given.

In Chapter 2 a molecular mechanics analysis of cinchona and ephedra alkaloids is given. This conformational study has revealed that for quinidine and all quinidine derivatives four different minimum energy conformations exist, two closed conformations 1 and 2 and two open conformations 3 and 4. In case of quinine and quinine derivatives three minimum energy conformations have been identified (closed 1, closed 2, open 3). For ephedrine nine minimum energy conformations have been found and in case of N-methylephedrine seven minima were identified. A rigid fitting study of the calculated conformations of cinchona and ephedra alkaloids revealed that excellent similarities exist between all the minimum energy conformations of quinine and (N-methyl)ephedrine.

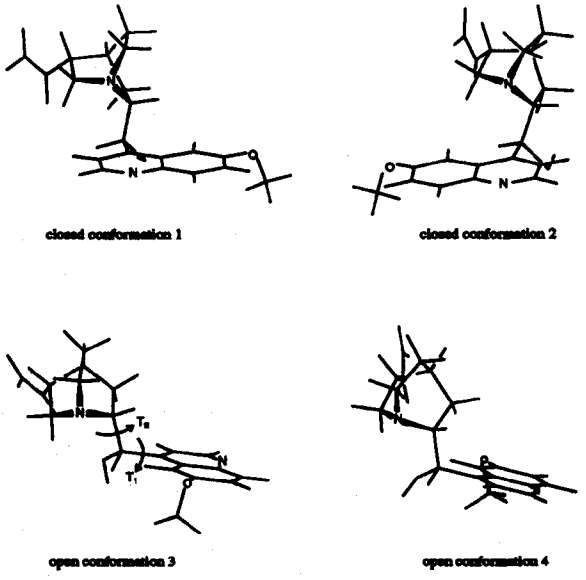

The four minimum energy conformations of quinidine.

In Chapter 3 a conformational analysis of cinchona alkaloids in solution is given. The results have been obtained by using several NMR techniques. We have demonstrated that the conformation of cinchona alkaloids can be influenced by varying the substituent at the benzylic position, by changing its configuration, by protonation of the quinuclidine nitrogen, by the nature of the solvent, or by complexation with osmium tetraoxide. Chloro cinchona alkaloid derivatives attain the closed conformation 2 almost exclusively. For the ester derivatives also a preference was found for the closed conformation 2. But now the equilibrium between closed conformation 2 and open conformation 3 is solvent dependent. For the methoxy derivatives the distinct preference for the closed conformation 2 has vanished. Either conformation 2 or 3 is now found in excess, depending on the solvent. The cinchona alkaloids themselves (with a hydroxy substituent at C_9) prefer the open conformation 3 in all solvents. The fact that epicinchona alkaloids

are found in the open conformation 4 suggests that the configuration of the benzylic C_9 position is important in determining the overall conformation.

In Chapter 4 a study of conformational effects of cinchona alkaloid-substrate interactions is presented. Because we are especially interested in the use of cinchona alkaloids as chiral bases and ligands we have studied effects of protonation and complexation on the conformation of the alkaloids in solution. Additional NMR data of thiol-alkaloid interactions and results from a molecular docking study are used to propose a transition state for the asymmetric Michael addition between aromatic thiols and conjugated alkenones.

In Chapter 5 the molecular orbital calculations on some cinchona and ephedra alkaloids and on model compounds are adressed. With the calculational results we have explained in some detail the experimentally obtained conformational data.

In Chapter 6 further attention has been paid to the Michael addition between aromatic thiols and alkenones. We have described initial experiments in which ephedra alkaloids are used as chiral catalyst. Based on results with these catalysts we have concluded that steric arguments might be less important to obtain high e.e.'s than previously believed.

SAMENVATTING

Het feit dat enantiomeren in principe verschillende eigenschappen bezitten in een chirale, dus natuurlijke, omgeving vormt een belangrijke reden voor de sterke belangstelling voor de stereoselectieve synthese. De natuurlijk voorkomende cinchona en ephedra alkaloiden worden veel toegepast in de chemie:

- als chirale katalysatoren in stereoselectieve synthese. Ze zijn met succes toegepast in koolstof-koolstof, koolstof-zwavel, koolstof-selenium en koolstof-fosfor bindingsvormende reakties.
- als farmaceutisch werkzame verbindingen.
- als chirale splitsings middelen.

Het succes van de cinchona en ephedra alkaloiden in al deze toepassingen is te danken aan hun vermogen om zeer specifiek en selektief interakties aan te gaan. In dit proefschrift worden de resultaten besproken van een konformatie studie van cinchona en ephedra alkaloiden. Omdat we vooral geinteresseerd zijn in hun gebruik als chirale katalysatoren (base, ligand) zijn ook de effekten op de konformatie bestudeerd van protonering en van komplexering.

In hoofdstuk 1 worden de cinchona en ephedra alkaloiden geintroduceerd. Ook worden de verschillende routes besproken waarlangs stereoisomeren verkregen kunnen worden.

In hoofdstuk 2 worden de resultaten besproken van een molekulaire mechanica analyse van cinchona en ephedra alkaloiden. Voor quinidine en alle quinidine derivaten zijn vier verschillende konformaties gevonden, twee 'gesloten' konformaties en twee 'open' konformaties. Voor quinine en alle quinine derivaten werden drie konformaties gevonden, twee 'gesloten' konformaties en een 'open' konformatie. In het geval van ephedrine werden negen verschillende konformaties gevonden, terwijl voor N-methylephedrine zeven konformaties werden gevonden. Met behulp van een rigid fitting programma werden alle berekende minimum energie konformaties van de cinchona alkaloiden vergeleken met die van de ephedra alkaloiden. Er werd een grote overeenkomst gevonden tussen de konformaties van beiden klassen van alkaloiden.

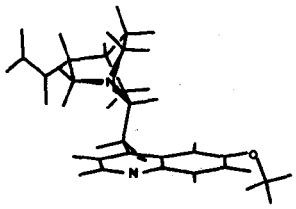

closed conformation 1

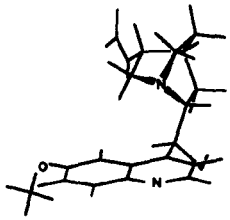

closed conformation 2

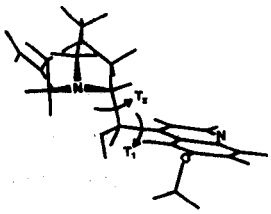

open conformation 3

open conformation 4

De vier minimum energie konformaties van quinidine.

In hoofdstuk 3 wordt een konformatie analyse van cinchona alkaloiden in oplossing besproken. De resultaten werden verkregen door gebruik te maken van verschillende NMR technieken. We hebben aangetoond dat de konformatie van cinchona alkaloiden bepaald wordt door de aard van de benzylische substituent en ook door de konfiguratie van het benzylische koolstof atoom. Ook het oplosmiddel bleek in staat te zijn de konformatie van cinchona alkaloiden te beinvloeden. Cinchona alkaloiden met een chloor atoom aan het benzylische koolstof bleken een sterke voorkeur te bezitten voor de gesloten konformatie 2. Voor ester derivaten werd welliswaar ook een voorkeur gevonden voor de gesloten konformatie 2, maar nu minder uitgesproken. Ook de open konformatie 3 komt voor. De verhouding tussen de gesloten konformatie 2 en de open konformatie 3 wordt bepaald door de polariteit van het oplosmiddel. In het geval van methoxy

derivaten is de uitgesproken voorkeur voor de gesloten konformatie 2 geheel verdwenen. Open konformatie 3 of gesloten konformatie 2 komt nu in overmaat voor, afhankelijk van het oplosmiddel. De cinchona alkaloiden zelf (dus met een hydroxy groep aan het benzylische koolstof) worden uitsluitend in de open konformatie 3 gevonden. Het feit dat epicinchona alkaloiden gevonden worden in de open konformatie 4 geeft aan dat de konfiguratie van het benzylische koolstof atoom belangrijk is.

In hoofdstuk 4 wordt een konformatie studie beschreven van cinchona alkaloid-substraat interakties. Omdat we vooral geinteresseerd zijn in het gebruik van cinchona alkaloiden als chirale base en als chiraal ligand hebben we de effekten van protonering en komplexering op de konformatie bestudeerd. Ook wordt een voorstel besproken voor de geometrie van de overgangstoestand van de asymmetrische Michael additie tussen aromatische thiolen en gekonjugeerde alkenonen. Additionele NMR data van alkaloid-aromatische thiol interakties en resultaten van een molekulaire docking studie zijn hiervoor gebruikt.

In hoofdstuk 5 worden molekulaire orbital berekeningen aan cinchona en ephedra alkloiden besproken. Met behulp van de resultaten van deze berekeningen worden vele experimentele observaties van het konformatie gedrag van cinchona alkaloiden verklaard.

In hoofdstuk 6 wordt verdere aandacht besteed aan de asymmetrische Michael additie van aromatische thiolen en gekonjugeerd alkenonen. De resultaten van reakties waarin ephedra alkaloiden gebruikt worden als chirale katalysator dienen als uitgangspunt voor een discussie over de belangrijkste faktoren die bepalend zijn voor het succes van de reaktie.